Molecular Mechanisms of Fragile X Syndrome Investigated by Mass Spectrometry-Based Proteomics

Dissertation

zur Erlangung des Grades eines

Doktors der Naturwissenschaften

der Mathematisch-Naturwissenschaftlichen Fakultät

und

der Medizinischen Fakultät

der Eberhard-Karls-Universität Tübingen

vorgelegt

von

Katarina Matic

Aus Split, Kroatien

Juni - 2015

Tag der mündlichen Prüfung: 10.09.2015.

Dekan der Math.-Nat. Fakultät: Prof. Dr. W. Rosenstiel

Dekan der Medizinischen Fakultät: Prof. Dr. I. B. Autenrieth

1. Berichterstatter: Prof. Dr. Boris Macek

2. Berichterstatter: Prof. Dr. Olaf Reiss

Prüfungskommission: Prof. Dr. Boris Macek

Prof. Dr. Olaf Riess

Prof. Dr. Alfred Nordheim

Prof. Dr. Mathias Jucker

Erklärung / Declaration:

Ich erkläre, dass ich die zur Promotion eingereichte Arbeit mit dem Titel:

„Molecular Mechanisms of Fragile X Syndrome Investigated by Mass Spectrometry-Based Proteomics“

selbständig verfasst, nur die angegebenen Quellen und Hilfsmittel benutzt und wörtlich oder inhaltlich übernommene Stellen als solche gekennzeichnet habe. Ich versichere an Eides statt, dass diese Angaben wahr sind und dass ich nichts verschwiegen habe. Mir ist bekannt, dass die falsche Abgabe einer Versicherung an Eides statt mit Freiheitsstrafe bis zu drei Jahren oder mit Geldstrafe bestraft wird.

I hereby declare that I have produced the work entitled "Molecular Mechanisms of Fragile X Syndrome Investigated by Mass Spectrometry-Based Proteomics", submitted for the award of a doctorate, on my own (without external help), have used only the sources and aids indicated and have marked passages included from other works, whether verbatim or in content, as such. I swear upon oath that these statements are true and that I have not concealed anything. I am aware that making a false declaration under oath is punishable by a term of imprisonment of up to three years or by a fine.

Tübingen, den 15.06.2015. .....

Datum / Date Unterschrift /Signature

Statement of contributions:

The aim of the research work described in the first part of the thesis ("Quantitative phosphoproteomics of murine *Fmr1*-KO cell lines provides new insights into FMRP-dependent signal transduction mechanisms") was to analyze the influence of FMRP on major signal transduction networks. To that end, we performed a global analysis of the proteome and phosphoproteome of *Fmr1*$^{-}$ and *Fmr1*$^{+}$ mouse embryonic fibroblast (MEF) cell lines using stable isotope labeling by amino acids in cell culture (SILAC) and high resolution mass spectrometry.

Cells were constructed and provided by Dr. Davidovic L and Dr. Bardoni B. Eninger T and I did the sample preparation: growing the cells, proteome and phosphoproteome preparation, and performed the processing of MS raw files and complete downstream analysis of the retrieved results. Western blot analysis was done by Dr. Davidovic L. Manuscript was written by Eninger T and me with the help of Prof. Dr. Macek B and Dr. Davidovic L.

This data represent the first global large-scale analysis of proteome and phosphoproteome of the *Fmr1*-KO MEF cell lines, a commonly used *Fmr1*-KO model. By doing the analysis I contributed to the conformation of downregulation of the MEK/ERK pathway in absence of FMRP, with decreased phosphorylation on ERK1/2. In addition, my analysis showed differential expression of several proteins involved in mTOR, Wnt, p53 and MAPK signaling cascades, that were known to be associated with autism, but not with FXS. I detect significant increase of p53 and proteins linked to the p53 signaling. Therefore, my work will ultimately lead to a better understanding of the molecular mechanisms dysregulated in FXS.

Katarina Matic, MD

I confirm that the above description of Ms. Matic's contributions to the manuscript is correct.

Prof. Dr. Boris Macek

Table of Contents

LIST OF ABBREVIATIONS

AMPA	α-Amino-3-hydroxy-5-Methyl-4-isoxazolePropionic Acid
ANOVA	Analysis of Variance
AQUA	Absolute Quantification
ARG	Arginine
ATP	Adenosine Triphosphate
AUC	Area Under Curve
C18	Octadecyl Carbon Chain
CAN	Acetonitrile
CID	Collision Induced Dissociation
DIV	Day in Vitro
DMEM	Dulbecco's Modified Eagle Medium
DNA	Deoxyribonucleic acid
ESI	Electrospray Ionization
FDR	False Discovery Rate
FMRP	Fragile X Mental Retardation Protein
FXS	Fragile X Syndrome
GSK	Glycogen Synthase Kinase
H/L	“Heavy” to “Light” Ratio
HCD	High Energy Collision Dissociation
HET	Heterozygous Knock-Out
HITS-CLIP	High-Throughput Sequencing of RNA Isolated by Crosslinking Immunoprecipitation
HPLC	High Pressure Liquid Chromatography
ICAT	Isotope-Coded Affinity Tags
ID	Intellectual disability
IMAC	Metal Ion Affinity Chromatography
ITRAQ	Isobaric Tags for Relative and Absolute quantification
KEGG	Kyoto Encyclopedia of Genes and Genomes
KO	Knock-Out
LC	Liquid Chromatography
LFQ	Label-Free Quantification
LMEM	Linear Mixed Effects Model
LTD	Long Term Depression
LTP	Long Term Potentiation
LTQ	Linear Trap Quadrupole
LYS	Lysine
M/Z	Mass-to-Charge Ratio

MALDI	Matrix Assisted Laser Desorption Ionization
MBR	Match Between Run
MEF	Mouse Embryonic Fibroblast
MGLUR	Metabotropic Glutamate Receptor
MPEP	2-Methyl-6-(PhenylEthynyl)Pyridin
MRNA	Messenger Ribonucleic acid
MS	Mass Spectrometry
MS/MS	Tandem Mass Spectrometry
NLS	Nuclear Localization Signal
NMDA	N-Methyl-D-Aspartate
PAR-CLIPS	Photoactivatable Ribonucleoside-Enhanced Crosslinking and Immunoprecipitation
PEP	Posterior Error Probability
PI	Isoelectric Point
PPI	Protein-Protein Interaction
PPM	Part Per Million
PRI	Protein-RNA interaction
PSILAC	Pulsed Stable Isotope-Labeling by Amino Acids in Cell Culture
PTM	Post-Translational Modification
PVDF	Polyvinylidene Difluoride
RGG	Arginine-Glycine-Glycine
RT	Room Temperature
SCX	Strong Cation Exchange Chromatography
SD	Standard Deviation
SDS-PAGE	Sodium dodeecyl sulfate polyacrylamide gel electrophoresis
SER	Serine
SILAC	Stable Isotope-Labeling by Amino Acids in Cell Culture
TDZD	Thiadiazolidinone
TFA	Triflouroacetic Acid
THR	Threonine
TIO_2	Titanium Dioxide Chromatography
TPA	Total Protein Approach
TYR	Tyrosine
UV	Ultraviolet
WT	Wild Type
XIC	Extracted Ion Current

SUMMARY

Fragile X syndrome (FXS) is the leading cause of inherited intellectual disability (ID) and autism. This neurodevelopmental disorder is caused by silencing of the *FMR1* gene and lack of its product, Fragile X Mental Retardation Protein (FMRP). FMRP, an RNA-binding protein, is highly expressed in the brain and plays an important role in the transport and translation of many different mRNA targets. Lack of FMRP causes disruption in synapse morphology and function, as well as disruption in synaptic plasticity. These molecular and synaptic abnormalities cause FXS symptoms like ID, autism, hyperactivity, epilepsy and anxiety. Therefore, understanding of the molecular pathogenesis of FXS is also important for other neurodevelopmental and psychiatric disorders. In last two decades, extensive research in basic neurobiology and pathophysiology led to significant advances in FXS field. However, although caused by only one gene, the molecular mechanisms of FXS are not yet well understood. Since FMRP is characterized as a translational regulator with multiple mRNA targets, it is crucial to understand the changes of the proteome in the absence of FMRP. As multiple FMRP-regulated proteins are involved in conserved neuronal signal transduction pathways, it is also necessary to study FMRP-dependent changes in the phosphoproteome dynamics. In my thesis I applied mass spectrometry-based proteomics to address several aspects of the disorder in different FXS models, such as *Fmr1*-KO cell lines and mice.

To analyze the influence of FMRP on major signal transduction networks, I first performed a global analysis of the proteome and phosphoproteome of *Fmr1*$^{-}$ and *Fmr1*$^{+}$ mouse embryonic fibroblast (MEF) cell lines using stable isotope labeling by amino acids in cell culture (SILAC) and high resolution mass spectrometry. In this study I detected 6,703 proteins and 9,181 phosphorylation events, and mapped 266 significantly changing proteins and 142 phosphorylation sites onto major signal transduction pathways. My results confirmed a downregulation of the MEK/ERK pathway in absence of FMRP, with decreased phosphorylation on ERK1/2. Several proteins involved in mTOR,

Wnt, p53 and MAPK signaling cascades were also significantly regulated; they were previously shown to be associated with autism, but not with FXS. Additionally, I detected a significant increase of p53 and proteins linked to p53 signaling, as well as a decreased level of the major prion protein (Prp) in *Fmr1*$^{-}$ cells. Decreased p53 signaling is the likely cause for previously observed dysregulation of cell cycle control in FXS, whereas reduced levels of Prp could contribute to the cognitive deficits observed in the FXS patients. These proteins and signal transduction pathways may represent novel targets for treatment of FXS symptoms.

In the second part of the thesis, I used the same MEF cell line in order to analyze potential substrates of glycogen synthase kinase 3β (GSK-3β), an emerging therapeutic target for treatment of FXS. I used two inhibitors of GSK3-β kinase, lithium and TDZD-8, to identify potential substrates of the kinase in *Fmr1*$^{-}$ and *Fmr1*$^{+}$ cells. Lithium treatment was poorly reproducible on the proteome and phosphoproteome level, reflecting its reported low specificity for GSK3- β, whereas TDZD-8 treatment showed good reproducibility between biological replicates. Of a total of 7,285 detected phosphorylation events, 91 were significantly decreased upon TDZD-8 treatment in *Fmr1*$^{+}$ and 146 in *Fmr1*$^{-}$ MEF cells – these phosphorylation events were likely targets of GSK-3β. Overlap of these potential substrates was poor in *Fmr1*$^{+}$ and *Fmr1*$^{-}$ cells, pointing to different substrates of the GSK-3β kinase in *Fmr1*$^{+}$ and *Fmr1*$^{-}$ MEF cells. Importantly, downregulation of multiple phosphorylation events on *MAP1B*, a well characterized GSK-3β substrate whose mRNA is a known FMRP target, was observed only in *Fmr1*$^{+}$ MEF cell line. In healthy neurons, *MAP1B* is coordinating microtubule dynamics. Since abnormal axon branching is one of the leading symptoms of FXS, I postulate that the lack of regulation of *MAP1B* by GSK-3β is the likely cause for aberrant morphology of neurons in FXS. Functional enrichment analysis revealed an implication of the potential GSK-3β substrates in different processes in MEF cell lines. For example, in *Fmr1*$^{-}$ MEFs potential substrates seem to be more involved in cell cycle, DNA replication and RNA processing. Since downregulation of DNA damage/repair pathway in FXS patients was recently reported, this data will shed new

light on differential activity of GSK-3β in *Fmr1*$^{+}$ and *Fmr1*$^{-}$ MEF cells and deepen our understanding of molecular mechanisms regulated by this kinase.

In the third part of my thesis, I postulated that increased protein synthesis in FXS is accompanied by increased protein degradation in order to maintain cellular homeostasis. Since increased protein synthesis and degradation lead to increased protein turnover, I used stable isotope labeling ("dynamic SILAC" approach) to measure protein turnover rate in mouse primary cortical neurons derived from the WT and *Fmr1*-KO model. Analysis showed that most of the proteins have a similar half-life in WT and *Fmr1*-KO, although calculated median protein half-life was higher in *Fmr1*-KO neurons than in WT. Functional enrichment analysis showed that proteins with the lowest turnover rates are involved in oxidative phosphorylation, Alzheimer's, Parkinson's and Huntington's diseases, whereas proteins with the highest turnover rates are involved in phagosome, Wnt signaling pathway and gap junction, for both, WT and *Fmr1*-KO neurons. The experimental design employed did not allow for detection of low SILAC incorporation rates and proteins with very short half-lifes and further optimization of experimental conditions is needed to fully address differences in protein turnover between *Fmr1*-KO and WT cells.

In the fourth and final part of the thesis, I investigated molecular mechanisms of the genetic "rescue" of the FXS, recently reported to occur in *Fmr1*-KO mice after reduction of activity of the mGluR5 receptor. To that end, I performed a proteome-wide quantitative comparison of protein levels in the hippocampi between WT, *Fmr1*-KO mice and *Fmr1*-KO/*mGluR5*-het cross mice (the "rescued" FXS model), obtained from the laboratory of Mark Bear (MIT). Pearson correlation of protein intensities showed good technical reproducibility between biological replicates and also showed that different genotypes are very similar to each other – of 5,238 detected proteins, only about 198 were significantly changing between genotypes. Yet, pairwise comparison of *Fmr1*-KO and WT revealed proteins that are known to be involved in memory, learning and long

term potentiation. Moreover, the data suggests disturbed mitochondrial transcription regulation in FXS model. One of the significantly changing proteins, the major prion protein, had a lower expression level in *Fmr1*-KO in comparison with WT. Since I detected the same expression pattern in MEF cell lines, I postulate that Prp plays a significant role in FXS pathogenesis. In the FXS rescue model, most of the significantly changing proteins are involved in metabolic processes, with the exception of Citron Rho-interacting kinase which is functionally linked to *Fmr1* gene and it is interacting with mGluR5 receptor, and therefore may be involved in the rescue mechanism. I also addressed absolute protein levels in analyzed mouse models. This approach showed no difference in the total proteome abundance between the three genotypes; however, it did show that proteins with higher upregulation levels in *Fmr1*-KO are more abundant that those that were found to be downregulated. This imbalance may be the cause of the overall increased protein levels previously detected in brains of FXS mice. However, a portion of changing proteins is rather small and therefore not significant and further experiments need to be performed to address this.

Overall, this thesis presents an extensive proteomics analysis of the different cellular and animal models of FXS. Combined, these approaches compile a substantial source of information for the FXS research community. In addition, this data is contributing to the better understanding of FXS pathophysiology and development of a potential new treatments.

ZUSAMMENFASSUNG

Das Fragile X Syndrom (FXS) ist die Hauptursache bei erblich bedingter geistiger Behinderung (ID) sowie bei Autismus. Diese Entwicklungsstörung des Nervensystems wird durch Ausschalten des *FMR1* Gens und das Fehlen seines Produkts, des Fragile X Mental Retardation Proteins (FMRP), ausgelöst. FMRP, ein RNA-bindendes Protein, liegt im Gehirn hoch exprimiert vor und spielt beim Transport und bei der Translation vieler verschiedener Ziel-mRNAs eine bedeutende Rolle. Das Fehlen von FMRP führt zur Zerstörung der Morphologie und Funktion der Synapsen, wie auch zur Zerstörung der synaptischen Plastizität. Diese molekularen und synaptischen Anomalien führen zu FXS Symptomen wie ID, Autismus, Hyperaktivität, Epilepsie und Angstzuständen. Das Verständnis der molekularen Pathogenese des Fragile X Syndroms ist deshalb nicht nur relevant für die FXS Patienten, sondern auch für andere Entwicklungsstörungen des Nervensystems und psychiatrische Erkrankungen. In den letzten zwei Jahrzehnten führten umfassende Grundlagenforschungen in der Neuro- und Pathophysiologie zu signifikanten Fortschritten im FXS-Bereich. Obwohl die Ursache nur an einem einzelnen Gen liegt, ist der molekulare Mechanismus von FXS noch wenig erforscht. Seitdem FMRP als Translationsregulator zahlreicher Ziel-mRNAs beschrieben ist, ist es unumgänglich ein Verständnis über die Änderungen im Proteom bei Abwesenheit von FMRP zu erlangen. Da viele FMRP-Zielmoleküle in konservierten neuronalen Signaltransduktionswegen eingebunden sind, ist es auch wichtig, FMRP-abhängige Veränderungen in der Dynamik des Phosphoproteoms zu studieren. In meiner Dissertationsarbeit führte ich Massenspektrometrie-basierende Proteomanalysen durch, um verschiedene Aspekte einer Störung in verschiedenen FXS-Modellen, wie *Fmr1*-KO Zelllinien und Mäuse, zu untersuchen.

Um den Einfluss von FMRP auf die wesentlichen Signalübertragungsnetzwerke zu analysieren, führte ich zuerst, unter Verwendung von SILAC (Stable Isotope Labeling by Amino Acids in Cell Culture) und hochauflösender Massenspektrometrie, eine

umfassende Analyse des Proteoms und des Phosphoproteoms von *Fmr1*$^{-}$- und *Fmr1*$^{+}$-embryonalen Maus-Fibroblastenzelllinien (MEF) durch. Bei dieser Studie detektierte ich 6 703 Proteine und 9 181 Phosphorylierungsstellen, darunter 266 Proteine und 142 Phosphorylierungsstellen, die signifikant reguliert waren und in wichtigen Signaltransduktionswegen vorkommen. Meine Ergebnisse bestätigten eine Herunterregulierung des MEK/ERK-Signalweges mit verminderter Phosphorylierung von ERK1/2 bei Abwesenheit von FMRP.

Auch viele in mTOR-, Wnt-, p53- und MAPK-Signalkaskaden involvierte Proteine waren signifikant reguliert; sie waren zuvor mit Autismus, aber nicht mit FXS in Zusammenhang gebracht worden. Außerdem detektierte ich sowohl einen signifikanten Anstieg von p53 und von Proteinen, die mit dem p53-Signalweg in Verbindung stehen, als auch einen verminderten Expression von wichtigen Prionproteinen (Prp). Der abgeschwächte p53-Signalweg ist vermutlich der Grund für die zuvor beobachtete Fehlregulation der Zellzykluskontrolle in FXS, dahingegen könnte ein verminderter Prp-Anteil zu den in FXS-Patienten beobachteten kognitiven Mängeln beitragen. Diese Proteine und Signaltransduktionswege können neue Zielstrukturen für die Behandlung von FXS-Symptomen sein.

Im zweiten Teil meiner Dissertationsarbeit verwendete ich dieselbe MEF-Zelllinie, um potentielle Substrate der Glykogen-Synthase-Kinase 3β (GSK-3β), ein neu aufkommendes therapeutisches Zielmolekül zur Behandlung von FXS, zu untersuchen. Ich verwendete zwei Inhibitoren der GSK3-β-Kinase, Lithium und TDZD-8, um mögliche Substrate der Kinase in *Fmr1*$^{-}$- und *Fmr1*$^{+}$-Zellen zu identifizieren. Die Behandlung mit Lithium war sowohl auf Proteom-, als auch auf Phosphoproteomebene schlecht reproduzierbar, was seine bereits bekannte geringe Spezifität gegenüber GSK3- β widerspiegelt, während die Behandlung mit TDZD-8 eine gute Reproduzierbarkeit zwischen biologischen Replikaten zeigte. Unter insgesamt 7 285 detektierten Phosphorylierungsstellen waren nach TDZD-8-Behandlung 91 in *Fmr1*$^{+}$- und 146 in *Fmr1*$^{-}$

-MEF-Zellen signifikant zurückgegangen – diese Phosphorylierungsstellen waren wahrscheinlich GSK-3β-Targets. Die geringe Überlappung dieser potentiellen Substrate in *Fmr1*$^{-}$- und *Fmr1*$^{+}$-Zellen deutet auf verschiedene Substrate der GSK3- β-Kinase in *Fmr1*$^{+}$- und *Fmr1*$^{-}$-MEF-Zellen hin. Nennenswert ist, dass die Herunterregulierung mehrerer Phosphorylierungsstellen auf *MAP1B*, einem gut beschriebenen Substrat der GSK3β, dessen mRNA als ein Zielmolekül von FMRP bekannt ist, nur in der *Fmr1*$^{+}$ -MEF-Zelllinie gesehen wurde. In gesunden Neuronen koordiniert *MAP1B* die Mikrotubuli-Dynamik. Da die abweichende Verzweigung der Axone eines der führenden FXS-Symptome ist, postuliere ich, dass die fehlende Regulation von MAP1B durch GSK-3β der mögliche Grund für die abweichende Morphologie der Neuronen in FXS ist. Eine Anreicherungsanalyse auf funktionaler Ebene zeigte die Auswirkung potentieller GSK-3β-Substrate in verschiedenen MEF-Zelllinien. Zum Beispiel scheinen in *Fmr1*$^{-}$ -MEFs die potentiellen GSK-3β-Substrate mehr im Zellzyklus, in der DNA-Replikation und in der RNA-Prozessierung involviert zu sein. Da kürzlich von einer Herunterregulation des DNA-Schädigung/-Reparatur-Systems in FXS-Patienten berichtet wurde, werden diese Daten Aufschluss über verschiedene Aktivitäten der GSK-3β in *Fmr1*$^{+}$- und *Fmr1*$^{-}$-MEF-Zellen liefern und unser Verständnis für den, durch diese Kinase regulierten, molekularen Mechanismus vertiefen.

Im dritten Teil meiner Dissertationsarbeit postuliere ich, dass die gesteigerte Proteinsynthese in FXS durch eine erhöhte Proteindegradierung begleitet wird, um die zelluläre Homöostase zu erhalten. Da eine erhöhte Proteinsynthese und –degradation zu einem erhöhten Proteinumsatz führt, verwendete ich die stabile Isotopenmarkierung (dynamischer SILAC-Versuch), um die Proteinumsatzrate in primären kortikalen Neuronen von WT-und *Fmr1*-KO-Mausmodellen zu messen. Die Analyse zeigte, dass die Mehrzahl der Proteine ähnliche Halbwertszeiten im WT und im *Fmr1*-KO haben, obwohl die berechnete mediane Proteinhalbwertszeit in *Fmr1*-KO-Neuronen höher war als im WT. Eine Anreicherungsanalyse auf funktionaler Ebene zeigte, dass die Proteine mit den niedrigsten Umsatzraten in oxidativen Phosphorylierungsprozessen, Alzheimer-,

Parkinson- und Huntington-Erkrankungen beteiligt sind, während die Proteine mit den höchsten Umsatzraten im Phagosom, Wnt-Signalweg und Gap Junction involviert sind. Diese Ergebnisse waren konsistent in WT und Kmr1-KO Neuronen. Das angewendete Versuchskonzept gestattete nicht die Detektion geringer SILAC-Inkorporationsraten und Proteine mit sehr kurzen Halbwertszeiten, d.h. es ist eine weitere Optimierung der experimentellen Konditionen nötig, um Unterschiede in der Proteinumsatzrate zwischen *Fmr1*-KO- und WT-Zellen vollständig zu erfassen.

Im vierten und letzten Teil meiner Dissertation untersuchte ich den molekularen Mechanismus des genetischen "Rescues" von FXS, von dem kürzlich berichtet wurde, dass er in *Fmr1*-KO-Mäusen nach Reduktion der Aktivität des mGluR5-Rezeptors aufgetreten sei. Zu diesem Zweck führte ich eine proteomweite, quantitative Vergleichsstudie der Proteingehalte zwischen den Hippocampi von WT- und *Fmr1*-KO-Mäusen und *Fmr1*-KO/*mGluR5*-het gekreuzten Mäusen (FXS-"Rescue"-Model) durch. Die Mäuse kamen aus dem Labor von Mark Bear (MIT). Die Pearson-Korrelation demonstrierte eine gute Reproduzierbarkeit zwischen den biologischen Replikaten und zeigte außerdem, dass verschiedene Genotypen zueinander sehr ähnlich sind – von 5 238 detektierten Proteinen zeigten nur 198 signifikante Unterschiede zwischen Genotypen. Dennoch legten paarweise Vergleiche von *Fmr1*-KO und WT Proteine offen, von denen bekannt ist, dass sie eine Funktion im Gedächtnis, beim Lernen und bei der Langzeitpotenzierung haben. Darüber hinaus deuten die Daten auf eine gestörte mitochondriale Transkriptionsregulation im FXS-Model hin. Eines der signifikant regulierten Proteine, das maßgebliche Prionprotein, zeigte im Vergleich zum WT ein niedrigeres Expressionslevel in *Fmr1*-KO. Da ich das gleiche Expressionsmuster in MEF-Zelllinien detektierte, postuliere ich, dass Prp eine signifikante Rolle in der FXS-Pathogenese spielt. Im FXS-"Rescue"-Model sind die meisten signifikant regulierten Proteine in metabolische Prozesse involviert. Ausnahme ist die Citron-Rho-interagierende Kinase, die funktional mit dem *Fmr1*-Gen verbunden ist und mit dem mGluR5-Rezeptor interagiert und damit in den "Rescue"-Mechanismus involviert sein

kann. Ich habe auch den absoluten Proteingehalt in den analysierten Mausmodellen bestimmt. Dieser Versuch zeigte keinen Unterschied in den gesamten Proteinmenge aller drei Genotypen, aber er zeigte, dass Proteine mit höherer Expressionsrate in *Fmr1*-KO mehr vertreten sind, als jene mit niedrigerer Expressionsrate. Dieses Missverhältnis kann die Ursache für den allgemeinen Anstieg des, zuvor in Gehirnen von FXS-Mäusen detektierten, Proteingehalts sein. Jedoch ist der Anteil regulierter Proteine ziemlich gering und daher nicht signifikant. Um weiter Erkenntnisse zu erlangen, müssen weitere Experimente durchgeführt werden

In ihrer Gesamtheit demonstriert diese Dissertationsarbeit eine umfangreiche proteomische Analyse verschiedener zellulärer und tierischer FXS-Modelle. Zusammenfassend lässt sich sagen, dass diese Experimente zur Erstellung einer umfangreichen Informationsquelle für die FXS-Forschungsgemeinschaft beigetragen haben. Außerdem leisten diese Daten einen Beitrag zum besseren Verständnis der Pathologie bei FXS und zur Entwicklung potentiell neuer Behandlungsstrategien.

I INTRODUCTION

In an era where medical science has succeeded in curing patients from a variety of diseases through breakthroughs in understanding of the fundamental mechanisms of biological systems, it is fascinating to reflect on how much information is still relatively unknown within certain biological disciplines. One of areas that reflect this notion is in the field of neuroscience: in this broad and complex discipline, the amount of information is exponentially growing and to follow up on all of these different avenues makes for a very daunting task. One broad area of neuroscience are neurodevelopmental disorders (NDDs), which are not only medically relevant but also present a platform to understand basic principles of neuronal development and biology. Here I focus on Fragile X syndrome, a rare NDD linked to a severe dysregulation of protein synthesis in neurons, whose connection to other neurodevelopmental disorders, especially autism, makes it a relevant and interesting disorder to study the molecular pathogenesis mechanisms relying on protein homeostasis in the brain.

I.1. Fragile X Syndrome

Fragile X syndrome (FXS), also known as Martin Bell or Escalante's syndrome, was first described in 1943, when Martin and Bell described a family in which, as they believed, intellectual disability was transmitted in an X-linked manner [1]. FXS affects approximately 1:5000 males and 1:10,000 females worldwide [2]. Although it is classified as a rare disorder, it is the most common form of hereditary intellectual disability [2] and has been connected to a plethora of other neurodevelopmental disorders [3-6], including autism [6]. Its X-linked recessive inherited form of intellectual disability was first identified in 1969 when Lubs observed constriction in the end of the long arm of the X chromosome in four members of the same family (**Figure I.1**) [7]. Approximately 15 years later, observed constriction of the fragile site was localized to the chromosome

band Xq27.3 [8]. In 1991, the corresponding gene was identified and named the Fragile X mental retardation 1 (*Fmr1*) [9].

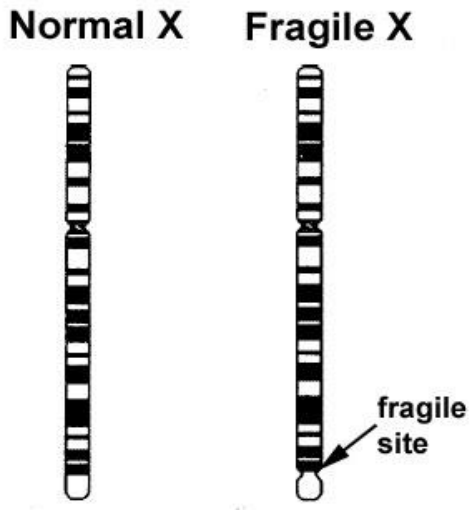

Figure I.1 | Normal and Fragile X chromosome. *Fragile X chromosome has a fragile site in the end of the long chromosome arm (Xq27.3) that appears to have a constriction upon microscopic observation. (Source: www.geneticsperiod4.wikispaces.com/Fragile-X%20Syndrome).*

Expansion of the *Fmr1* gene is the main cause of the disorder. In the 5' untranslated region of the gene, normal individuals have approximately 5-50 CGG trinucleotide repeats. Individuals with ~ 50-200 CGGs repeats are classified as premutation carriers [10], with increased *Fmr1* transcripts, but decreased levels of Fragile X mental retardation protein (FMRP) [11, 12]. If the number of the CGG repeats exceeds 200, the gene becomes hypermethylated, resulting in transcriptional silencing and lack of FMRP [9, 13]. This condition is defined as a full mutation [10] (**Table I.1**). Around 15 % of male patients have incomplete or partial methylation which normally leads to reduced production of FMRP and a milder degree of the symptoms [14, 15]. In very rare cases, apart from the CGG repeat expansion, FXS can be initiated through deletions [16-19] and point mutations [20] that lead to the production of the nonfunctional protein.

Table I.1 | Number of CGG repeats from normal individual to the FXS patient.

	Number of CGG trinucleotide repeats
Normal	5-50
Premutation	50-200
Full mutation	>200

Individuals affected by FXS show different symptoms that are typically patient-specific. The most prominent symptom is mild to severe intellectual disability (ID) [21-23]. Other developmental symptoms include memory and learning difficulties [24], decreased motor function, and speech impairment [13, 25, 26]. Some individuals show behavioral and emotional features such as attention deficit and hyperactivity [27], anxiety [28] and autistic behavior (in ca. 30% of cases) [29]. Furthermore, in ca. 20% of cases this disorder is characterized by seizures [30, 31] and sensory integration problems (**Figure I.2**). The most prominent physical symptom of FXS is macroorchidism [32]. Others may include long narrow face with prominent jaw and ears [33, 34], hypotonia, increased joint laxity and high palate [13, 25, 26], but the physical phenotype is not necessary present. Although FXS affects both genders, females tend to have milder symptoms than males. This comes from the fact that females have another X chromosome with normal *Fmr1* gene that can produce some FMRP. For example, around one third of females with a full mutation do not show any sign of cognitive impairment, while others have mild to severe cognitive, behavioral or social difficulties [35].

I.1.1. FMRP and its function

Fmr1 gene encodes for FMRP, a highly conserved RNA-binding protein. In various tissues, as a result of alternative splicing, *Fmr1* can produce 12 protein isoforms with molecular weight between 67-80 kDa [36].

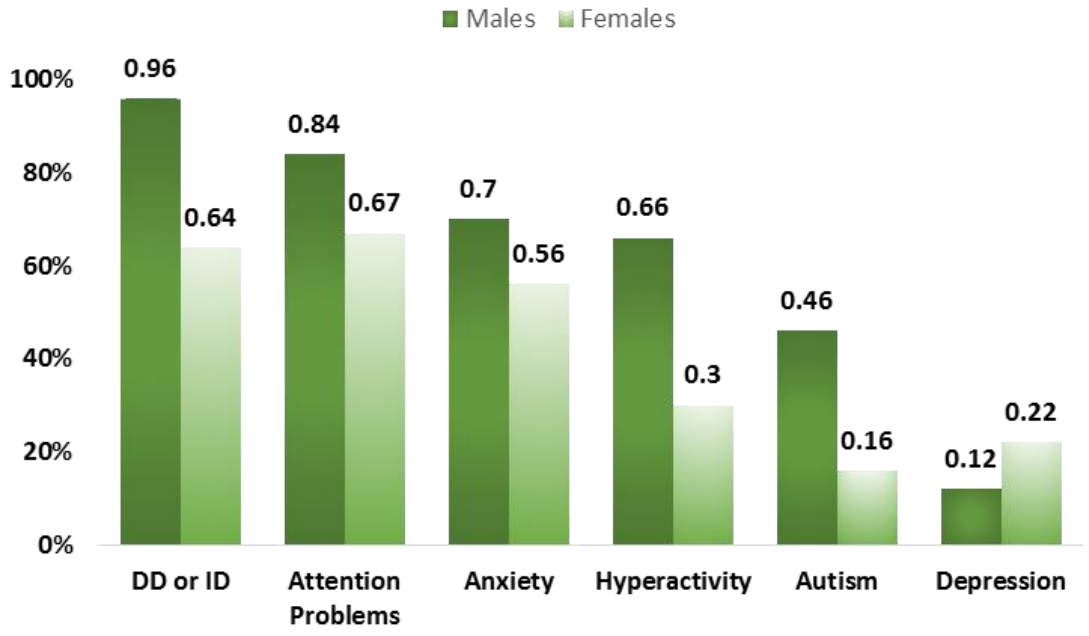

Figure I.2 | Percentage of children with FXS and co-occurring conditions. *(Source: http://www.cdc.gov/ncbddd/fxs/data.html and [37]).*

Expression of the different FMRP isoforms is not tissue-specific [36], although FMRP is highly abundant in the brain and testis [38]. In the brain, it is primarily expressed in neurons and it is predominantly located in the cytoplasm [38]. FMRP has several functional domains that are capable to bind mRNA. The central region of the protein contains two K Homology domains (KH1 and KH2) and the C–terminal end has arginine-glycine-glycine (RGG) box [39]. FMRP contains a nuclear localization signal (NLS) and although it is mainly localized in cytoplasm, some isoforms can shuttle between the nucleus and cytoplasm [40]. Through its domains, FMRP binds approximately 4% of mRNA in a mammalian brain [41] and has been associated with actively translating polyribosomes [42, 43]. It is believed that FMRP is suppressing translation by stalling ribosomal translocation on their respective mRNA targets (**Figure I.3**) [44].

Therefore, FMRP has an important role towards the regulation of protein synthesis and neuronal development [45].

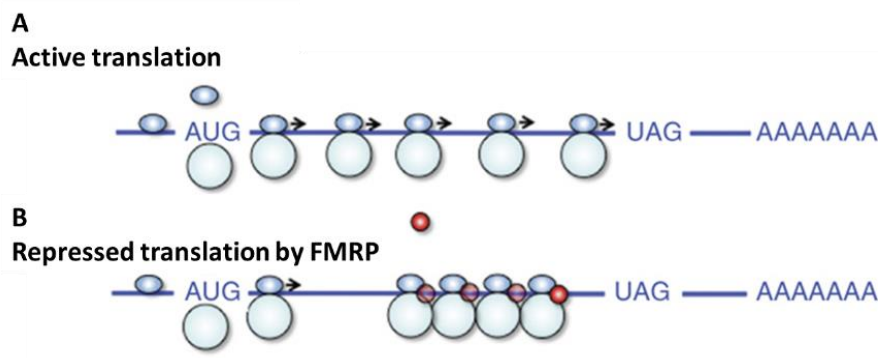

Figure I.3 | Model of translational suppression via FMRP. A) *Process of active translation in which mRNAs are translated into protein. The small ribosomal subunit (40S) binds to an AUG codon on the mRNA and recruits the large ribosomal subunit (60S). Translation is complete when ribosomes dissociate at the stop codon (UAG).* ***B)*** *Translation is repressed by FMRP, on specific mRNAs, in a complex that includes target mRNA and a few condensed ribosomes (adopted and modified from [46]) .*

A recent study, using HITS-CLIP (high-throughput sequencing of RNA isolated by crosslinking and immunoprecipitation) method based on ultraviolet (UV) covalent cross-linking of mRNA and mRNA binding protein, followed by immunopercipitation and sequencing technologies [47], identified more than 800 mRNA targets of FMRP and interestingly, these targets seem to be equally represented in the pre- and postsynapse [44]. Another study used PAR-CLIP (photoactivatable ribonucleoside-enhanced crosslinking and immunoprecipitation) method based on incorporation of photoreactive ribonucleoside analog – 4-thiuridine into RNA transcripts which after UV irradiation crosslink with RNA – binding proteins and therefore can be immunoprecipitated. In this study more of 8,000 mRNA targets for FMRP was identified [48]. Reported numbers of mRNA targets of FMRP seem to be quite high, implicating that FMRP could bind more than one third of total mRNA, questioning the specificity of the detected interaction.

Moreover, recently published work showed that reported targets disproportionally represent the most abundant mRNAs and mRNAs with the longest coding sequence [49].

I.1.2. Translational regulation of FMRP

In the absence of FMRP, translation is dysregulated and protein synthesis is elevated. It is believed that this dysregulation is the main cause of the symptoms in fragile X patients. Several studies of the fragile *X* mouse model have shown that global cerebral protein synthesis is elevated in vitro and in vivo [10, 50, 51]. Thus far, it is unclear whether this elevated protein synthesis is arising from dysregulation of the primary mRNA targets of FMRP, or from a downstream secondary effect mediated by its targets. In addition, the prediction that some protein levels are high because of the loss of translational repression can be misleading because degradation mechanisms could restore protein levels to normal. Therefore, this data should be confirmed on the protein level. Modern proteomic workflows allow quantification of changes on the protein levels in a global and high throughput fashion. So far, several proteomic studies of FXS were performed. Quantitative proteomic analysis of synaptosomes from *Fmr1*-KO and WT cortical neurons revealed more than 100 proteins with altered expression in the absence of FMRP, including proteins related to autism and epilepsy [52]. Another study revealed 23 proteins with differential expression involved in cell differentiation, neurite outgrowth, and synaptic vesicle release in the mice hippocampi [53], while heterozygous dfmr1 Drosophila allowed profiling of 1,617 proteins [54].

I.1.3. FXS models

During the past 20 years of FXS research, the research community has created more than 20 distinct animal models and cell lines in order to study different aspects of this disorder. Diversity of these models is ranging from the *Aplasyia* model which was used to gain a better understanding of the associated memory and learning deficits, *Gryllus*

[55] and zebra finch *[56]* for speech related deficits, to *Drosophila* [57-59] and mouse models [60]. Of course, some of the models are controversial, but models such as *Drosophila* and especially mice are very well established and often used within the fragile X research community.

Generation of the *Fmr1*-KO mouse in 1994 [60] created a reliable FXS model that recapitulates several cellular and behavioral phenotypes that are normally found in fragile patients, such as abnormalities in dendritic spine [61], hyperactivity, impairments in spatial learning and social behavior [62], audiogenic seizures [63, 64], and macroorchidism [60].

Another important model used to answer fundamental molecular aspects are cell lines. For example, primary neurons were used to achieve a clearer understanding of synaptic dysfunction in FXS [52]. Immortalized *Fmr1*-KO cell line, called STEK was established in 2002. It was derived from *Fmr1*-KO mouse embryos and SV40-immortalized. This cell line was used to examine the role of FMRP as a transporter associated with mRNPs, translational repressor in stress granules and to investigate FMRP domains involved in polyribosomal association [65, 66]. Next generation of the STEK cell line was obtained in naturally immortalized *Fmr1*-KO mouse embryonic fibroblasts (MEFs) [67]. This cell line was used to identify novel FMRP mRNA targets [67, 68] and to identify dysregulated proteins and phosphorylation events (discussed later) in the absence of FMRP [69].

I.1.4. mGluR5 theory of FXS

The concept that synapses are able to strengthen or weaken over time was first suggested by Santiago Ramón y Cajal in the end of 19th century [70]. Since then, the knowledge about synapses and their function have dramatically grown. Modification of the synapse in response to an increase or decrease in its activity is called synaptic plasticity [71]. Two mechanisms are underlying this process – long term potentiation (LTP) and long-term depression (LTD). Long lasting neuronal changes caused by LTP or LTD are dependent on two synaptic activity processes: local protein synthesis driven by

translation of existing mRNAs and new protein synthesis through transcription and translation [72]. All changes are mainly caused by the release of the neurotransmitter glutamate and response of the ionotropic glutamate receptors, α-amino-3-hydroxy-5-methyl-4-isoxazolepropionic acid (AMPA), N-methyl-D-aspartate (NMDA) and metabotropic glutamate receptors (mGluRs).

Today, two forms of LTD are known: LTD activated by postsynaptic NMDA receptors and LTD dependent on the group1 mGluR activation [73]. While both LTDs require long term protein synthesis, LTD dependent on the mGluR activation requires local protein synthesis as well [74, 75]. In 1997 it was shown that FMRP is synthesized in response to mGluR5 activation [76], while later it was suggested that FMRP binds mRNA of mGluRs and inhibits their translation [50, 77]. The study of the *Fmr1* knockout mouse suggests a connection between the exaggerated mGluR5 signaling and FXS [78]. This was confirmed by two approaches – pharmacological and genetic. Upon treatment of *Fmr1*-KO mice with mGluR5 antagonists such as MPEP and Fenobam [78-80], reversal of many FXS abnormalities was achieved. In genetic approach, *Fmr1* mutant mice with reduced *mGluR5* expression (*Fmr1*-KO/*mGluR5* het KO cross – genetic rescue model) showed correction of most of the symptoms like seizures, hippocampal synaptic plasticity, ocular dominance plasticity, protein synthesis, and dendritic spine density [78]. The fact that most of the FXS symptoms can be explained by increased LTD and a consequent increase in protein synthesis was coined as the mGluR5 theory of FXS (**Figure I.4**) [81, 82]. This theory led to an intriguing concept that FXS and related genetic disorders (including to a certain extent autism), could be treatable by mGluR5 antagonists.

I.1.5. Role of Glycogen synthase kinase in FXS

Glycogen synthase kinase 3 (GSK-3) is a serine/threonine kinase, encoded by two genes, GSK-3α and GSK-3β [83]. Both genes are ubiquitously expressed, but GSK-3β is prevalently expressed in the brain [84].

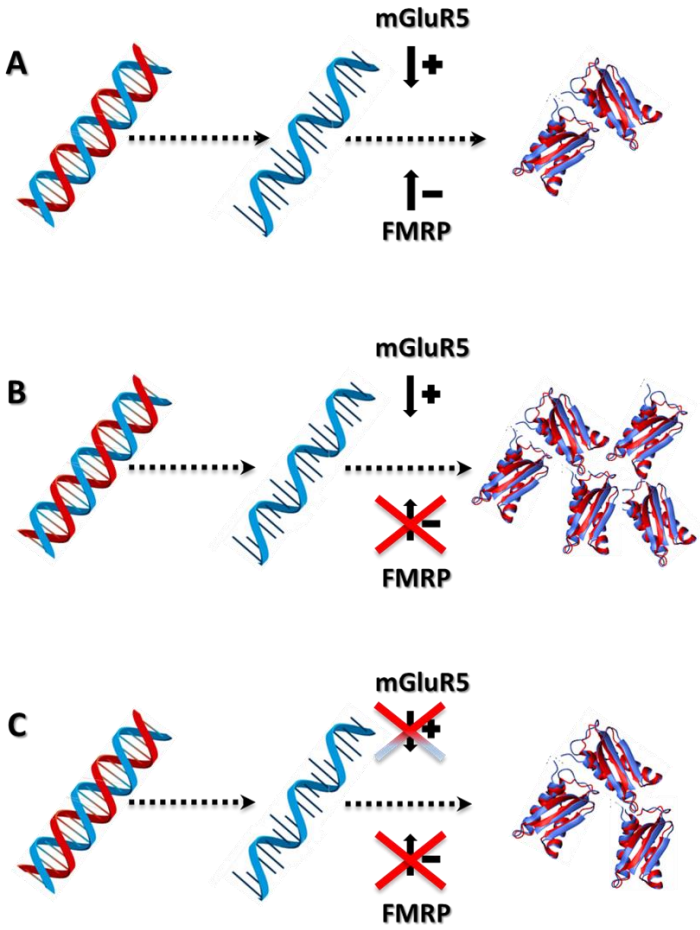

Figure I.4 | mGluR theory. A) *In a normal translational process, mGluR5 has an increasing translation rate, while FMRP is repressing it;* ***B)*** *In FXS, the lack of FMRP causes an increase in the translation rate;* ***C)*** *When mGluR5 expression is reduced upon lack of FMRP, the translational rate reverts back to the normal rate.*

While kinase activation can be enhanced by phosphorylation on tyrosine 279 in GSK-3α and tyrosine 216 in GSK-3β [85], main regulation is driven by inhibitory phosphorylation on serine 21 in GSK-3α and serine 9 in GSK-3β [86].

GSK-3 plays an important role in various neurophysiological processes, such as neurogenesis, gliogenesis, cell migration, cell morphology, and axonogenesis [87], as a part of Wnt signaling pathway, sonic hedgehog (SHH), Notch pathway [87] and different apoptotic pathways [88]. Therefore, it is not surprising that GSK-3 has an impact in the

pathophysiology of multiple disorders, such as mood disorders, Alzheimer's disease, diabetes and cancer, and was recently implicated to be involved in general inflammation [85]. Increased activation of GSK-3β has been found in the FXS mouse model and this activity is associated with excessive mGluR5 signaling [89]. Using lithium (unspecific GSK-3β inhibitor), significant improvement was accomplished in *Drosophila* and mouse FXS models [90]. Therefore, more effort has been directed towards the inhibition of GSK-3β as a potential avenue for FXS treatment. Today, there are lot of potential inhibitors of GSK-3β [86]. However, lithium is a preferred choice since it has been used as a mood stabilizer to treat bipolar disorders for over 50 years. Although the therapeutic mechanisms are not completely understood, it was shown that lithium can reverse mGluR-dependent LTD [91], hyperactivity [92], learning deficits, dendritic spine shape, anxiety [93] and macroorchidism [94]. Unfortunately, unspecific binding of lithium can also cause a variety of side effects. In order to reduce side effects, more specific inhibitors were developed, such as thiadiazolidinone (TDZD) derivates. TDZD families are non-adenosine triphosphate (ATP) competitive GSK-3 inhibitors that bind to unique regions within the kinase. One of them, TDZD-8, has been shown to increase the inhibitory serine 9 phosphorylation on GSK-3β and specifically inactive the kinase [95].

I.2. Biological function of proteins

I.2.1. Proteome

Genome sequencing opened a new window within biology. While it is essential to understand the genome architecture, it is also important to keep in mind that during development the genome is static, but its expression, as measured by the levels of its products (RNA and proteins), is dynamic [96]. Transcription and degradation of mRNA as well as protein synthesis and degradation play an essential role towards the understanding of biological processes. It is clear that studying these molecules one at a time is not satisfactory, especially when considering that the number of proteins and

their variants is much larger than the number of genes. Therefore, the concept of the proteome, all proteins that are expressed by the genome in a cell, tissue or an organism at a certain time point or under certain conditions, was proposed in 1995 [97]. The research field that studies the proteome is called proteomics and is used to investigate protein function, protein-protein interactions and post-translational modifications (PTMs) [98].

I.2.2. Protein modifications

One primary factor contributing to protein diversity is the result of covalent post-translational amino acid modifications [99]. The possibility to add modifications opens the space for various protein functions such as change in protein activity, cellular localization and protein-protein interaction [100]. Since the proteome is dynamic, different stimuli can change cellular activity which is often driven by protein modifications. The knowledge about the spectrum of different modifications is growing rapidly. For example, it is estimated that around 5% of the human proteome consists of enzymes [101] that are able to attach more than 200 known post-translational modifications [102]. Until recently, it was considered that protein modifications are independent off each other. However, it is becoming increasingly evident that crosstalk between different modifications can be responsible for the overall cellular activity within a certain state [103].

Protein modifications can be both reversible and irreversible. A classic example of a reversible modification is the activation or deactivation of kinases in cellular pathways that leads to the addition or removal of phosphate groups. Irreversible modifications usually involve proteolytic cleavage, for example in the insulin case when proinsulin is cleaved to become active insulin [100]. Since PTMs are very important in protein function, any misbalance can lead to improper cellular function or disease. Considering

that PTMs cannot be studied at the genome or transcriptome level, mass spectrometry has become a powerful tool for both the detection and quantification of PTMs.

I.2.2.1. Protein phosphorylation

Knowledge about protein phosphorylation as a regulatory physiological mechanism originates back to 1955 [104]. Today, this is one of the most important and well-studied reversible modifications. It occurs in both prokaryotes and eukaryotes. In eukaryotes protein phosphorylation typically occurs on serine, threonine, tyrosine and, to a smaller extent, on histidine residues. Prokaryotic organisms predominantly employ histidine and aspartate phosphorylation which serves as the hallmark of prokaryotic cell signaling, known as two component signal transduction. In addition, phosphorylation of cysteine, arginine and lysine was reported, but its function remains unclear [105-108]. Regulation of phosphorylation is carried out by two enzymes – a kinase that phosphorylates in an almost exclusively conserved mechanism with adenosine triphosphate (ATP) as a phosphate group donor; and phosphatase that dephosphorylates proteins. The importance of this modification stems from the fact that it plays a role in many different processes such as cell cycle control, receptor-mediated signal transduction, differentiation, proliferation, transformation, and metabolism, therefore its ability to regulate different enzymes and receptors in a rapid fashion can be crucial in many pathological states [109]. It has been estimated that in eukaryotes, more than a third of the proteome is phosphorylated and that about 520 protein kinases are responsible for more than 700,000 phosphorylation events [110].

The low abundant nature of protein phosphorylation adds an extra challenge towards its identification due to fact that phosphorylated proteins are mostly present in a small fraction of total proteins [111]. Thus, phosphoprotein and phosphopeptide enrichment strategies have to be employed in order to study this modification. These include antibody-based enrichment [111], immobilized metal affinity chromatography (IMAC)

[112], strong cation exchange chromatography (SCX) [113] or titanium dioxide chromatography (TiO_2) [114]. Depending on the complexity of the sample, peptides can be separated and enriched by SCX followed by TiO_2 chromatography enrichment. Although challenging, phosphopeptide enrichment coupled with advanced MS technology is a primary choice for large scale analysis of the phosphoproteome.

SCX is based on the difference in the solution charge states of phosphorylated and nonphosphorylated peptides. Its stationary phase is negatively charged, and it binds positively charged peptides. In acidic conditions, tryptic digested peptides carry on average a net charge of +2, due to protonation of N-terminal amino groups and the side chains of lysine and arginine. On the other hand, singly phosphorylated peptides carry net charge on average a net charge of +1 due to presence of negatively charged phosphate group. Therefore, singly phosphorylated peptides bound to the stationary phase will elute earlier than average unmodified peptides in a shallow salt gradient (**Figure I.5**)[115]. Consequently, phosphopeptides are enriched in the early SCX elution fractions.

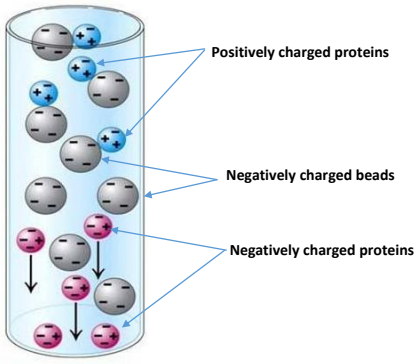

Figure I.5 | Cation exchange chromatography. *Positively charged proteins/peptides bind negatively charged stationary phase, while negatively charged proteins/peptides are not binding. When all positively charged proteins/peptides are bound to the column, they can be eluted using the salt gradient. (Source: www.wikibooks.org).*

TiO_2 is a type of metal oxide affinity chromatography which relies on high affinity absorption of the phosphate groups. In acidic conditions, TiO_2 serves as an anion exchange column in which phosphopeptides are bound, and can be eluted under alkaline conditions. Next to phosphopeptides, acidic peptides are binding TiO_2. To overcome this issue 2,5-dohydroxy benzoic acid (DHB) can be used due to the fact that it binds to TiO_2 stronger than acidic peptides, but weaker than phosphopetides (**Figure I.6**) [109]. However, DHB can interfere with column separation efficiency and contaminate mass spectrometer. An alternative is to use high level of triflouroacetic acid (TFA) which can protonate acidic residues and overcome nonspecific binding to TiO_2 [116].

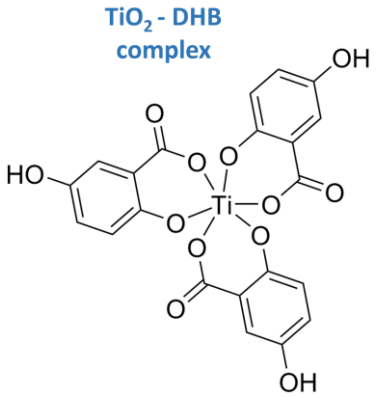

Figure I.6 | Depiction of TiO_2 in complex with 2,5-dihydroxy benzoic acid (DHB). *(adopted and modified from[109]) .*

I.2.3. Protein turnover

Cells are living in a dynamic state in which proteins are constantly synthesized and degraded [117]. Protein synthesis and/or degradation can be changed due to a physiological, developmental or pathological state of the cell [118]. Thus, protein expression levels are reflecting the balance between these processes and their dynamic interplay is called protein turnover [119]. Until recently, gene expression at the mRNA level was used as an estimation of protein abundance. However, through the rise of new

techniques it became clear that this correlation is very variable and that the change in the protein abundance can be only partially explained by mRNA level [120].

In early studies, detection of radioactive amino acids coupled with inhibition of protein synthesis was used to determine protein turnover. However, translational inhibition by actinomycin or cyclohexamide may not reflect turnover rate under physiological conditions due to their toxicity and possible disruption in normal cellular activity [121]. In addition, tagging strategies together with western blotting and fluorescent detection techniques can be used. From a biological standpoint, tagging the protein could change its stability, but also time and cost investments are not negligible [122]. Recent advances in mass spectrometry combined with stable isotope labeling allows for the measurement of protein turnover, for example using dynamic stable isotope labeling by amino acids in cell culture (SILAC, see I.3.4.2. section for details).

I.3. Mass spectrometry-based proteomics

Understanding living organisms and their functions is essential in molecular bioscience. The central dogma of molecular biology demonstrates that a gene is transcribed into mRNA and mRNA is translated into a protein. However, this process is not straightforward: one gene can produce more than one protein due to alternative splicing, sequence polymorphisms and post-translational modifications [123].

During the last two decades, the rise of high throughput "-omics" technologies has paved the way for major discoveries in systems biology. The first branch, genomics, can essentially map the entire genome of an organism. Furthermore, genes can have different expression patterns in different cell types and specific conditions. Technology that allows the analysis of gene expression (mRNA) is called transcriptomics. Complementary to genomics and transcriptomics is proteomics, which has become the method of choice to study gene expression at the protein level. Due to the rapid development in mass spectrometry (MS), MS-based proteomics has become the dominant technology for studying proteins, protein-protein interactions (PPIs) and post

translational modifications (PTMs), directly contributing to a better understanding of the organisms and their functions[124].

I.3.1. Shotgun proteomics

Initial proteomic approaches used protein separation based on the charge and molecular weight, known as two-dimensional gel electrophoresis, which generates protein spots which can then be analyzed using MS. Due to limitations such as depth of coverage, low protein amount in a spot, a low dynamic range of detection and time consumption, further approaches were developed: top-down and bottom-up proteomics [125]. Top-down proteomics typically uses the whole protein in analysis by MS, while in bottom-up or “shotgun” proteomics enzymatically digested proteins are measured by MS. The goal of the “shotgun” proteomics is to analyze the complex protein mixtures that are extracted from the cell or tissue, and digested by specific enzymes such as trypsin or LysC, using a combination of liquid chromatography and tandem mass spectrometry[126].

I.3.2. Sample preparation and instrumentation

For a long period of time, MS was restricted to small and thermostable compounds due to lack of proper ionization techniques [127]. A breakthrough came with the development of two “soft” ionization techniques - electrospray ionization (ESI) and matrix assisted laser desorption/ionization (MALDI). These two ionization techniques introduced MS into protein research and were awarded a Nobel Prize in chemistry in 2002. This advance made mass spectrometry the preferred method to gain key insights into the composition, regulation and function of molecular complexes and pathways [128]. Modern mass spectrometers are measuring the mass-to-charge ratio (m/z) of the compounds in the sample. Measuring the mass of intact proteins is more challenging than measuring the mass of peptides. MS is less sensitive for the proteins as they are

more difficult to separate, ionize and analyze in a mass spectrometer then peptides. In addition, complex mixtures of multiply charged protein molecules can lead to identical masses for two or more different proteins [129]. Thus, a “shotgun” proteomic approach is the most suitable for robust protein identification. In this approach, proteins are extracted from a biological sample (tissue or cell culture) and digested to peptides, which are typically 10-20 amino acids long. Complexity of the resulting peptide mixture can be reduced by various separation techniques, such as isoelectric focusing of peptides according to their isoelectric point (pI) [130]. Alternatively, 1D SDS-PAGE separation can be performed before in-gel protein digestion [131], and extraction of peptides for LC-MS analysis. Peptides resulting from protein digestion are typically loaded onto a nanoscale HPLC column filled with reversed-phase material, and eluted according to their hydrophobicity in a gradient of increasing organic solvent. After elution, peptides are ionized and measured by MS (**Figure I.7**).

I.3.3. Mass spectrometry and peptide fragmentation

A mass spectrometer typically consists of three parts: an ion source, a mass analyzer and an ion detector. There are several types of ion sources, mass analyzers and ion detectors. Further description of a mass spectrometer is focused on the LTQ-Orbitrap system which is used to analyze all experiments described in this thesis.

As previously mentioned, after elution from the HPLC column, peptides are ionized by electrospray ionization (ESI). ESI uses electrical potential to transfer ions from solution into the gas phase of the mass spectrometer. In ESI, eluting peptides are electrostatically dispersed through the application of high voltage. Next, the solvent is evaporated and charged peptide ions are produced [132]. Complex peptide mixtures, especially those derived by trypsin (that leaves positively charged residues at C termini) are commonly analyzed in the positive ion mode. Ions are entering the mass spectrometer through a

transfer capillary. In the vacuum system of the mass spectrometer, ions are guided by ion optics into the mass analyzer. To determine the m/z ratios of the intact peptide (precursor) ions, ions are trapped in an electrostatic field in the Orbitrap cell, and they move around central electrode.

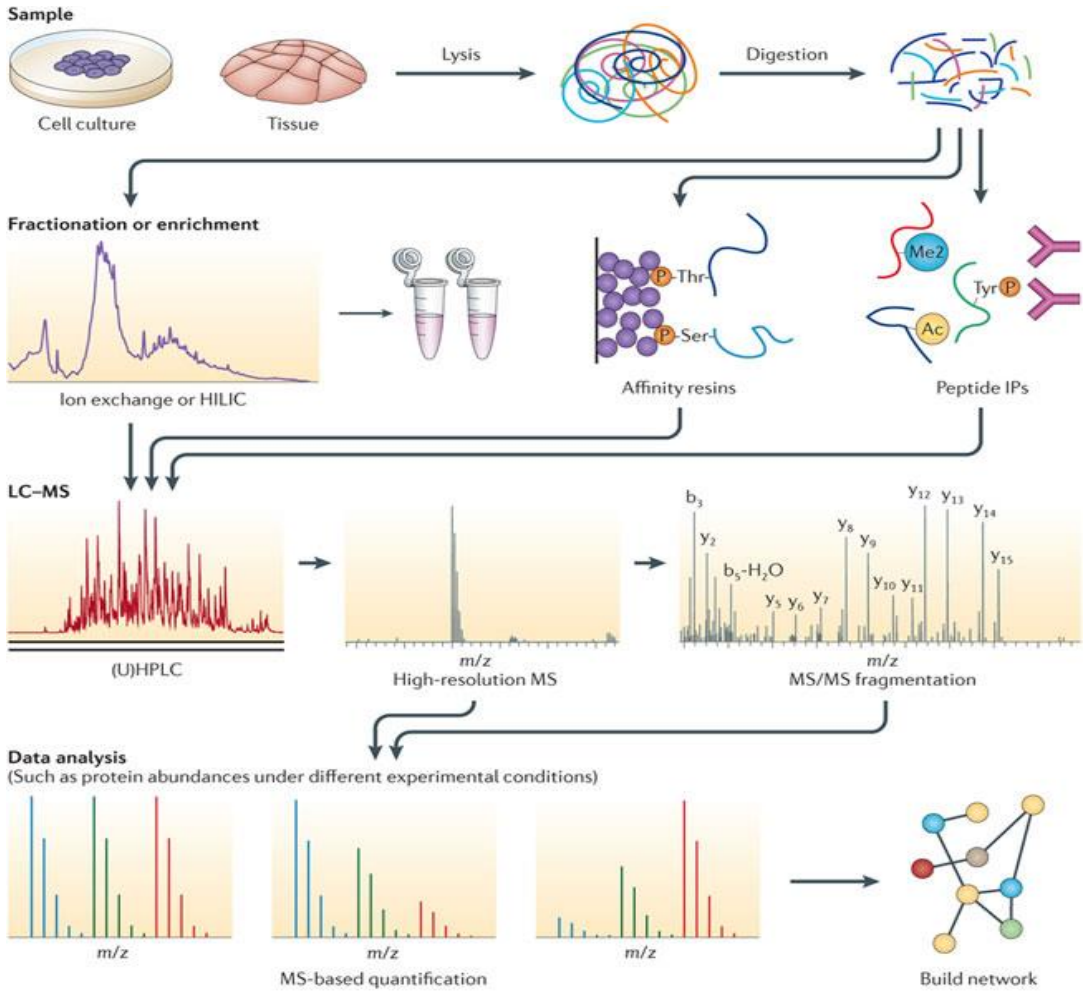

Figure I.7 | Common mass spectrometry- based proteomics workflow. *Proteins are extracted from the biological sample and digested by protease. Resulting peptide mixture can further be fractionated, or enriched in case of PTMs. Next, peptides are separated using reversed phase high performance liquid chromatography (HPLC) and subjected to mass spectrometry analysis. Mass of the peptide is recorded in high resolution full scan (MS) and fragmented in tandem mass spectrometry (MS/MS). MS precursor ion can be used to obtain quantification data, whereas MS/MS data is used to identify peptides. Further analysis is achieved using bioinformatics tools (adopted from [133]).*

Frequencies of individual axial oscillations of peptide ions with different masses are detected by their current image and the produced signal is converted into a mass to charge spectrum using the Fourier transform algorithm [134]. Ionized peptides normally appear as isotopic clusters due to C^{12}/C^{13} ratio [129]. These peaks are separated by 1 Da, which can be easily detected by the Orbitrap mass analyzer due to its high resolution and mass accuracy (**Figure I.8**).

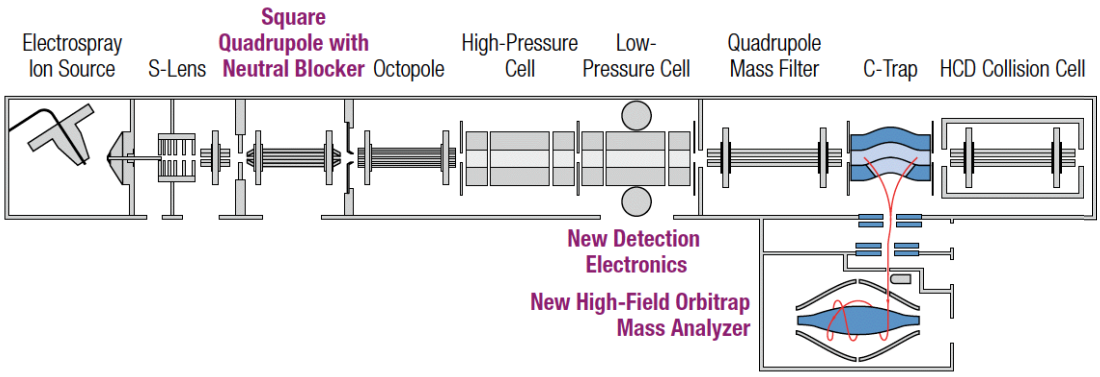

Figure I.8 | Schematic for the LTQ Orbitrap Elite hybrid mass spectrometer. *This mass spectrometer combines a linear ion trap and an Orbitrap mass analyzer (adopted and modified from [135]).*

In order to retrieve the information about primary structure (sequence) of the peptide, the most abundant ions are isolated, fragmented and recorded as MS/MS (tandem MS) spectra in process called dependent data analysis. Fragmentation of the isolated peptides is achieved by collision of the peptides with inert gas molecule (e.g. helium) in a process called collision induced dissociation (CID). The most common fragment ions generated by CID are *b* and *y* fragment ions (**Figure I.9**). While a precursor ion spectrum (MS spectrum) is acquired in the Orbitrap, a MS/MS spectrum is usually acquired in the ion trap mass analyzer with high speed and sensitivity, but low resolution. High resolution MS and low resolution MS/MS approach is called “high-low” strategy.

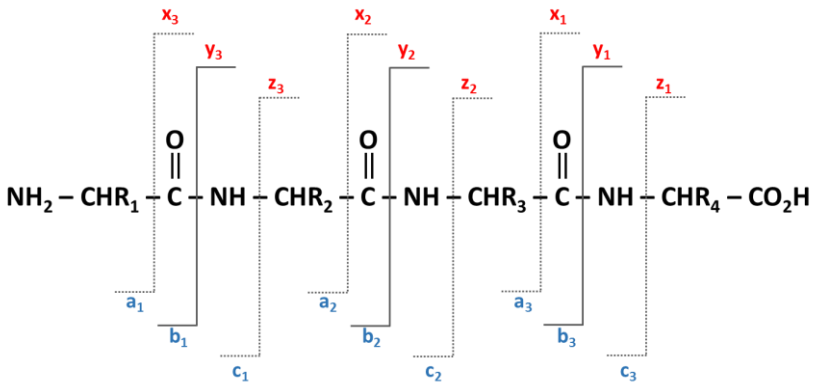

Figure I.9 | Collision induced dissociation peptide fragmentation. *Peptides can be fragmented into a, b- and C ions on the N-terminal or x, y and z ions on the C terminal, respectively (adopted from [109]).*

Another possibility is to acquire MS/MS spectra in the Orbitrap analyzer using high energy collision dissociation (HCD) collision cell. In this approach both type of spectra are acquired at a high resolution and mass accuracy ("high-high" approach). It is important to have high resolution MS spectra in order to apply more stringent mass tolerance during database search, and therefore reduce the search space (the number of theoretical peptides sequences matched to measured MS spectra) and increase search accuracy and specificity. However, acquisition of high resolution MS spectra requires additional time, which may compromise sequencing speed. Therefore, acquisition of high or low resolution MS/MS spectra is usually a compromise between sequencing speed of the instrument and the quality of the acquired spectra.

Today it would be impossible to manually process MS raw data due to tremendous amount of data acquired. Therefore, several computational tools for protein identification have been developed. Several different methods were proposed to assign an amino sequence to the MS spectrum, such as extracting the amino acid sequence from the fragmentation spectrum (*de novo* sequencing) or correlating to the spectra libraries [136]. However, most often acquired spectra are compared to theoretical spectra obtained by *in silico* digestion. Search engines use different algorithms for MS spectral matching based on probability scoring like Mascot [137] and Andromeda [138] or

cross-correlation (Sequest [139]). The MS spectrum is correlated to a theoretical peptide and the best statistical match allows the peptide to be identified [140]. These identifications can result in true and false positive matches, therefore they are evaluated with target-decoy-based based approach [141]. Derived false discovery rate (FDR) helps to determine the number of false positive identifications in a dataset.

I.3.4. Quantitative proteomics

Although identification of proteins is important, it is not sufficient to completely understand biological processes. Understanding of protein dynamics in a cell over time or changes in functional perturbations is essential. The ability to determine protein abundance for thousands of identical proteins in different states, treatments, or perturbations can be measured by MS and makes proteomics method of choice for quantitative data. Two main approaches can be used in order to gain this information – labeling approach and label-free approach, which can result in relative or absolute quantitative data.

I.3.4.1. Labeling techniques

In order to detect the abundance level of a protein from different samples, peptides are differentially labelled by stable isotopes which can then be distinguished upon MS analysis. The labelled samples are mixed in equaimolar amounts and analyzed by MS. When all labeled forms of the peptide are observed, distinct by the mass difference introduced by labeling, respective signal intensities are compared and quantification (protein abundance levels) is achieved.

Stable labeling can be introduced by chemical tagging, enzymatic labeling and metabolic incorporation [142, 143] (**Figure I.10**).

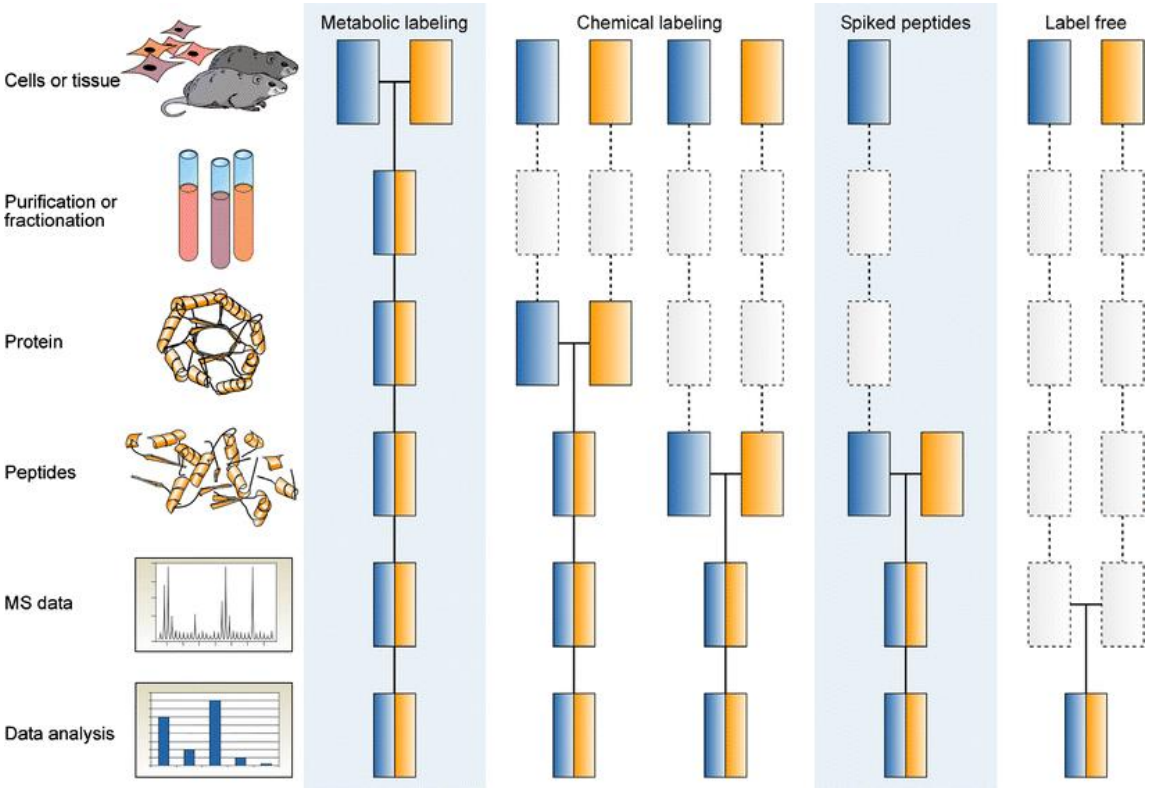

Figure I.10 | Labeling techniques in quantitative proteomics. *Colors represents different experimental conditions. Depending on the used approach samples can be combined at different steps during sample preparation. Horizontal lines indicate combining the samples, while dashed lines pinpoint when experimental variation in sample preparation can occur (adopted from [144]).*

In chemical labeling approaches, samples can be labeled prior to or after protein digestion. For example, in isotope-coded affinity tags (ICAT) , the tag is covalently bound to free cysteines [145], while in tandem mass tags (iTRAQ or TMT) it is bound to primary amines [146, 147]. Transfer of "heavy" oxygen (^{18}O) by a protease during protein digestion is the main enzymatic labeling strategy [148]. Frequently used metabolic labeling is based on incorporation of the labels into living cells by growing the cells in media supplemented with "heavy" stable isotopes. Additionally, metabolic labeling can be achieved through ^{15}N labeling [149]. While ^{15}N labeling is primarily used for microbes and plants, stable isotope labeling by amino acids [150] is the method of the choice in

mammalian systems [124]. Due to fact that labeling occurs in living cells, the accuracy of quantification will not be affected by errors introduced in sample preparation, since samples are combined directly after cell harvest.

I.3.4.2. Stable isotope labeling by amino acids in cell culture (SILAC)

SILAC is a very powerful and widely applicable metabolic labeling method in which two cell populations are grown in media containing either a “light” or “heavy” form of an amino acid. The “heavy” version of the stable amino acid isotope contains a fixed number of ^{13}C, ^{15}N and/or ^{2}H atoms. Arginine and lysine are extensively used amino acids for two practical reasons: when performing a classical tryptic digest, we are ensuring that each tryptic peptide is going to have at least one isotope label, and it is crucial to use essential amino acids to ensure complete labeling of the proteins in the cell population. In classical cell culture, complete labeling (>95%) is achieved after 5-6 cells doublings. As mentioned before, after complete labeling, cells are harvested and equally mixed. As most physical and chemical properties of the labeled peptides are not changed, peptides co-elute at the same time. In the mass spectrometer peptides can be distinguished from each other due to the mass shift introduced via “heavy” labeled amino acids (Figure I.11). Intensities from the SILAC pairs (“heavy” and “light” peptides) are measured by MS to allow a relative comparison of the thousands proteins from the experiment [143].

Since original SILAC was established, additional applications were developed through the years. Dynamic SILAC is an approach for measuring protein turnover. Turnover can be measured by “heavy” isotope labeling over time from unlabeled cell culture or vice versa. Incorporation of the “heavy” isotope over the time can be measured by MS [151] (**Figure I.12**). However, by definition protein turnover is a balance between protein synthesis and protein degradation.

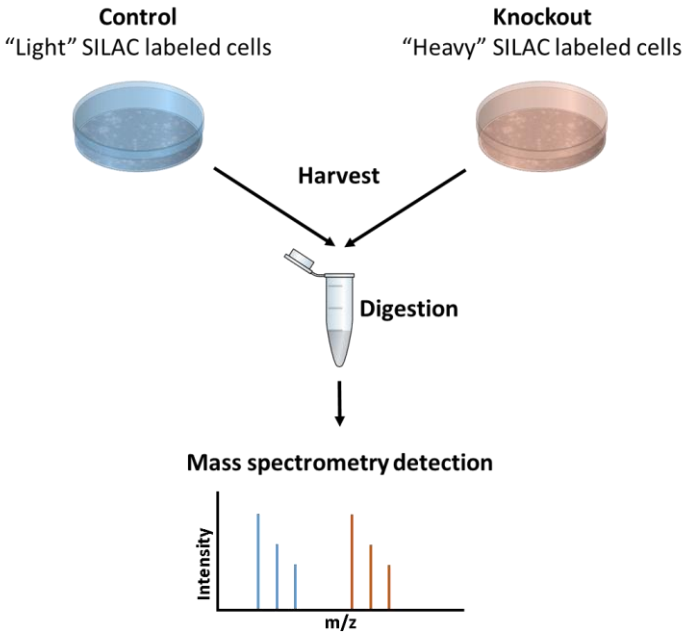

Figure I.11 | SILAC typical workflow. *Control ells are grown in "light" and knockout cells in "heavy" medium. After complete labeling of the cells (around 5 cell doubling times), "light" and "heavy" cells harvested and mixed in equal amounts. Next, proteins are digested and following peptide mixture is measured on the mass spectrometer.*

Thus, increased "heavy to "light" ratios of the particular protein can indicate fast protein synthesis or low protein synthesis combined with rapid protein degradation [120]. Another application is pulsed SILAC (pSILAC) developed for a direct comparison of protein translation rates between two samples. Firstly, both cell lines are grown in "light" isotope containing medium. After one cell population is perturbed, the medium is exchanged to medium containing "medium"-"heavy" isotope amino acids in one cell population and "heavy" isotope amino acids in another cell population. After a certain amount of time, cells are harvested, equally mixed and measured by MS.

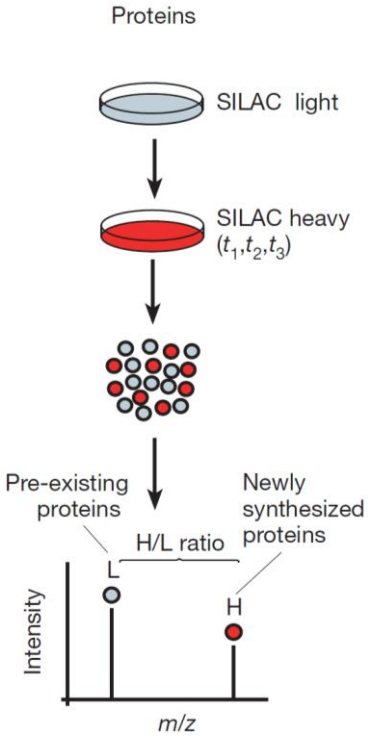

Figure I.12 | Dynamic SILAC typical workflow. *Cells are grown in "light" and, at the certain point, switched to the "heavy" medium. While synthesizing, proteins are incorporating "heavy" amino acids, which can be measured by MS, while collecting different time points. (adopted from [152]).*

Preexisting proteins remain in the "light" form, while newly synthesized proteins will contain "medium"-"heavy" or "heavy" isotope label, therefore the difference in this ratio shows the difference in translation of the corresponding proteins [120].

Next to the application of relative quantification, protein turnover and translation, SILAC can be used to study temporal changes [153] or protein-protein interactions [154]. Additionally, SILAC labeling can be applied to neuronal cell culture, although maximum label efficiency is lower (~80%) than in the normal cell culture due to the fact that neurons are not dividing [155]. Also, SILAC labeling was expanded to in vivo labeling of higher organisms like fruit fly [156] or mouse [157].

I.3.4.3. Label-free approaches

As a result of the rapid development of LC-MS instrumentation, quantification by label-free approaches became more popular and robust. The main assumption of this approach is that under controlled conditions, different samples that are measured separately by MS can be compared. Label-free quantification (LFQ) can be obtained by MS spectral counting (the number of MS/MS spectra acquired for the corresponding protein) or by measuring MS ion current level (areas under the curve (AUC) or extracted ion current (XIC)) (**Figure I.13)** [158].

Advantages of this approach are: lower costs, since it does not involve additional chemistry or sample preparation steps;the fact that quantification of the many samples can be simultaneously performed; and support of the higher dynamic range (1:60) in the comparison with labeling techniques (1:20) [159]. However, some disadvantages include differences in sample preparation, ionization efficiency and variation in chromatography retention times between LC-MS runs. Label-free approaches are therefore less accurate than stable isotope-based quantitative approaches.

I.3.4.4. Absolute quantification

Absolute quantification is determination of the absolute abundance of the protein, defined in moles or copy numbers This information can be extremely useful within the medical field, particularly when looking for biomarkers as a diagnostic tool [160] and moreover when modeling biological systems [161]. Most of the techniques applied for the absolute quantification rely on the internal standards with a known concentration (peptide or protein). For example, one of the popular techniques is called AQUA (Absolute Quantification). AQUA employs spiking of a known amount of synthetically produced stable isotope label peptide into a sample. The absolute amount of the peptide of interest is determined by comparing MS signal between the spike-in standard and peptide of interest [162].

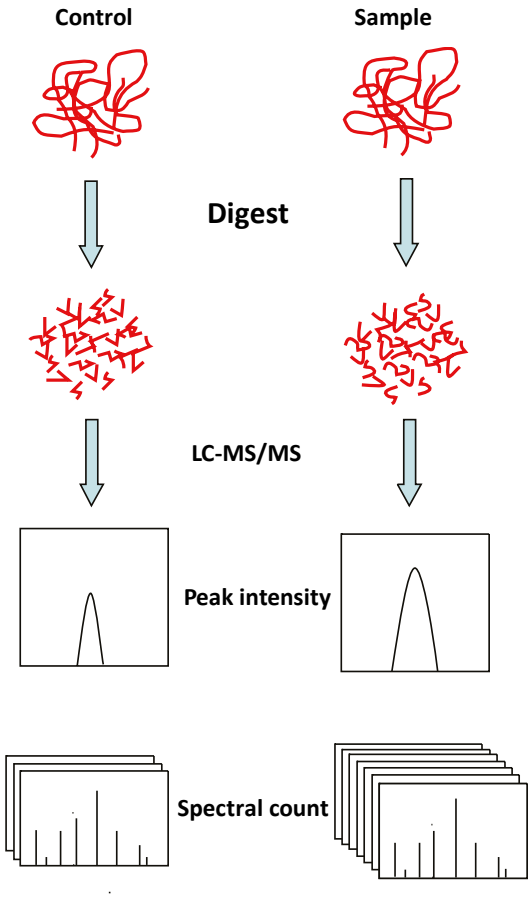

Figure I.13 | Label-free typical workflow. *Different samples (control and sample) are processed and measured separately. Label-free quantification is based on comparison of peak intensity (MS ion current), or by MS spectral count of the same peptide. (adopted from[163]).*

As an alternative to the internal standards, label-free approaches can be used for absolute quantification. A recently developed approach known as the total protein approach (TPA) utilizes the LFQ intensity from a particular protein and is divided by the total MS signal (sum of all LFQ intensities). Moreover, the resulting ratio can be transformed into copy number per cell by dividing the ratio by molecular weight and multiplying it by the Avogadro constant and protein content of the cell [164].

II. AIMS AND OBJECTIVES OF THE THESIS

Although FXS is a monogenic disease, different clinical symptoms indicate that FMRP is involved in the regulation of multiple factors that modulate gene translation and major signal transduction pathways in neurons. In order to understand molecular mechanisms by which FMRP regulates protein synthesis, it is essential to understand its influence on the neuronal proteome and phosphoproteome. Motivated by the lack of data on the proteome level during absence of FMRP in neurons, my main aim was to use proteomics to identify and quantify protein expression and phosphorylation levels in several cellular and animal models of FXS. To this end, I defined the following specific objectives:

1) Analysis of signal transduction pathways involved in the pathogenesis of FXS at the phosphoproteome level in SILAC-labeled murine *Fmr1*$^{-}$ and *Fmr1*$^{+}$ fibroblastic cell lines
    a. Identification and quantification of proteins and phosphorylation sites dysregulated as a consequence of FMRP loss
    b. Bioinformatic analysis of the proteomics results to identify regulatory pathways involved in FXS
2) Identification of potential new GSK-3β substrates in SILAC-labeled murine *Fmr1*$^{-}$ and *Fmr1*$^{+}$ fibroblastic cell lines using GSK-3β inhibition by lithium and TDZD-8
    a. Analysis of the significant changes in phosphoproteome after inhibiting the GSK-3β kinase with lithium (unspecific inhibitor) and TDZD-8 (specific inhibitor)
    b. Identification of potential GSK-3β substrates upon treatments
    c. Analysis of differential GSK-3β activity in *Fmr1*$^{-}$ and *Fmr1*$^{+}$ fibroblastic cell lines based on detected potential substrates
3) Measurement of protein turnover based on dynamic-SILAC method in primary cortical neuronal culture (*Fmr1*-KO and WT)
    a. Large-scale analysis of protein turnover in primary neuronal cell culture

   b. Comparison of the turnover between WT and *Fmr1*-KO in cortical neuronal culture model

4) Analysis of pathways involved in the pathogenesis and genetic rescue of FXS at the proteome level in mouse hippocampus
   a. Proteome-wide quantitative comparison of protein levels in the hippocampi of WT, *Fmr1*-KO and *Fmr1*-KO/*mGluR5*-het cross mice
   b. Absolute quantification of protein levels between WT, *Fmr1*-KO and *Fmr1*-KO/*mGluR5*-het cross mice

III MATERIALS AND METHODS

III.1. Materials

III.1.1. List of chemicals and consumables

Name	***Company***
0.05% Trypsin-EDTA (1X), Phenol Red	Gibco/ Invitrogen
2,5-dihydrobenzoic acid	Sigma-Aldrich
*20*LumiGLO and 20*Peroxide*	Cell Signaling New England Biolabs
Acetic Acid	Sigma-Aldrich
Acetonitrile	Merck KGaA
Ammonium Bicarbonate	Merck KGaA
Ammonium Sulphate	Merck KGaA
Anti-GAPDH	Pierce Antibody
Anti-rabbit IgG, HRP-linked Antibody	Cell Signaling New England Biolabs
Anti-prion protein PrP antibody	AbCam
Arginine (Arg0)	Silantes
Arginine (Arg6, Arg10)	Silantes
Bensonase	Merck KGaA
Blotting Papier	VWR
Bovine Serum Albumin	Sigma-Aldrich
Bradford Reagent	Bio-Rad Laboratories
C8/C18 Extraction Discs	Empore™
Calcium Chloride	Merck KGaA
Cell scraper	Greiner
Chloroform	VWR
Corning® 500mL Vacuum Filter/Bottle System	Corning
Dialyzed FBS	Invitrogen
Dimethylsulfoxid	Sigma-Aldrich
Dithiothreitol	Merck KGaA

Name	Company
DMEM medium	PAA or PAN Biotech
DPBS	PAA Laboratiories
EDTA	Sigma-Aldrich
Ethanol	Merck KGaA
Fmr1- MEF cell line	Kind gift from Dr. Davidovic
Fmr1^{+} MEF cell line	Kind gift from Dr. Davidovic
Formic Acid	Merck KGaA
Glycerol	Merck KGaA
Glycerol-2-Phosphate	Sigma-Aldrich
GSK-3beta (D5C5Z) XP® Rabbit mAb	Cell Signaling New England Biolabs
Hippocampal mouse tissue	Kind gift from Prof. Bear
Hygromycin B	Sigma-Aldrich
Immobiline Drystrips	GE Healthcare
InstantBlue	Biozol
Iodoacetamide	Sigma-Aldrich
IPG-buffer pH 3-10	IPG-buffer pH 3-10
IPTG	Euromedex
Isopropanol	Merck KGaA
L-glutamine	Gibco
Lithium chloride solution	Sigma-Aldrich
LumiGLO® reagent	Cell Signaling New England Biolabs
Lys-C	Wako
Lysine (Lys0)	Silantes
Lysine (Lys4, Lys8)	Silantes
Methanol	Merck KGaA
Mineral Oil	Bio-Rad Laboratories
NeuroPAN Basal-Media	PAN Biotech
n-octylglucoside	Roche
NuPAGE 12% Bis-Tris Gel	Life Technologies (Invitogen)
NuPAGE LDS Sample Buffer	Life Technologies (Invitogen)

Name	Company
NuPAGE® MOPS SDS Running Buffer	Life Technologies
Penicilin/Streptomycin	PAN
Phospho-GSK-3-beta (Ser9)Rabbit mAb	Cell Signaling New England Biolabs
Potassium Chloride	Merck KGaA
Potassium Hydrogen Phosphate	Merck KGaA
Protease Inhibitor Cocktail (tablets)	Roche
ReproSil-Pur C18-AQ 3 µm resin	Dr. Maisch GmbH
Resource S Column	GE Healthcare
Roti®-Fluoro PVDF membrane	Roth
SeeBlue® Plus2 Prestained Standard	Life Technologies
Sep-Pak C18 Cartridges	Waters
Sodium Orthovanadate	Sigma-Aldrich
Sponge Pad for Blotting (8)	Life Technologies (Invitogen)
TDZD-8	Sigma-Aldrich
Thiourea	Merck KGaA
Titanium dioxide Beads	Sachtopore
Transfer Buffer	Life Technologies (Invitogen)
Triethylammonium Bicarbonate	Sigma-Aldrich
Trifluoroacetic Acid	Merck Millipore
Tris Base	Sigma-Aldrich
Trypsin	Promega
Tween 20	Merck KGaA
Urea	Merck KGaA
Whatman™	GE Healthcare
ß-mercaptoethanol	BDH

III.1.1. List of instruments

Instrument	*Company*
3100 Offgel Fractionator	Agilent Technologies
ÄKTA System	GE Healthcare
Borosilicate Emitters	Thermo Scientific
Cell culture incubator	Thermo Fisher Scientific
Centrifuge (table-top)	Eppendorf
Column Oven	Sonation
Easy-LC nano-HPLC	Proxeon Biosystems
Electrospray ionization source	Proxeon Biosystems
Fusion SL Imager	Peg Lab
LTQ-Orbitrap Elite	Thermo Fisher Scientific
LTQ-Orbitrap XL	Thermo Fisher Scientific
Nano ES Ion Source (ES380)	Thermo Scientific
Spectrophotometer (A_{595})	Thermo Electron Corporation
Stage-tip Centrifuge	Sonation
Vacuum Centrifuge	Eppendorf
XCell II Blot Module	Invitrogen
XCell SureLock Mini-Cell Electrophoresis	Invitrogen

III.2. Methods

III.2.1. Quantitative phosphoproteomics of murine *Fmr1*-KO cell lines provides new insights into FMRP-dependent signal transduction mechanisms

This chapter of the thesis was adopted from Matic et al [69].

III.2.1.1. Cell culture and SILAC labeling

A spontaneously immortalized fibroblastic murine *Fmr1*-KO cell line was established from mouse embryonic fibroblasts (MEFs) derived from *Fmr1*-null C57Bl/6J embryos (mouse strain gR2700 available from Jackson Laboratory). *Fmr1*-KO MEFs cells were then transfected with a pTL10 vector containing *FMR1* isoform 1 human cDNA or with an empty pTL10 vector [165]. Simultaneously, cells were cotransfected with a pIREShyg3 plasmid (Clontech-BD Bioscience) containing Hygromycin B resistance. This procedure resulted in two stable cell lines: one stably re-expressing FMRP, termed as STEK-59 (*Fmr1*$^{+}$ MEFs), and one *Fmr1*-KO cell line further referred to as STEK-87 (*Fmr1*$^{-}$ MEFs). MEF cells were cultured in DMEM medium (Dulbecco's modified eagle medium, High Glucose (4,5 g/L), PAA or PAN Biotech) lacking arginine, lysine and L-glutamine. L-glutamine (2 mM, Gibco), penicillin/streptomycin (100 U/ml, PAN), Hygromycin B (from *Streptomyces hygroscopicus*, 150 µg/mL, Sigma-Aldrich) and dialyzed FBS (10 %, Invitrogen) were added to the medium. The "light" SILAC media was further supplemented with 73 mg/L L-lysine Lys0 and 42 mg/L L-arginine Arg0 (both from Silantes), whereas 73 mg/L "heavy" L-lysine Lys8 (13C6,15N2-L-Lysine, Silantes) and 42 mg/L "heavy" L-arginine Arg10 (13C6,15N4-L-Arginine, Silantes) were added to the "heavy" SILAC medium. Both cell lines (*Fmr1*$^{+}$ MEFs and *Fmr1*$^{-}$ MEFs) were grown in an incubator (37°C, 5 % CO2) in either "light" or "heavy" SILAC DMEM medium.

III.2.1.2. Protein extraction

To extract SILAC labeled proteins from cell culture, cells were washed twice with 5 mL DPBS (PAA Laboratories) and put on ice to prevent protein degradation during the following denaturation step with a buffer containing 6 M urea, 2 M thiourea and 10 mM Tris-Base. Protease- (complete Mini EDTA-free Proteinase Inhibitor Cocktail) and phosphatase inhibitors (glycerol-2-phosphate, sodium fluorite, and sodium orthovanadate) were added. DNA and RNA were removed during 10 min incubation with benzonase (EMPROVE® bio; Merck) on room temperature (RT) followed by centrifugation at 2800 x g (4000 rpm, 10°C, 25 min). The DNA- and RNA- containing precipitate was removed afterwards.

III.2.1.3. In-solution protein digestion and isoelectric focusing

Extracted proteins from each cell line were mixed 1:1 ("light" to "heavy" according to Bradford assay, Bio-Rad Laboratories). Protein mixtures were digested according to the protocol published by Macek et al. [166]. Portions of the tryptic peptides, 100µg per sample, were further fractionated according to their isoelectric point on 3100 OffGel fractionators (Agilent) by Off-Gel separation using manufacturer's instructions. Focusing was done with 13cm Immobiline DryStrips pH 3-10 (GE Healthcare), resulting in 12 fractions per sample. Current was limited to 50 µA and fractionation completed as soon as 20 kVh were reached. Fractions were acidified using acidic acid (30 % ACN, 10 % TFA and 5 % acetic acid in water) before desalting on StageTips, described by Ishihama [167].

III.2.1.4. Phosphopeptide enrichment

Phosphopeptide enrichment was done as described previously [168] with following modifications: 5 mg of digested peptides per sample (a portion of tryptic digestion described in previous section) were separated using strong cation exchange (SCX) chromatography with a linear gradient of 0-35 % of SCX solvent B over 32 min which resulted in 16 fractions. The resulting 16 fractions were pooled to eleven fractions

according to the SCX chromatogram. The flow-through, containing unbound peptides was collected separately. Eleven fractions per replicate plus flow-through were further processed via TiO_2 chromatography. Hereafter phosphopeptides were eluted in three steps with elution buffer (40 % ammonium hydroxide solution in 60 % acetonitrile, pH 10.5**)**. The TiO_2 chromatography was done once or twice per fraction depending on phosphopeptide quantities expected from SCX chromatogram. Enrichment of the flow-through was done five times.

III.2.1.5. Nano-LC-MS/MS analysis

All peptides were measured on Easy-LC nano-HPLC (Proxeon Biosystems) coupled to an LTQ Orbitrap Elite mass spectrometer (Thermo Fisher Scientific) for the proteome or an LTQ Orbitrap XL (Thermo Fisher Scientific) for the phosphoproteome measurements. Liquid chromatography was done on a 15 cm fused silica emitter with an inner diameter of 75 µm and a tip diameter of 8 µm in-house made nano-HPLC column, packed with reversed-phase ReproSil-Pur C18-AQ 3 µm resin (Dr. Maisch GmbH). Peptides were flushed with HPLC solvent A (0.5 % acetic acid) at a flow rate of 500 nL/min with the maximum pressure of 280 Bar. Elution was done using segmented 90 min gradient (LTQ Orbitrap Elite) or 130 min (LTQ Orbitrap XL) of 5 - 90 % HPLC solvent B (80 % ACN, 0.5 % acetic acid) at a flow rate of 200 nL/min. The eluted peptides were ionized in an electrospray ionization (ESI) source (Proxeon Biosystems) set to positive ion mode. Full scan MS spectra were acquired in the Orbitrap analyzer in a mass range from m/z 300 - 2000 at a resolution of 120,000 (LTQ Orbitrap Elite) or 60,000 (LTQ Orbitrap XL), followed by fragmentation in LTQ mass analyzer of the top-20 (LTQ Orbitrap Elite) or top-5 (LTQ Orbitrap XL) most intense precursor ions with collision induced dissociation (CID) at a target value of 5000 charges. Dynamic exclusion was used to exclude fragmented masses for 90 sec. In addition, for phosphoproteome measurement (LTQ Orbitrap XL), ions were fragmented by multi stage activation (MSA) on the neutral loss ions at -98, -49 and -32.6.

III.2.1.6. Data processing and analysis

The mass spectrometry data were processed using MaxQuant suite V 1.3.0.5 [169, 170]. Spectra were searched using andromeda search engine [138] against the proteome database of *Mus musculus* (UniProt complete proteome database, downloaded on 25. December 2012), consisting of 50,697 protein entries and 247 commonly observed lab contaminants. Mass tolerance for the first search was set to 20 ppm, and for the main search to 6 ppm. SILAC multiplicity was set to two. Lys0, Arg0 and Lys8, Arg10 were defined as “light” and “heavy” samples, respectively. Full tryptic specificity was required and a maximum of two missed cleavages were allowed. Carbamidomethylation of cysteine was set as fixed modification while oxidation, acetylation (on N-term) and phosphorylation on Ser/Thr/Tyr were chosen as variable modifications. Initial mass tolerance for the precursor ion was set to 6 parts per million (ppm) and for the fragment ions 0.5 Da. For quantification of proteins, minimum two peptides with at least seven amino acids had to be detected. The maximum allowed posterior error probability (PEP) was set to 1 and the false discovery rate (FDR) to max 1 % for peptides and proteins. Re-quantification was enabled while “second peptide search” option was disabled.

The localization probabilities of potential phosphorylation events on Ser/Thr/Tyr were calculated based on the posttranslational modification (PTM) score. Quantification of phosphorylation sites was normalized with the respective protein abundance, provided the protein was quantified in unmodified form.

III.2.1.7. Bioinformatic analysis

Perseus V 1.3.0.4, a module from the MaxQuant suite [169], was used for comparison of SILAC ratio distributions and calculation of the Pearson correlation coefficient in both, proteome and phosphoproteome measurements. This was done by extraction of the H/L ratios from ProteinGroups.txt file, generated in MaxQuant. Contaminants, reverse hits or proteins identified only by modification site were removed, values were Log2

transformed and the Pearson correlation coefficient calculated for the H/L ratios of both replicates.

Calculation of significantly changing proteins and phosphorylation sites was also done in Perseus V 1.3.0.4 using two-tailed “Significance B” test; $p \leq 0.05$. “Significance B” test is based on the assumption that the most of the data is following normal distribution. For calculation of significantly changing proteins, data must be log transformed to ensure equal treatment for up- and down-regulation. Test is using 15.87 and 84.13 percentile as an asymmetric estimate for a standard deviation. This deviation is applied on the protein subsets which are binned based on their intensity. Therefore this test is considering shift of the ratio from the normal distribution and intensity level [169]. H/L ratios were transformed to Log2, whereas intensities of peptides or phosphorylation sites were Log10 transformed. For significance of phosphorylation sites, H/L ratios were normalized by corresponding protein H/L ratios.

In the same module we performed functional enrichment analysis of Gene Ontology, Pfam and KEGG terms for increased and decreased classified proteins and phosphorylation sites. We applied truncation based on Benjamini-Hochberg [171] corrected p-values with threshold value of 0.05 to test whether specific annotation terms are significantly enriched or depleted among the chosen set of proteins of interest. The adjusted p-values were +/-log10 transformed and visualized in Excel. List of proteins and phosphorylation sites from class 1-3 were divided based on their increasing or decreasing level separately uploaded to STRING (The Search Tool for the Retrieval of Interacting Genes) database [172, 173] to look for known and predicted protein interactions. We requested the highest confidence score of 0.9 for the predicted protein interaction and discarded disconnected nodes.

The available list of FMRP protein-RNA interaction (pri) or protein-protein interactions (ppi) manually curated from the literature [174] was updated with recent references (notably ref 9) and used to appreciate the overlap between dysregulated proteins in the present datasets of protein levels and phosphorylation events.

III.2.1.8. Western-blotting

Work in this chapter was done by Laetitia Davidovic, Physiopathology of Mental Retardation, Valbonne, France.

Cell extracts were analysed by western blotting as described previously [174, 175].The following primary antibodies were used: 1C3 against FMRP (1:500, [38]); 3Fx against FXR1P and cross-reacting with FXR2P (1:500, [176]), anti-β-actin monoclonal antibody (1:20,000; Sigma), anti-β-tubulin monoclonal antibody (1:500, clone E7, Iowa Developmental Hybridoma Bank, USA), anti-cPLA2 (1:1,000, Santa Cruz) and anti-Prp (1:500, clone SAF70, [177]). Digital acquisition of chemiluminescent signal was performed using the Las-3000 Imager system (Fujifilm). Quantitation of western-blot was performed using the ImageJ software and normalized to the β-actin or β-tubulin signal. GraphPad 4 software was used for statistical analysis.

III.2.2. Inhibition of GSK-3β kinase in murine *Fmr1*-KO cell lines

This chapter of the thesis is manuscript in preparation from Matic el al.

III.2.2.1. Inhibition of GSK-3β

Two stable cell lines, STEK-59 (*Fmr1*$^{+}$ MEFs) and STEK-87 (*Fmr1*$^{-}$ MEFs) were established as described the in previous section (III.2.1.1.) [165]. In order to inhibit GSK-3β, both cell lines were treated with 20 mM lithium (unspecific inhibitor) or 5 μM TDZD-8 (specific inhibitor) at different time points (0, 0.5, 1, 3, 6, and 12hours). Inhibition of the kinase was determined through the increase of the phosphorylation event at the Ser-9 site of the kinase by western blot. We used Anti-Phospho-GSK-3-beta (Ser9) antibody (1:1000, Cell Signaling) to detect Ser-9 phosphorylation and GSK-3-beta (1:1000, Cell Signaling) to

detect kinase as a loading control. In both cell lines, inhibition was achieved at 3 hours when treated with lithium, and 1 hour when treated with TDZD-8 (see Results).

III.2.2.2. Cell culture and SILAC labeling

Cell lines were cultured in DMEM medium (PAA or PAN Biotech) in deficiency of arginine, lysine and L-glutamine. Medium was supplied with L-glutamine (2 mM, Gibco), penicillin/streptomycin (100 U/ml, PAN), Hygromycin B (from *Streptomyces hygroscopicus*, 150 µg/mL, Sigma-Aldrich) and dialyzed FBS (10 %, Invitrogen). Two triple SILAC experiments were constructed. *Fmr1*$^{+}$ MEFs and *Fmr1*$^{-}$ MEFs treated with lithium were grown in the "light" SILAC medium. Both cell lines without the treatment were grown in "medium" SILAC medium, and *Fmr1*$^{+}$ MEFs and *Fmr1*$^{-}$ MEFs treated with TDZD-8 were grown in "heavy" SILAC medium. Cell lines, with or without corresponding treatment, were grown in an incubator at 37°C, with 5 % CO2. In addition, 12 hours prior to treatment cells were put in the starvation medium (medium without FBS).

III.2.2.3. Sample preparation

Sample preparation was done as described previously (III.2.1.2., III.2.1.3.). Each approach was performed in biological replicates. Briefly, after cell treatments, proteins were extracted. Extracted proteins were mixed in equal amounts, "light" to "medium" to "heavy", resulting in two samples per biological replicate. Mixed proteins were digested. For the proteome part, portion of digested proteins (60 µg) was used for Offgel separation. The remaining sample (3.5 mg) was acidified with TFA to 0.1% concentration (v/v) and used for phosphopeptide enrichment. Afterwards, solid phase extraction was performed. Shortly, samples were loaded on to Sep-Pak Vac 1cc C18 Cartridges. Prior to loading, columns were activated with Methanol and equilibrated with Solvent A* (2% acetonitrile / 1% TFA). After loading the sample, column was washed with Solvent A (0.5% acetic acid) and peptides were eluted with 80% ACN / 6% TFA. Next, peptides were

incubated with TiO2 beads (1:2, bead to protein ratio) for 10 min. Beads were washed with Solvent B and peptides were eluted with 5% NH3.H2O, pH 11.0 in to 20% FA. Samples were evaporated in the SpeedVac (Eppendorf) until 50 µl and purified on StageTips [167].

III.2.2.4. LC - MS analysis

All samples were measured on Easy-LC nano-HPLC (Proxeon Biosystems) coupled to an LTQ Orbitrap Elite mass spectrometer (Thermo Fisher Scientific) as described previously (II.1.5.). Elution was performed using segmented 90 min gradient (proteome measurement) or 130 min (phosphoproteome measurement). Full scan MS spectra were acquired in the Orbitrap analyzer in a mass range from m/z 300 - 2000 at a resolution of 120,000, followed by fragmentation of 15 most intense ions in HCD collision cell with normalized collision energy of 35%. The resulting fragments were detected at a resolving power of 15,000 in the Orbitrap analyzer.

III.2.2.5. Data processing and analysis

Data was processed in the same manner as described in III.2.1.6. section with following exception. MaxQuant suite 1.5.1.0. was used for processing with multiplicity three, Lys0, Arg0 for “light”, Lys4, Arg6 for “medium” and Lys8, Arg10 for “heavy” samples. Requantify option was disabled and phosphorylation events ratios were not normalized by their respected protein ratios.

Perseus V 1.5.0.15 [169], was used for calculation of the Pearson correlation and two-tailed “Significance B” test as described before.

Functional enrichment analysis of Gene Ontology and KEGG terms was done using DAVID online tool [178, 179]. We applied truncation based on Benjamini-Hochberg [171] corrected p-values with threshold value of 0.05. List of decreasing phosphorylation sites from class 1-3 were uploaded to STRING (The Search Tool for the Retrieval of Interacting

Genes) database [172, 173] to look for known and predicted protein interactions with the highest confidence score of 0.9 for the predicted protein interaction and discarded disconnected nodes.

III.2.3. Dynamic SILAC of WT and *Fmr1*-KO primary cortical neurons

III.2.3.1.SILAC labeling of primary cortical neurons

Work in this chapter was done by Laetitia Davidovic, Physiopathology of Mental Retardation, Valbonne, France.

Primary cortical neurons were obtained from C57BL/6J mouse embryos as previously described [68]. Neurons were seeded in NeuroPAN-Basal-Media (PAN Biotech) lacking arginine and lysine. Medium was supplemented 73 mg/L “heavy” L-lysine Lys8 (13C6, 15N2-L-Lysine, Silantes) and 42 mg/L “heavy” L-arginine Arg10 (13C6, 15N4-L-Arginine, Silantes). Neurons were collected at the following time points: 2, 3, 4, 5, 6 and 10 DIV.

III.2.3.2. Sample preparation

Samples were prepared as described previously (III.2.1.2., III.2.1.3.). Shortly, at the corresponding time points, proteins were extracted. Protein concentration was determined using Bradford assay (Bio-Rad Laboratories). 10 µg of each sample was digested. After digestion was done, samples were acidify to pH 2 and loaded on the StageTips [180].

III.2.3.3. LC-MS analysis

All samples were subjected to nano-LC-MS/MS measurements on the LTQ-Orbitrap Elite (Thermo Fisher Scientific) as described previously (III.2.1.5.). Separation was performed using a linear 90 min gradient as described in III.2.2.4. section.

III.2.3.4. Data processing and analysis

Data was processed as described in III.1.6. section with the exception of multiplicity two, Lys0, Arg0 for "light" and Lys4, Arg6 for "heavy" samples.

Perseus V 1.5.0.15 [169], was used for calculation of the Pearson correlation and box plots were created using online tool (http://boxplot.tyerslab.com).

Protein half-lives were calculated using approach adopted from Schwanhausser et al [152]. In this approach, it is assumed that "light" labeled proteins are exponentially decaying with the degradation rate constant (k_{dp}). This rate can be calculated using the formula

$$k_{dp} = \frac{\sum_{i=1}^{m} log_e(r_{t_i} + 1)t_i}{\sum_{i=1}^{m} t_i^2}$$

where m represents the number of time points (t_i), and r_{t_i} the "heavy" to "light" ratio of the specific protein at each time point. When we have calculated k_{dp}, half-life of the protein ($T_{1/2}$) can be extracted from the formula

$$T_{1/2} = \frac{log_e 2}{k_{dp}}.$$

Functional enrichment analysis of Gene Ontology, Pfam and KEGG terms was performed for all quartiles in WT and *Fmr1*-KO, separately, as described in III.2.1.7. section with exception of threshold value of 0.01 (Benjamini-Hochberg corrected p-values).

III.2.4. Global identification of differentially regulated proteins in mouse models of Fragile X Syndrome

This chapter of the thesis is manuscript in preparation from Matic el al.

III.2.4.1. Mouse model, preparation of the tissue

Work in this chapter was done by Emily Osterweil, Department of Brain and Cognitive Sciences, Massachusetts Institute of Technology, USA.

Fmr1-KO mutant mice (Jackson Labs) were crossed with *Grm5* mutants (Jackson Labs) to produce *Fmr1*-KO/*mGluR5*-het mice. *Fmr1*-KO/*mGluR5*-het, *Fmr1*-KO and wild type littermates were kept on the C57BL/6J background. All mice were treated according to the NIH and MIT guidelines, and maintained in 12 : 12 hours light : dark cycle [81].
Experiments were performed blind to genotype.
At the P25-32 male littermates were killed by rapid decapitation and hippocampi were rapidly dissected [181].

III.2.4.2. Protein extraction and digestion

Hippocampal tissues were homogenized in denaturation buffer (6 M urea/2 M thiourea in 10 mM Tris buffer) with 1% of *N*-Octyl-β-d-glucopyranoside. Homogenized tissues were centrifuged 5 min at 13000 rpm to remove the foam, precisely balanced, then centrifuged at 20 000 rpm in the prior cooled ultra-centrifuge at 4°C for 1 hour. Next, the

protein extracts were collected and methanol/chloroform precipitation was performed. Protein concentration was determined by Bradford assay (Bio-Rad). Extracted proteins, 10 µg per a sample, were digested as described in III.2.1.3. section.

III.2.4.3. Nano-LC-MS/MS analysis

The peptides were measured on an EASY-nLC II nano-LC (Proxeon Biosystems) coupled to either LTQ Orbitrap Velos mass spectrometer (Thermo Fisher Scientific) or LTQ Orbitrap Elite mass spectrometer (Thermo Fisher Scientific). The peptides were separated by liquid chromatography using 15 cm PicoTip fused silica emitter of 75 µm inner diameter (ID) and an 8 µm Tip ID (New Objective) packed in-house with reversed-phase ReproSil-Pur C18-AQ 3 µm resin (Dr. Maisch GmbH). Sample was loaded onto the column using Solvent A (0.5% acetic acid) at 700 nL/min with maximum back pressure of 280 Bar and subsequently eluted using a segmented gradient of 5-90% solvent B (80% ACN in 0.5% acetic acid) at the constant flow rate of 200 nL/min over 230 min. Full scans for the MS spectra were acquired between 300 – 2000 Thompson at the resolution of 60,000 (LTQ Orbitrap Velos) and 120,000 (LTQ Orbitrap Elite). In the linear ion trap the 15 (LTQ Orbitrap Velos) or 20 (LTQ Orbitrap Elite) most intense ions were selected for the further fragmentation with collision induced dissociation (CID) at a target value of 5000 charges.

III.2.4.4. MS data processing

Acquired raw data were processed with MaxQuant software (v.1.3.0.5) [169] as described before (III.2.1.6.). To perform label-free quantification we enabled the label-free algorithm and used the “match between runs” option. Raw files were matched within time window of 2 minutes as follows. Due to robust recalibration of peptide retention times performed by MaxQuant software all LC-MS/MS runs were matched between each other.

III.2.4.5. Bioinformatic analysis

III.2.4.5.1. Data preparation and imputation of missing values

After removal of decoy proteins, commonly observed lab contaminants, and proteins only identified by a modification site ("Only identified by Site") we extracted the label-free (LFQ) intensities of the remaining protein groups. The resulting data matrix consisted of 5,238 rows (protein groups) and 27 columns (nine replicates for each genotype) containing label-free intensities. For further analysis we required a minimum of nine valid columns for each protein group to retain cases in which a protein is completely missing in two out of three genotypes. Label-free intensities were log10-transformed and missing values were imputed to simulate protein abundances near the detection limit as described in Deeb at al [182] using values 1.4 for 'downshift' and 0.3 for width, respectively (**Supplementary Figure III.1**).

III.2.4.5.2. Normalization and filtering

LFQ intensities across the different measurements were normalized according to the Quantile method [183] using function 'normalize.quantiles' form the 'preprocessCore' R-package (**Supplementary Figure III.2**). To increase statistical power in finding differential proteins, we removed proteins with no or only negligible variation of expression across the genotypes prior to hypothesis testing. To that end we calculated pairwise ratios of averaged LFQ intensities between different genotypes and determined outliers of the resulting distribution. We calculated the significance of each protein ratio with respect to the distance of the median of the distribution of all protein ratios as well as its signal intensity. This approach was introduced in [169] to determine the significance of proteins ratios in a typical quantitative MS-based proteomics experiment and referred to as "Significance B" (p_{sigB}). All proteins with $p_{sigB} > 0.1$ in a pairwise comparison were not considered in hypothesis testing for differential expression.

III.2.4.5.3. Linear mixed effect model analysis of variance

Based on the imputed, normalized, and log-transformed LFQ intensities we applied analysis of variance (ANOVA) to test for differential expression between pairs of genotypes. We modeled the expression values as response of a linear mixed effects model (LMEM) consisting of one fixed effect (genotype), and two random effects (the different batches of experiments and the general error term). The modeling and ANOVA was performed in R using functions 'lmer' and 'anova', respectively, which are part of the R-package 'lmerTest'.

Proteins having a p-value below 0.015 were considered as potential candidates for differential expression between the phenotypes. We chose this threshold based on empirically observed p-values of positive controls in our dataset, e.g. the expression mGluR5 is known to be reduced by a factor of two in the *mGluR5*-het model compared to *Fmr1*-KO and WT, respectively.

For false discovery estimation among all tested hypotheses we adjusted the p-values for multiple hypothesis testing by the method of Benjamini & Hochberg [184]. For the list of potential differential proteins we report the false discovery rate as the maximal adjusted p-value in the corresponding list. Principle component analysis was performed in R using the function 'prcomp'.

III.2.4.6. Calculation of absolute protein abundances

We calculated absolute amounts for each protein using the total protein approach (TPA) described in [164]. Briefly, individual LFQ intensities were divided by the sum of all LFQ intensities of every protein of a sample which corresponds to the total MS signal of the proteome in that sample.

III.2.4.7. String analysis

List of significantly changing proteins from ANOVA analysis was separately uploaded to STRING database [172, 173] for each pairwise comparison to look for known and

predicted protein interactions. We use 0.4 confidence score for the predicted protein interaction and discarded disconnected nodes.

III.2.4.8. Western blot validation

Equal amounts of the protein extract, 20µg, were loaded on the SDS-PAGE gel, followed by separation at 200V for 1 hour. Proteins were transferred to a PVDF membranes using XCell II™ Blot Module (Invitrogen) and membranes were blocked overnight with PBS and 1% Tween20. Membranes were washed in PBST and incubated for 1 hour using the following antibodies: Anti-prion protein PrP antibody (1:5000, AbCam), Anti-Fragile X Mental Retardation Protein Antibody (1:500, Millipore) and Anti-GAPDH (1:2000, Pierce Antibody).

After washing, incubations with HRP linked secondary antibody against mouse or rabitt were done for 1 hour (1:4000, Cell Signaling Technology). LumiGLO® reagent (Cell Signaling Technology) and Fusion SL Imager (PegLab) were used to visualize the proteins.

IV RESULTS

IV.1. Quantitative phosphoproteomics of murine *Fmr1*-KO cell lines provides new insights into FMRP-dependent signal transduction mechanisms

This chapter of the thesis was adopted from Matic et al [69].

To compare the proteome and the phosphoproteome of the *Fmr1*$^{-}$ and the control *Fmr1*$^{+}$ MEF cell lines, two SILAC experiments in a reverse labeling manner were performed. SILAC-labeled cells were lysed, their proteins extracted and digested with trypsin. Smaller portions of the digests were separated by isoelectric focusing (for proteome measurement), whereas the larger portion was subjected to two stages of phosphopeptide enrichment, using SCX and TiO_2 chromatographies (for phosphoproteome measurement). All LC-MS/MS measurements were performed on the LTQ-Orbitrap mass spectrometers and MS data were processed by MaxQuant software package (**Figure IV.1**).

As a quality control step, we checked incorporation of SILAC labels. Incorporation was verified in dedicated mass spectrometry runs and calculated using the formula

$$\frac{\tilde{X}\left(\frac{H}{L}\right)}{1+\tilde{X}\left(\frac{H}{L}\right)} * 100$$

in which, (H/L) refers to the unnormalized ratio of the quantified peptide with the "heavy" label to the corresponding "light" peptide. Mass spectrometry runs confirmed full labeling of the MEF proteome (**Table IV.1**).

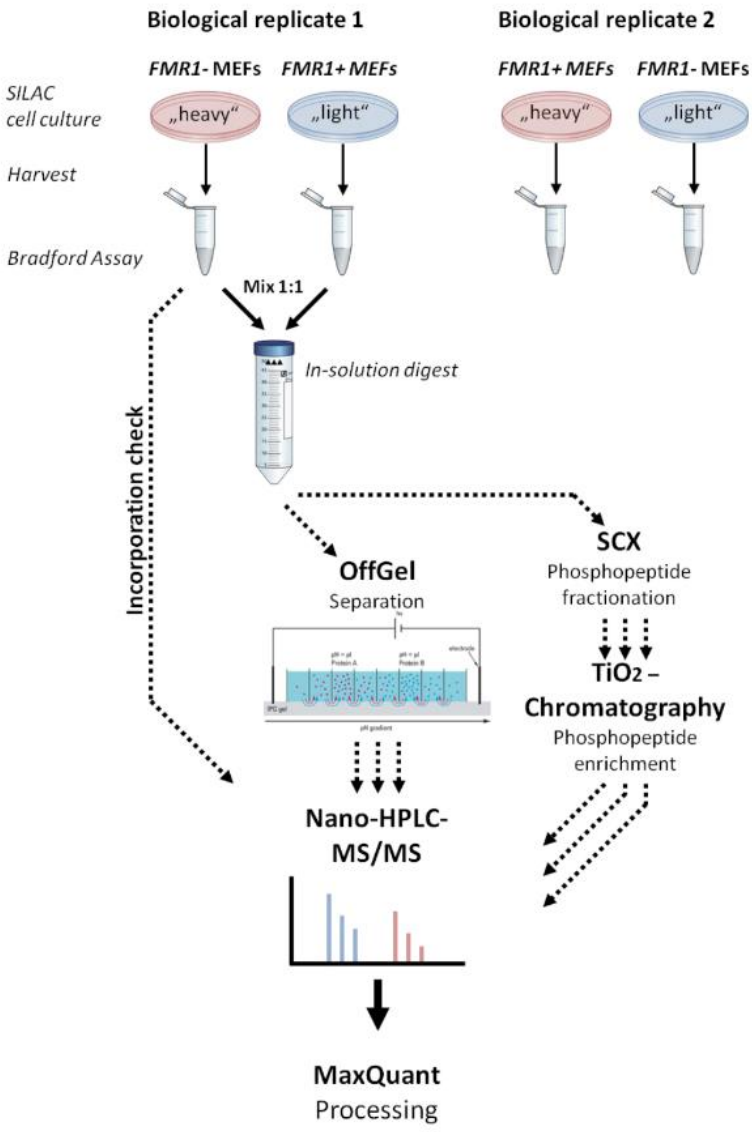

Figure IV.1 | Proteomic and phosphoproteomic workflow for two replicates of SILAC labeled cells. *Fmr1$^-$ MEFs and Fmr1$^+$ MEFs cells were grown in SILAC labeled medium for 14 days. In biological replicate 1 Fmr1$^-$ MEFs were "heavy" and Fmr1$^+$ MEFs "light" labeled, while in biological replicate 2 labeling was inversed. After labeling, cells were harvested, followed by cell lysis and protein extraction. Full incorporation of SILAC amino acids was confirmed. After 1:1 mixing of "heavy" and "light" cell lysates and subsequent in-solution digestion, one part was used for the proteomic workflow, which includes separation by OffGel and measurement by nano-HPLC MS/MS on a LTQ-Orbitrap Elite and further processing by MaxQuant software. The larger part of digested proteins was fractionated by SCX and phosphopeptides were enriched by TiO2 chromatography before subsequent measurements by nano-HPLC MS/MS on a LTQ-Orbitrap XL.*

Table IV.1 | Incorporation rates of "heavy" isotopes of arginine and lysine in cells after 9 days of growth in SILAC media. "*Heavy" isotopes were incorporated during cell growth. The rate describes the percentage of "heavy" amino acid isotopes in the cells proteins. Cells were considered fully labeled since the incorporation rate was high (above 95 %).*

	Fmr1^{+} *MEF*	**Fmr1^{-} *MEF***
Arginine	0.968	0.966
Lysine	0.966	0.965
Combined	0.967	0.965

"Heavy" (Arg10, Lys8) and "light" (Arg0, Lys0) labeled cell lysates were mixed in equal amounts based on Bradford measurements. Digested peptides were measured by MS in order to verify mixing using the formula

*Measured Protein Concentration * $\tilde{X}$ (H/L) = True Protein Concentration*

in which mixing error is calculated based on the median of unnormalized evidences (**Table IV.2**).

Table IV.2 | SILAC heavy/light mixing error. *Summary of unnormalized proportions of "heavy" labeled evidences compared to "light" labeled evidences. The numbers of detected and quantified evidences are listed additionally.*

	Median (H/L)	***Detected evidences***	***Quantified evidences***
Proteome biological replicate 1	0.87	65,857	63,461
Proteome biological replicate 2	0.77	65,169	62,686
Phosphoproteome biological replicate 1	0.88	24,406	23,683
Phosphoproteome biological replicate 2	0.67	18,785	18,262

Both of these quality steps, incorporation and mixing check, were done as a standard quality control for following SILAC experiments.

Pearson correlation coefficients between SILAC ratios measured in two biological replicates were r = -0.932 for the proteome and r = -0.708 for the phosphoproteome data, indicating high reproducibility at both levels (**Figure IV.2 A, B**). Inverse correlation is a consequence of inverse SILAC labeling.

IV.1.1. Overview of proteome and phosphoproteome results

Combined analysis of 24 MS runs from isoelectric focusing (proteome analysis) and 44 MS runs from phosphopeptide enrichment resulted in 56,352 identified peptide sequences from 6,703 protein groups. Identified protein groups were filtered for contaminants, reverse (decoy) hits and proteins identified by modification site. The estimated false discovery rate (FDR) was 0.36 % at the peptide level and 2.09 % at the protein group level. From 6,235 detected endogenous MEF proteins, 4,195 were quantified in both replicates, of which 266 were changing significantly in both biological replicates (134 were increasing and 132 decreasing). Scatter plots of measured protein ratios are shown separately for both replicates in **Figure IV.2 C, D**.

The phosphoproteome analysis revealed 9,181 phosphorylation events on 2,494 proteins. Since we expected expression differences at both proteome and phosphoproteome levels, we normalized phosphopeptide ratios with protein ratios. The total number of quantified phosphorylation events that could be normalized by the respective protein ratio was 6,040, of which 142 showed significant changes in both replicates (86 phosphorylation sites were increasing and 56 phosphorylation sites were decreasing in *Fmr1*$^{-}$ cells compared to the *Fmr1*$^{+}$ cells). Distributions of phosphorylation events measured in both replicates are shown in **Figure IV.2 E, F**.

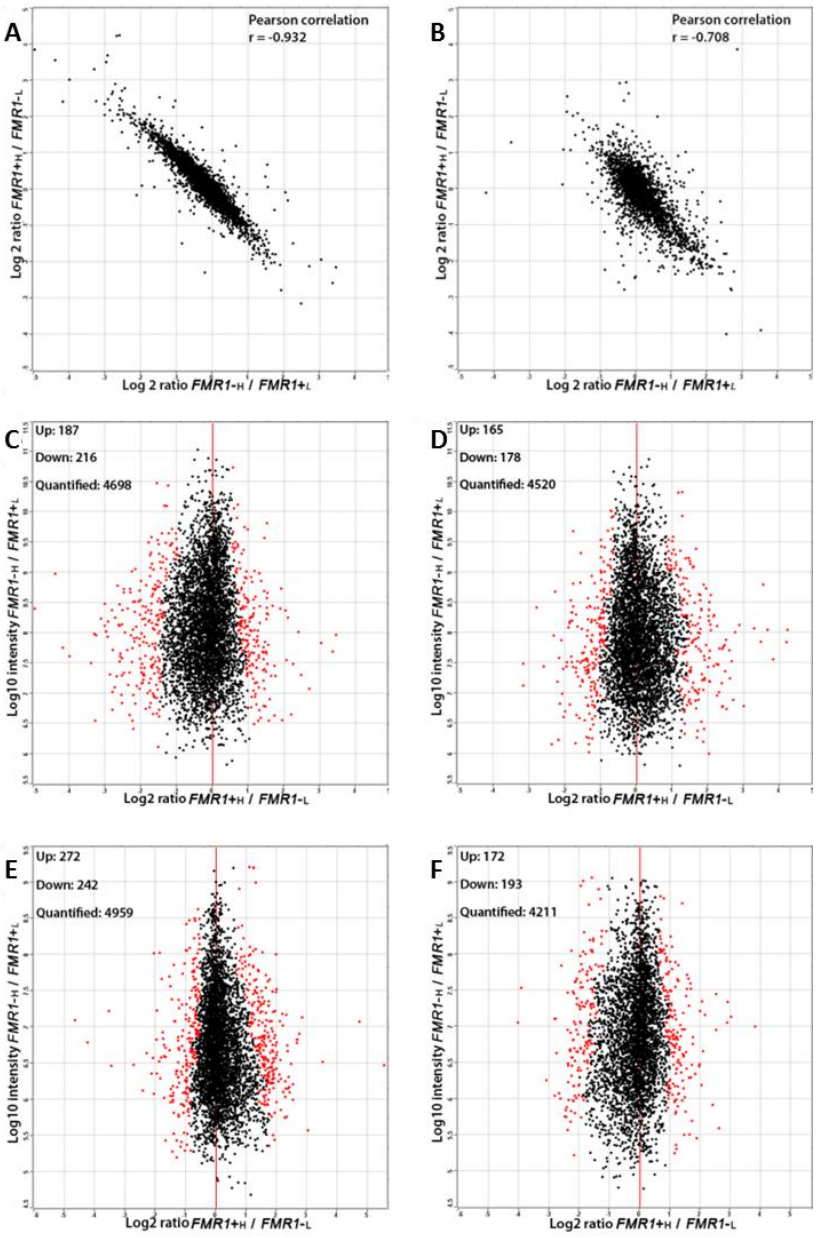

Figure IV.2 | Correlations of proteome and phosphoproteome

*Correlation between biological replicates at the **A)** proteome; and **B)** phosphoproteome level. Each dot represent a SILAC protein or phosphorylation site ratio measured in both biological replicates. Negative correlation is a consequence of inversed SILAC labeling.*

*Distributions of quantified proteins from **C)** biological replicate 1; **D)** biological replicate 2; **E)** phosphorylation sites replicate 1 and **F)** biological replicate 2. Intensity is log10, H/L ratios log2 transformed. Red dots represent significant ($p < 0.05$) outliers, which are reported separately for increased and decreased in Fmr1^{-} MEF.*

We next compared our quantified proteome dataset with reported mRNA targets or protein interactors of FMRP [44, 185-196] (see Material and Methods section). This comparison revealed 383 proteins, of which 23 were significantly changing in at least one biological replicate in our dataset. Surprisingly, the levels of only eight proteins were significantly increasing in *Fmr1*$^{-}$ MEFs, as should be expected for mRNA targets for which FMRP would repress translation [197], while 15 were significantly decreasing. This limited overlap can have several reasons, starting from the proteome coverage obtained in our study (we estimate that we quantified about one third of all expressed proteins in the cell), studied system (original mRNA data are derived from the mouse brain), and additional regulatory mechanisms that likely influence the final level of an FMRP target protein in the cell, such as protein degradation. All detected proteins and phosphorylation events of proteins that are known mRNA targets or protein interactors of FMRP are listed in **Supplementary Table IV.1**.

IV.1.2. Validation by western blotting

Work in this chapter was done by Laetitia Davidovic, Physiopathology of Mental Retardation, Valbonne, France.

The mass spectrometry-based quantification was further validated by western blot (**Figure IV.3**). Analysis using the anti-FMRP mAb1C3 confirmed the expression of FMRP in *Fmr1*$^{+}$ MEFs and its absence in *Fmr1*$^{-}$ MEFs (**Figure IV.3A**). Western-blot analysis with the 3Fx antibody recognizing the homologues of FMRP, all isoforms of Fxr1p and Fxr2p, showed that the lack of FMRP did not affect their levels of expression (**Figure IV.3B**). This confirms the mass spectrometry measurements and previous observations that the absence of FMRP is not compensated by upregulation of its homologues [198].

Two candidate proteins which were significantly dysregulated in the MS experiments were validated. First, semi-quantitative western-blotting analysis confirmed that *Fmr1*$^{-}$

MEFs express lower levels of the major prion protein (Prp) than *Fmr1*$^{+}$ MEFs (**Figure IV.3C left panel**), exhibiting a significant decrease of 62 % (p=0.0361; **Figure IV.3C right panel**). Since PrP has a role in the formation of synapses [199] and in memory processing in the rat hippocampus [200], we hypothesize that reduced levels of Prp could contribute to the cognitive deficits observed in the *Fmr1*-KO mouse. Second, a significant increase in cytosolic calcium-dependent phospholipase A2 (Pla2g4a known as cPLA2, **Figure IV.3D left panel**) levels which is increased by 82 % in *Fmr1*$^{-}$ MEFs as compared to *Fmr1*$^{+}$ MEFs (p=0.0079 was observed; **Figure IV.3D right panel**). cPLA2 releases arachidonic acid from membrane phospholipids. Importantly, cPLA2 participates in cerebellar long-term depression and motor learning [201]. It is tempting to speculate that abnormal overexpression of cPLA2 in the brain could participate in the cerebellar dysfunctions observed in *Fmr1*-KO mice [202]. Significantly higher concentrations of cPLA2 have been reported in red blood cells of patients with autism[203], linking cPLA2 to another form of cognitive disorder.

IV.1.3. Regulatory pathway analysis

For downstream bioinformatic analysis and pathway mapping, detected proteins and phosphorylation events were clustered into three classes based on quantification confidence as described in **Table IV.3**. Proteins and phosphorylation events that were not significantly changing in any of the replicates were not further considered. To investigate general processes and pathways that differ between the *Fmr1*$^{+}$ and *Fmr1*$^{-}$ MEFs, classified proteins and phosphorylation sites were used to perform functional enrichment analysis of Gene Ontology (GO), Pfam and KEGG terms.

The set of proteins and phosphorylation events with *increased* levels revealed significant overrepresentation of terms related to cell cycle, nucleotide metabolism and p53 pathway (proteome level), as well as vasopressin-regulated water reabsorption and ribosome (phosphoproteome level) (**Supplementary Table IV.2**).

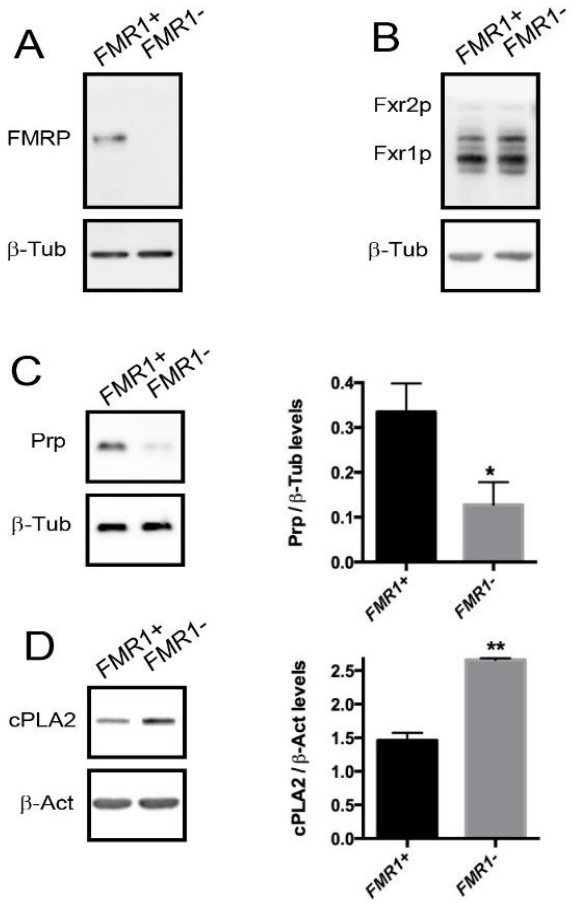

Figure IV.3 | Western-blot analysis of Fmr1-KO MEFS reexpressing (Fmr1$^+$) or not (Fmr1$^-$) FMRP. A) *Western-blot analysis of with anti-FMRP 1C3 antibody. β -tubulin (β-tub) signal is used to verify equal loading of lanes;* ***B)*** *Western-blot analysis of Fmr1$^+$ or Fmr1$^-$ MEFs with anti-Fxr1P/Fxr2p antibody #3FX recognizing the homologues of Fmrp, Fxr1p (short and medium isoforms) and Fxr2p. β -tubulin (β -tub) signal is used to verify equal loading of lanes;* ***C)*** *Representative western-blot of Prp protein levels in Fmr1$^+$ or Fmr1$^-$ MEFs. Densitometric quantification of western-blots reveal that depletion of Fmr1 leads to a significant decrease of Prp protein levels relative to Fmr1$^+$ cells;* ***C)*** *Representative western-blot of cPLA2 protein levels in Fmr1$^+$ or Fmr1$^-$ MEFs. Densitometric quantification of western-blots show that depletion of Fmr1 leads to a significant increase in cPLA2 protein levels. Data are presented as means ± SEM of n=5 experiments. The asterisks * and ** indicate respectively p<0.05 and p<0.01 of the Mann & Whitney test.*

Proteins and phosphorylation events with *decreased* levels pointed to significant overrepresentation of functions related to peroxisome proliferator-activated receptor (PPAR) pathway, lysosome and extracellular matrix interaction (proteome level), as well as gap junction, Alzheimer' s disease, long-term potentiation, long-term depression,

axon guidance, Wnt and MAP kinase pathways (phosphoproteome level) (**Supplementary Table IV.3**).

Table IV.3 | Classification of quantified proteins and phosphorylation sites. *Class 1 includes proteins or phosphorylation sites which were significantly changing in both replicates. Class 2 consists of proteins phosphorylation sites which were significantly changing in at least one replicate, and have the same trend in both replicates. Class 3 was significant in at least one replicate and had a missing value in the other replicate.*

	Proteins		***Phosphorylation sites***	
	Increased in *Fmr1*$^-$ KO	**Decreased in *Fmr1*$^-$ KO**	**Increased in *Fmr1*$^-$ KO**	**Decreased in *Fmr1*$^-$ KO**
Class 1	134	132	86	56
Class 2	77	75	131	129
Class 3	34	59	124	157
Classes 1+2+3	245	266	341	342

Next, the STRING [172, 173] database was searched for known and predicted protein-protein interactions among classified proteins and phosphorylation events detected in the dataset. The STRING analysis revealed strong clusters of cell cycle-related and ribosomal proteins among proteins with increased levels in *Fmr1*$^-$ cells (**Supplementary Figure IV.1A)**. Interestingly, a cluster of proteins of the ubiquitin/proteasome system was also present in that part of the dataset, pointing to a possible increase of protein degradation as a consequence of FMRP loss. Among proteins with decreased levels in *Fmr1*$^-$ cells, the STRING analysis detected several members of the gluthatione-S-transferase (GST) protein family, as well as PTEN/ phospholipase pathway and Notch signaling (**Supplementary Figure IV.1B**). The decrease in GST members can be linked to the increase in oxidative stress markers observed in the brain of *Fmr1*-KO mice [174, 204]. In phosphoproteome dataset, increased phosphorylation was observed on clusters of proteins related to pre-mRNA processing, DNA replication, ribosomal proteins and several proteins involved in nuclear transport, such as nucleoporins (**Figure IV.4A**),

revealing that FMRP influence on these processes is largely mediated at protein phosphorylation level. Among proteins with decreased phosphorylation levels in *Fmr1*$^{-}$ cells several proteins from the MAPK pathway were detected (**Figure IV.4B**). To gain a more detailed insight into differences in specific signal transduction networks, classified proteins and phosphorylation events onto highly conserved pathways from Kyoto Encyclopedia of Genes and Genomes (KEGG)[205] were mapped, focusing on the mTOR, p53, Wnt and MAPK pathways.

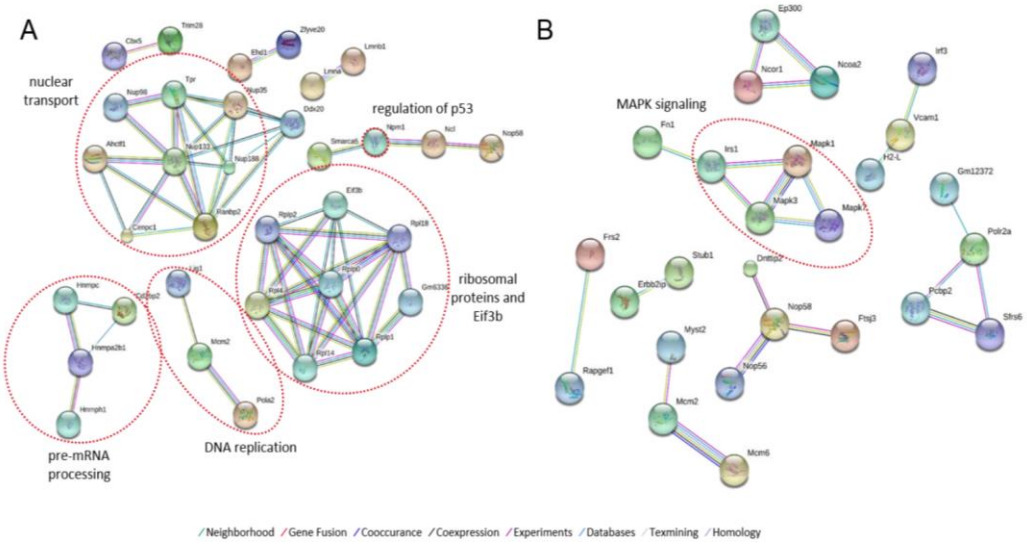

Figure IV.4 | Known and predicted protein interactions of detected phosphoproteins in Fmr1^{-} STEK cells. ***A)*** *proteins with increased phosphorylation;* ***B)*** *proteins with decreased phosphorylation. Interactions were retrieved from the STRING database using all phosphorylation sites from classes 1-3.*

IV.1.3.1. mTOR signaling Pathway

In *Fmr1*$^{-}$ cells, the levels of mTOR and the main proteins of the Akt-mTOR pathway were not significantly changing in steady states were not significantly changing

(**Supplementary Figure IV.2**). However, the data showed a significant decrease in the phosphorylation level on ERK (see below), as well as decreased phosphorylation levels of IRS1 and Rictor. Interestingly, a significant decrease in levels of PTEN was detected. PTEN is an inhibitor of the PI3K-AKT cascade pathway which is associated with memory and learning process [206] and whose downregulation is connected to autism[207] and FXS [208]. Also, significant increase of phosphorylation on the S6 protein was observed. Likely, this is consequence of activated p70 S6 kinase [209] and points to increase of mTOR activity and protein synthesis in *Fmr1*$^{-}$ MEFs.

The mammalian target of rapamycin (mTOR), a serine/threonine kinase is a signaling node that plays an important role in cellular processes such as protein synthesis and proliferation [210]. Notably, the mTOR/Akt pathway controls mGluR5-mediated activity-dependent protein synthesis involved in synaptic plasticity. There are contradictory statements on the contribution of the Akt-mTOR pathway on the exaggerated global protein synthesis in FXS. While Sharma et al. suppose a possible role for mTOR signaling in increased mGluR-LTD and assume a causal relationship between elevated mTOR signaling and over-activation of group 1 mGluRs [211], Osterweil et al. showed that mTOR does not contribute to the increased protein synthesis [212]. These authors also showed that ERK1/2 pathway is responsible for elevated protein synthesis, still the pathway by itself is not overactive, but rather hypersensitive to stimulation [211, 212].

IV.1.3.2. p53 Signaling Pathway

Dataset revealed significant increase of the p53 protein in *Fmr1*$^{-}$ cells as well as significant changes in eight other proteins linked to p53 signaling. Chk1, Cdk4/6, Cyclin B, Cdc2 and p53R2 were increased, whereas KAI, PTEN and TSAP6 were decreased (**Supplementary Figure IV.3**).

Using adult neuronal progenitor/stem cells (aNPCs) as a model, Luo et al. showed that FMRP regulates Cyclin D and Cdk4 mRNAs involved in cell cycle progression [213]. In addition, Liu et al showed that Cyclin B is upregulated in *Drosophila* FXS model [214],

which supports proposed involvement of FMRP in cell cycle control. Although there is to date very little evidence linking p53 signaling to FXS, recent reports show the involvement of FMRP in the DNA damage response [215, 216], a cellular response which triggers activation of the p53 pathway. Also, p53 mRNA is a putative target of FMRP since its 3'UTR harbors a G-quadruplex RNA structure [217] that is an RNA motif bound with high affinity by FMRP [189, 218]. Furthermore, there are several reports on the role of p53 in autism. Sheikh et al. examined a possible apoptosis signaling deregulation in the brain of autistic subjects and found increased levels of p53 [219]. Taken together, these results point to involvement of p53 and its downstream targets in dysregulated cell cycle control in FXS.

IV.1.3.3. WNT Signaling Pathway

The canonical Wnt pathway is crucial for activation of neuronal differentiation during neurogenesis and its inhibition induces hippocampus-dependent learning deficits [220, 221]. For this reason it was hypothesized that defective Wnt signaling might be linked to human mental disorders like FXS. Indeed, reduced Wnt signaling in aNPCs was found by Luo et al. in the hippocampus of *Fmr1*-KO mice [222]. Data revealed decrease of FRP level, which normally blocks Wnt canonical pathway (**Supplementary Figure IV.4**). Since it is reported that Wnt signaling is reduced in FXS, it is possible that this is one of the compensatory mechanisms. In addition, decreased levels of Knypek was detected. It was shown previously that Knypek influences synaptic formation and that is involved in AMPAR mobility[223]. In Wnt/calcium pathway significant decrease both in PLC levels and its phosphorylated forms, significant dephosphorylation of PKC, as well as significant dephosphorylation of the transcription factor NFAT was detected. Therefore, it can be hypothesized that calcium homeostasis and Wnt/calcium dependent gene expression may be affected in molecular pathogenesis of FXS.

IV.1.3.4. MAPK Signaling Pathway

The generated data points to a general downregulation of the canonical MAPK pathway, including related receptors and signaling nodes such as EGF-receptor, Ras and ERK1/2 (**Supplementary Figure IV.5**). It showed a decrease in ERK2 levels and a significant decrease in the phosphorylation status of ERK2 Thr183 and Tyr185, based on statistical significance mentioned in the methods section. Decreased levels of ERK1/2 and its phosphorylation are associated with cell proliferation, migration and differentiation, also in the central nervous system, and these processes are therefore expected to be affected in FXS [224]. Deficits in proper neurogenesis and neuronal differentiation in the absence of FMRP were previously described [225]. Importantly, a significant reduction in basal phosphorylation of ERK1/2 was also observed previously in the CA1 region of the *Fmr1*-KO hippocampus [212]. In addition, a significant increase of Filamin A (FLNA) levels with concomitant significant decrease in its phosphorylation levels was observed. Interestingly, it was previously reported that Filamin A phosphorylation modulates actin neuronal remodeling [214] and that its downregulation in *dfmr1*-null *Drosophila* participates in abnormal neuronal branching [226]. Importantly, in *Fmr1*$^{-}$ cells, significant increase in level of the cytoskeleton regulator PAK kinase was observed. This kinase was previously reported to be a drug target for FXS and autism therapy [227, 228].

IV.2. Inhibition of GSK-3β kinase in murine *Fmr1*-KO cell lines

This chapter of the thesis is manuscript in preparation from Matic el al.

GSK-3 plays important role in various processes through different pathways [87]. Its abnormal activity has been implicated in different diseases such as Alzheimer's disease, mood disorders, diabetes and cancer. Evidence that inhibition of GSK-3β can restore a number of abnormalities in FXS is an important indication of overlap between FXS and other diseases [86]. Therefore, GSK-3 is considered to be an important drug target, among other diseases, for the FXS. Based on the present literature, knowledge about GSK-3 implication in signaling pathways is not quite clear. In addition, from proposed GSK-3 substrates only a small portion is confirmed, leaving open space to investigate how many of these substrates are indeed regulated by GSK-3. Pharmacological blocking of the kinase can help to identify new substrates and provide better knowledge of its role in the signaling network. Here, we use triple SILAC based approach in order to compare changes on phosphoproteome level after applying two different GSK-3 inhibitors on the MEF cell lines. Both, *Fmr1*$^{+}$ MEF and *Fmr1*$^{-}$ MEF "light" cells were treated with unspecific GSK-3 inhibitor lithium for 3 hours, "medium" labeled cells were untreated, while "heavy" cells were treated with specific GSK-3β TDZD-8 inhibitor for 1 hour, respectively.

IV.2.1. Inhibitor treatment

An essential element towards finding new kinase substrates is the identification of downregulated phosphorylation events upon blocking the kinase. To this end, *Fmr1*$^{+}$ MEF and *Fmr1*$^{-}$ MEF cell lines were treated with 2 different inhibitors – 20mM unspecific GSK-3 inhibitor and 5μM specific GSK-3β TDZD-8 inhibitor at different time points (0, 0.5, 1, 3, 6, 12 hours). To test when the kinase is blocked, we performed Western blot analysis of different time points of MEFs cell lysates using antibody specific for phosphorylation of serine 9 in GSK-3β. Increased phosphorylation level demonstrates inhibition of the

GSK-3β kinase upon treatment [86]. The analysis showed an increased phosphorylation level of serine 9 after 1 hour in lithium, and 3 hours in TDZD-8 treatment (**Figure IV.5**). These time points were chosen for subsequent SILAC experiments.

IV.2.2. Proteome and phosphoproteome analysis

As a part of standard quality check, incorporation of the SILAC labels and mixing check were verified by MS (**Supplementary Table IV.4 and Supplementary Table IV.5**). Extracted proteins from SILAC-labeled cells were equally mixed, for each cell line separately, and digested with trypsin. A small portion of the digested proteins were further fractionated according to their isoelectric point for proteome measurement and the remaining portion was subsequently enriched for phosphopetides using TiO_2 enrichment.

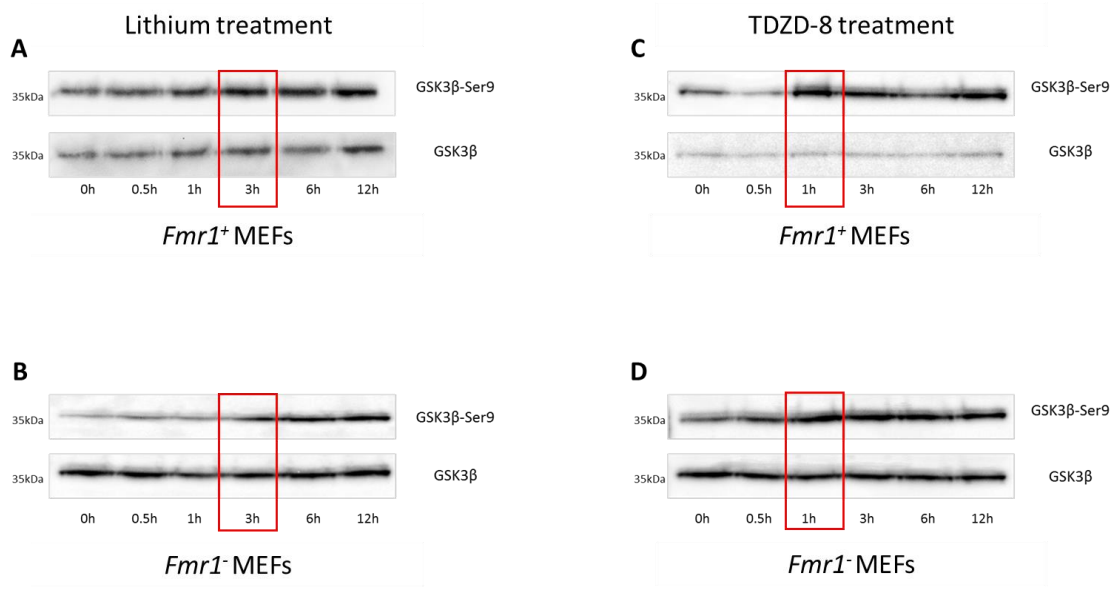

Figure IV.5 | Western blot analysis of GSK-3β inhibition. A) *Western blot analysis of lithium treatment in Fmr1⁺ MEFs**; B)** Western blot analysis of lithium treatment in Fmr1⁻ MEFs**; C)** Western blot analysis of TDZD-8 treatment in Fmr1⁺ MEFs**; D)** Western blot analysis of TDZD-8 treatment in Fmr1⁻ MEFs.*

Peptides were analyzed on the LTQ Orbitrap Elite coupled to the EASY-nLC. Experiments were performed in biological replicates and the resulting data was processed by MaxQuant software package [169] (**Figure IV.6**).

Combined analysis of 68 proteome and phosphoproteome MS runs resulted in identification of 51,048 peptide sequences (FDR 0.24%), 6,016 protein groups (FDR 1.41%) and 7,285 unique phosphorylation events (FDR 0.30%), of which 5,168 phosphorylation events were localized to a specific Ser/Thr/Tyr residue (**Supplementary Table IV.6**).

Correlation between biological replicates was similar for proteome and phosphoproteome level. Changes on both levels were not high which led to a generally low correlation and low reproducibility between biological replicates with exception of *Fmr1*$^{+}$ MEF cell line treated with TDZD-8 (**Supplementary Figure IV.6, Supplementary Figure IV.7**). This indicated that TDZD-8 is a more specific inhibitor of GSK-3β and therefore more suitable for analysis of its potential substrates.

In order to find phosphorylation events that are changing, we applied Significance B calculation (see Methods). In general, *Fmr1*$^{+}$ MEF cells were less affected by treatment than *Fmr1*$^{-}$ MEF cells implicating that *Fmr1*$^{-}$ cells are more sensitive to lithium and TDZD-8 treatments. Distributions for both cell lines are shown in **Supplementary Figure IV.8 and Supplementary Figure IV.9**.

For further bioinformatic analysis, phosphorylation events were clustered into three classes based on quantification confidence. A total of 180 phosphorylation sites in *Fmr1*$^{+}$ MEF cells and 276 sites in *Fmr1*$^{-}$ MEF cells were significantly changing in at least one biological replicate upon lithium treatment; in case of TDZD-8 treatment, 215 sites were significantly changing in *Fmr1*$^{+}$ MEF cells and 265 sites in *Fmr1*$^{-}$ MEF (**Figure IV.7**). Detailed classification is presented in **Table IV.4**.

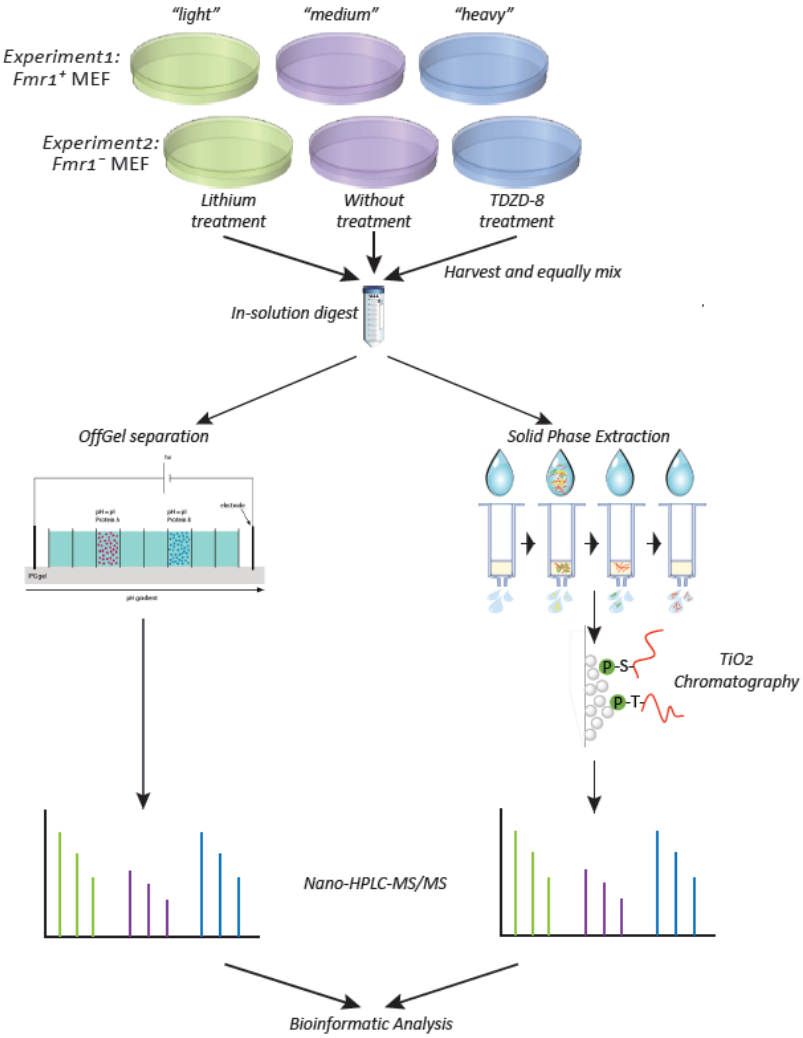

Figure IV.6 | Proteomic and phosphoproteomic workflow of MEF cells inhibitory treatment. *Fmr1⁻ MEFs and Fmr1⁺ MEFs cells were grown in SILAC labeled medium. In experiment 1, Fmr1⁺ MEFs treated with lithium were "light" and MEFs treated with TDZD-8 were "heavy" labeled, whereas untreated MEFs were labeled "medium". In the second experiment, the same labeling and treatment were applied on the Fmr1⁻ MEFs. After applied treatment, cells were harvested, lysed and proteins were extracted. Next, equally mixed proteins, for each experiment separately, were digested. Small part of peptides was used for offgel separation (proteome analysis), while another part was purified via solid phase extraction and sequentially incubated with TiO2 beads (phosphoproteome analysis). Samples were measures by nano-HPLC MS/MS on a LTQ-Orbitrap Elite and further processed using the MaxQuant software.*

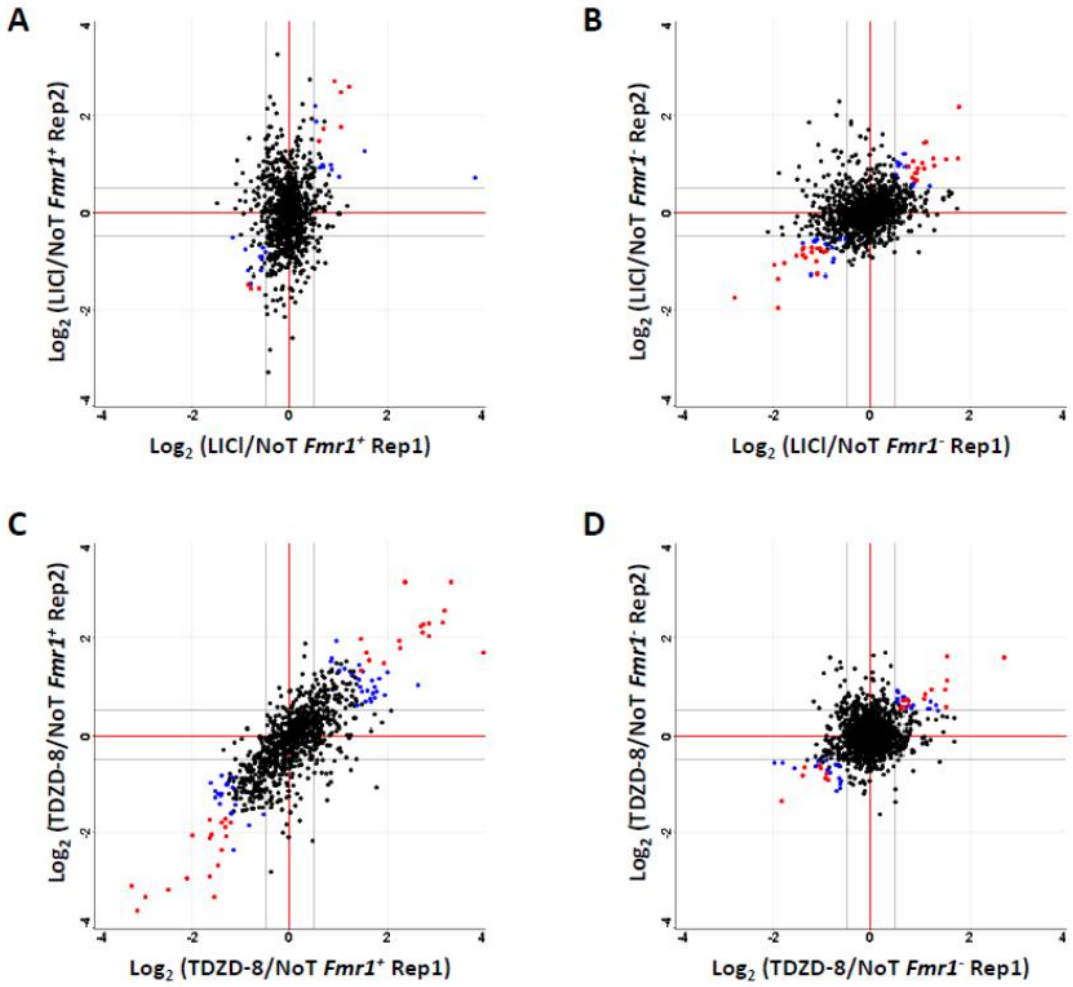

Figure IV.7. Distribution of significantly changing phosphorylation sites. A) *Significantly changing phosphorylation sites in lithium treatment in Fmr1⁺ MEFs;* ***B)*** *Significantly changing phosphorylation sites in TDZD-8 treatment in Fmr1⁺ MEFs;* ***C)*** *Significantly changing phosphorylation sites in lithium treatment in Fmr1⁻ MEFs;* ***D)*** *Significantly changing phosphorylation sites in TDZD-8 treatment in Fmr1⁺ MEFs. Red dots are representing phosphorylation sites that are significantly changing in both biological replicates (Group 1), blue dots are phosphorylation sites that are significantly changing in one biological replicate and have the same direction in another biological replicate (Group 2), and black dots are phosphorylation sites that are not significantly changing.*

Table IV.4 | Classification of quantified phosphorylation sites. A) *Significantly changing phosphorylation sites in lithium treatment;* ***B)*** *Significantly changing phosphorylation sites in TDZD-8 treatment. Class 1 includes phosphorylation sites which were significantly changing in both replicates. Class 2 consists of phosphorylation sites which were significantly changing in one replicate, and have the same trend in another replicate (with a cutoff of 0.7 and 1.41, which is around 1 SD). Class 3 was significant in one replicate and had a missing value in the second replicate.*

A

Lithium treatment	Fmr1^{+} *MEFs*			Fmr1^{-} *MEFs*		
	Class 1	**Class 2**	**Class 3**	**Class 1**	**Class 2**	**Class 3**
Downregulated	3	9	69	18	14	105
Upregulated	6	10	83	18	9	112
Total	9	19	152	36	23	217

B

TDZD-8 treatment	Fmr1^{+} *MEFs*			Fmr1^{-} *MEFs*		
	Class 1	**Class 2**	**Class 3**	**Class 1**	**Class 2**	**Class 3**
Downregulated	18	20	53	8	16	122
Upregulated	17	25	82	13	16	92
Total	35	45	135	21	30	214

IV.2.3. Identification of GSK-3β substrates

Due to low correlation and lack of reproducibility between biological replicates during lithium treatment, we decided to focus on TDZD-8 treatment. TDZD-8 is proven to specifically bind GSK-3β, therefore treatment with such inhibitor should cause less side effects. In order to identify GSK-3β kinase substrates in MEF cells we looked for decreased phosphorylation upon TDZD-8 treatment. In *Fmr1*$^{+}$ MEF cells a total of 91 phosphorylation sites showed decreased phosphorylation levels, whereas in *Fmr1*$^{-}$ MEF cells 146 phosphorylation sites showed decreased phosphorylation levels upon TDZD-8 treatment. These phosphorylation events were potential substrates of the GSK-3β

kinase. Next, we compared our list with a list of known and proposed substrates from the literature [229].

In *Fmr1*$^{+}$ MEF cells, inhibition by TDZD-8 confirmed one reported substrate (*MAP1B*), whereas in *Fmr1*$^{-}$ MEF cells it confirmed four reported substrates (*CTNND1*, *DPYSL2*, *DPYSL3* and *NDRG1*); all of them were significantly downregulated in at least one biological replicate (**Figure IV.8 A-D**). Interestingly, all six downregulated phosphorylation events from *MAP1B*, with GSK-3 motif, had a decreased phosphorylation level only in the *Fmr1*$^{+}$ MEF cell line, while in *Fmr1*$^{-}$ MEF was not regulated. *MAP1B* is known as a major substrate of GSK-3β and is involved in axonal growth regulation by binding microtubules in its phosphorylated state [230].

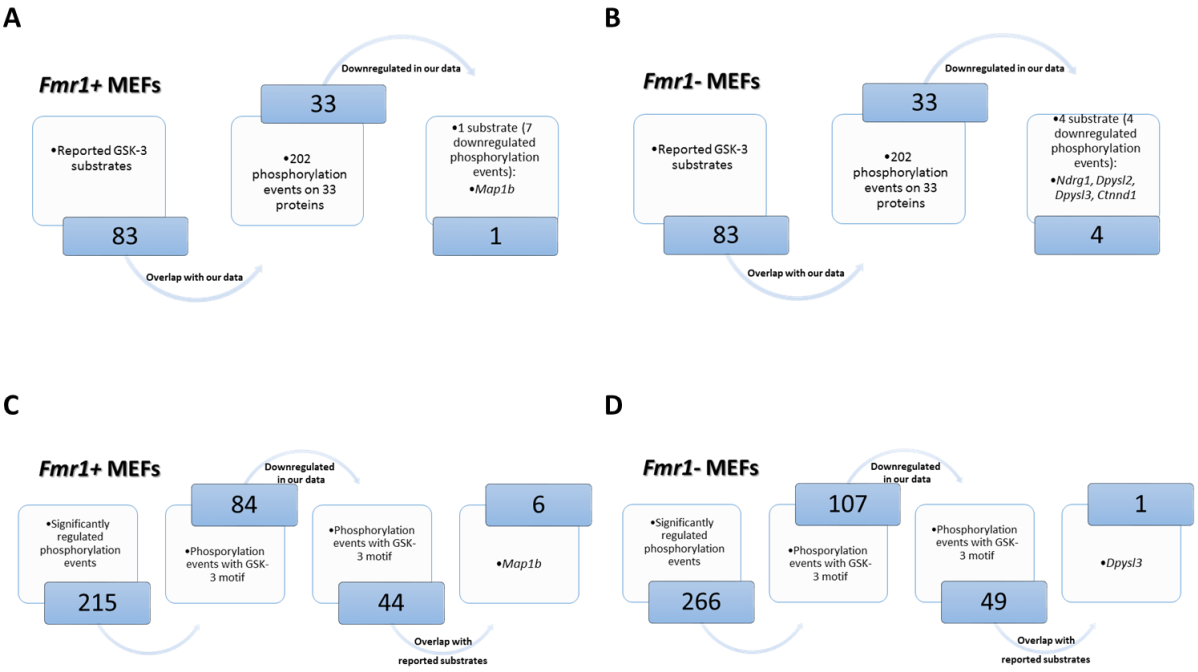

Figure IV.8 | Overview of overlap with known substrates and GSK motif in our phosphoproteome data upon TDZD-8 treatment. A) *Overlap with reported (known and proposed) substrates in Fmr1*$^{+}$ *MEFs;* ***B)*** *Overlap with reported (known and proposed) substrates in Fmr1*$^{-}$ *MEFs;* ***C)*** *Number of phosphorylation proteins with GSK motif in Fmr1*$^{+}$ *MEFs;* ***D)*** *Number of phosphorylation proteins with GSK motif in Fmr1*$^{+}$ *MEFs.*

The best known GSK-3β function is its involvement in the canonical WNT signaling pathway, where it is creating the "C" destruction complex via association with adenomatous polyposis coli (APC), axin and β-catenin. Once phosphorylated, β-catenin is degraded via ubiquitination/proteosome-dependent proteolysis. Dephosphorylation of β-catenin is important for its translocation to the nucleus and induction of transcription [231]. In our data, we confirmed the downregulation of β-catenin only upon lithium treatment in *Fmr1*$^{-}$ MEF (**Supplementary Figure IV.10**), while in other treatments (*Fmr1*$^{+}$, lithium and TDZD-8) we were not able to quantify it. However, we quantified another member of the catenin family, δ-catenin, where we measured a significant decrease in the phosphorylation level in *Fmr1*$^{-}$ MEF cells in both treatments, and in *Fmr1*$^{+}$ MEF is not significantly changing. δ-catenin is connected to mental retardation, learning deficits, synaptic plasticity, reduced LTP, spine and synapse morphogenesis and signaling of group I mGluR receptors [232-234]. Although a known GSK-3β target, δ-catenin was so far not connected with FXS and we propose that it could play an important role in molecular pathogenesis of the disorder.

We next compared potential substrates detected in *Fmr1*$^{+}$ MEFs and *Fmr1*$^{-}$ MEF cell lines (**Figure IV.9**) upon TDZD-8 treatment. Somewhat surprisingly, we found a poor overlap, pointing to the fact that different cell lines have distinct responses to GSK-3β inhibition. Although in Fmr1^{-} cells we detected a seemingly higher number of potential substrates, overall they were regulated to a much lower extent and most of them were quantified only in one replicate (class 3). This can be due to decreased specificity of the TDZD-8 in *Fmr1*$^{-}$ MEFs, or decreased specificity of the kinase (or both). Two common phosphorylation events belong to the same tumor protein D54, protein which have not been connected to the GSK-3β. This protein is known to play a role in cell growth, apoptosis and vesicle trafficking [235], which is in agreement with known GSK-3β functions.

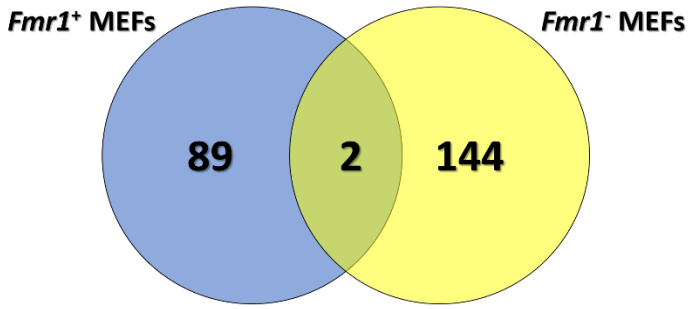

Figure IV.9 | Overlap of downregulated phosphorylation events upon TDZD-8 treatment in Fmr1⁺ and Fmr1⁻ MEFs.

List of the potential substrates, from class 1 and class 2, detected in this study in *Fmr1⁺* MEFs and *Fmr1⁺* MEFs is shown is **Table IV.5** and **Table IV.6**, respectively, while class 3 is shown in **Supplementary Table IV.7** and **Supplementary Table IV.8**.

IV.2.4. Functional enrichment analysis of potential GSK-3β substrates

In order to gain insights into the GSK-3β-mediated signaling, we performed functional enrichment analysis of Gene Ontology (GO) and KEGG terms of phosphoproteins that were significantly downregulated upon TDZD-8 treatment in *Fmr1⁺* and *Fmr1⁻* MEF cells. Processes related to focal adhesion, adherents junction and regulation of actin cytoskeleton were significantly overexpressed among potential GSK-3β substrates in *Fmr1⁺* MEF cells. Moreover, enrichment revealed overexpression of cytoskeletal protein binding, cytoskeleton organization and actin binding in *Fmr1⁺* MEFs, and cell cycle, division processes, ribonucleotide binding and GTPase and ATP binding in *Fmr1⁻* MEFs (**Supplementary Table IV.9**).

Table IV.5 | Potential substrates of GSK-3β in Fmr1⁺ MEFs (class 1 and class 2). *Table contains protein name of the potential substrate, presence of GSK-3 motif, overlap with known substrate [229], position of phosphorylated amino acid and phosphorylated residue.*

Protein.names	*GSK-3 motif*	*Reported substrates*	*Position*	*Amino.acid*
Acetyl-CoA carboxylase 1			79	S
Actin, cytoplasmic 1			239	S
Alpha-actinin-3			160	S
Cyclin-dependent kinase 17			146	S
Cofilin-2			3	S
Drebrin	+		142	S
E3 ubiquitin-protein ligase DTX3L	+		9	S
Filamin A-interacting protein 1-like	+		842	S
Filamin A-interacting protein 1-like			551	S
Golgi membrane protein 1			213	S
Heat shock protein beta-1			74	S
Heat shock protein beta-1			15	S
Interferon-activable protein 204	+		190	S
Interferon-activable protein 204	+		106	T
Microtubule-associated protein 1B		+	992	S
Microtubule-associated protein 1B	+	+	1497	S
Microtubule-associated protein 1B	+	+	1438	S
Microtubule-associated protein 1B	+	+	1422	S
Microtubule-associated protein 1B	+	+	1293	S
Microtubule-associated protein 1B	+	+	1775	S
Nestin	+		1837	S
Nestin	+		1565	S
Nexilin			296	S
PDZ and LIM domain protein 5	+		359	S
Phosphatase and actin regulator 4			593	S
Protein PML	+		17	S
Protein phosphatase 1 regulatory subunit 12A	+		299	S
Protein prune homolog 2	+		2638	S
Protein prune homolog 2			1682	S
Tyrosine-protein phosphatase non-receptor type 12			434	S
TBC1 domain family member 15			32	S
Tns1 protein	+		836	S
Tumor protein D54			166	S
tRNA methyltransferase 10 homolog A			21	T
Vinculin	+		346	S
Vinculin	+		290	S
Vinculin			721	S
14-3-3 protein zeta/delta			207	S

Table IV.6 | Potential substrates of GSK-3β in Fmr1$^-$ MEFs (class 1 and class 2). *Table contains protein name of the potential substrate, presence of GSK-3 motif, overlap with known substrate [229], position of phosphorylated amino acid and phosphorylated residue.*

Protein.names	*GSK-3 motif*	*Reported substrates*	*Position*	*Amino.acid*
Sperm-specific antigen 2 homolog			90	S
Tumor protein D54			166	S
Transmembrane protein 106B			34	S
Mitogen-activated protein kinase kinase kinase kinase 5			433	S
Supervillin			294	S
Arfip1 protein			132	S
Centrosomal protein of 170 kDa			443	S
GTP-binding protein RAD			25	S
cAMP-dependent protein kinase type II-beta regulatory subunit			112	S
Tyrosine-protein phosphatase non-receptor type 12			448	S
High mobility group protein HMGI-C	+		44	S
Cadherin-11			714	S
NAD kinase			48	S
Receptor-interacting serine/threonine-protein kinase 2			411	S
Epidermal growth factor receptor kinase substrate 8			684	S
Protein NDRG1		+	2	S
Septin-10			424	S
SH3 domain-containing kinase-binding protein 1			193	S
Echinoderm microtubule-associated protein-like 3			177	S
Ppp2r5d protein			565	S
Ribonuclease inhibitor			2	S
Suppression of tumorigenicity 5 protein			512	S
Ppfia1 protein			571	T
Plectin			4032	T

These differences could represent a consequence of a different activity of GSK-3β in *Fmr1*$^{+}$ and *Fmr1*$^{-}$ MEF cells.

To gain a better insight into predicted protein-protein interactions we searched proteins with significantly dowregulated phosphorylation events in the STRING database [172, 173]. The STRING analysis confirmed clusters from functional enrichment analysis. Proteins involved in adherent junction are clustering together in *Fmr1*$^{+}$ cells, and DNA

replication, RNA processing and cytoskeleton organization in *Fmr1*$^{-}$ cells (**Figure IV.10**). Results of functional enrichment and STRING analysis upon lithium treatment are shown in **Supplementary Figure IV.11** and **Supplementary Table IV.10**.

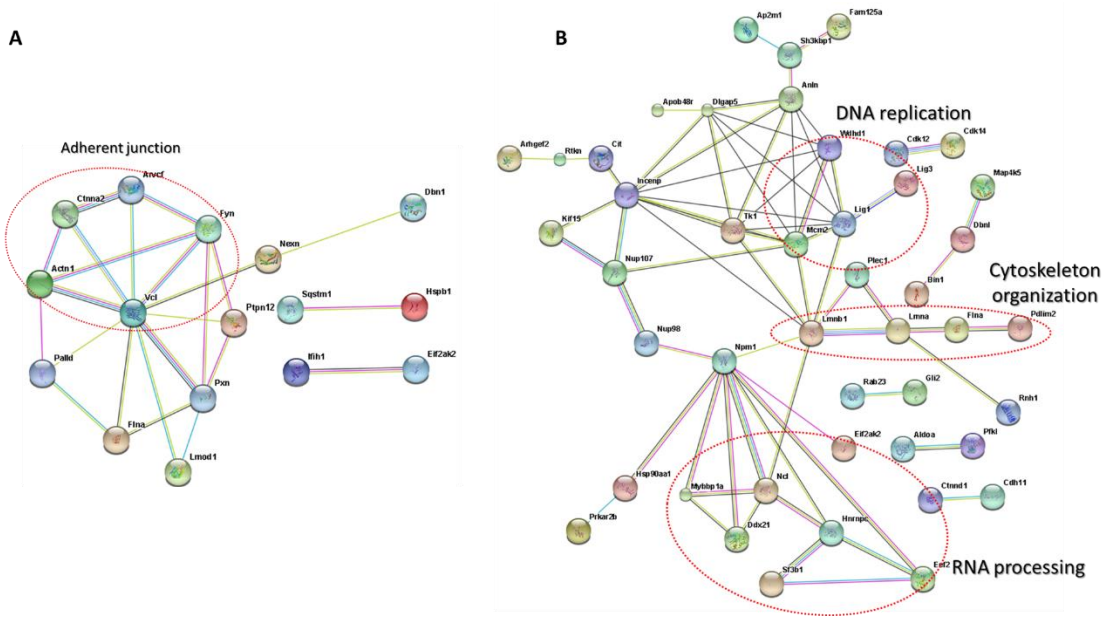

Figure IV.10 | Known and predicted protein interactions of detected phosphoproteins upon TDZD-8 treatment. A) *proteins with decreased phosphorylation in Fmr1*$^{+}$ *cell line;* ***B)*** *proteins with decreased phosphorylation in Fmr1*$^{-}$ *cell line.*

IV.3. Dynamic SILAC of WT and *Fmr1*-KO primary cortical neurons

Physiological, developmental or pathological state of the cell can change protein level through protein synthesis and/or protein degradation [118]. In this dynamic state, abundance of proteins is a consequence of protein turnover - balance between these

processes. Advances in proteomics have allowed large scale determination of the protein turnover and protein half-lives using SILAC metabolic labeling. In order to measure FMRP-dependent protein turnover, we performed dynamic SILAC labeling of WT and *Fmr1*-KO primary cortical neurons. Neurons were grown in "heavy" SILAC medium and collected at different time points (2, 3, 4, 5, 6 and 10 DIV). After cell lysis, proteins were extracted, digested with trypsin and resulting peptides were measured on LTQ-Orbitrap Elite. Acquired MS data were processed and incorporation of heavy SILAC label was quantified by MaxQuant [169] software package (**Figure IV.11**). Experiment was done in biological replicate.

Six time points from WT and *Fmr1*-KO neurons, in biological replicate, resulted in 24 runs. We identified 19,421 non-redundant peptides (FDR 0.25%) and 2,557 proteins (FDR 1.63%).

IV.3.1. Turnover rates in WT and *Fmr1*-KO cortical neurons

As a prerequisite to the turnover calculation, we checked for overall incorporation rates of the SILAC label in the analyzed neurons. Considering that proteins are constantly synthesizing and degrading, incorporation of "heavy" labeled proteins should increase with time and higher turnover proteins should incorporate the label faster. In our incorporation curves, we observed an almost identical increasing trend of incorporation in WT and *Fmr1*-KO neurons, respectively (**Figure IV.12**). However, *Fmr1*-KO neurons had slightly higher incorporation rate than WT neurons. In addition, our first time point (2 DIV) had an incorporation level around 50% and at the last time point (10 DIV) incorporation

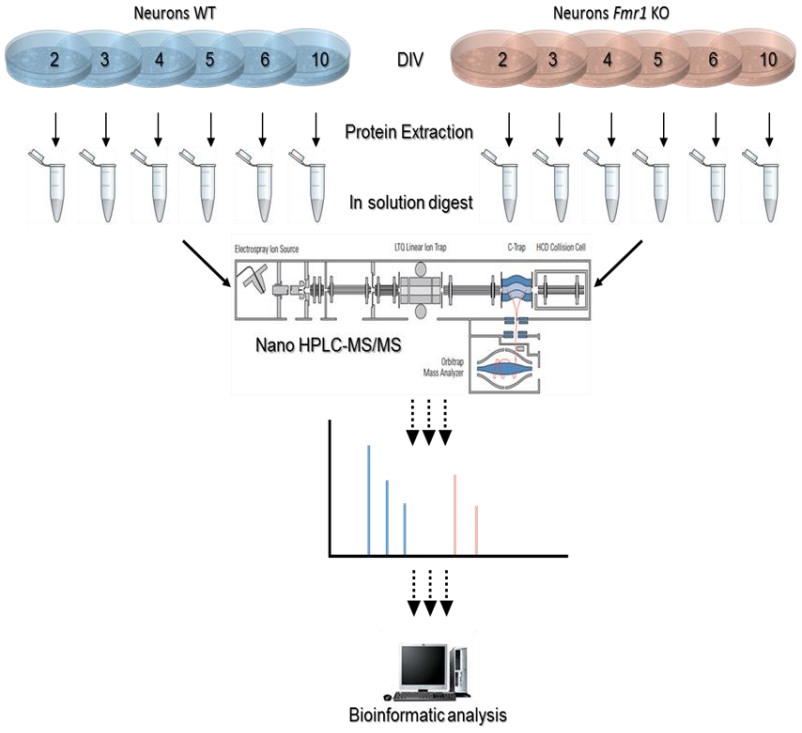

Figure IV.11 | Proteomic workflow for dynamic SILAC. *WT and Fmr1-KO cortical neurons were grown in SILAC labeled medium. Neurons were collected at different time points. After collection of the neurons, proteins were extracted and digested. Samples were measured by nano-HPLC MS/MS on a LTQ-Orbitrap Elite and incorporation of heavy SILAC label was quantified by MaxQuant software.*

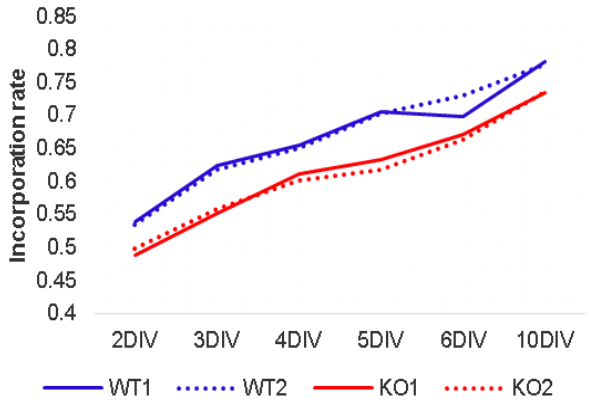

Figure IV.12 | Incorporation rate in WT and Fmr1-KO cortical neurons. *WT is shown in blue, and Fmr1-KO in red color. Solid lines present the first, and dashed lines the second biological replicate.*

was around 80% which is considered as maximal achievable labeling of neurons due to the fact that they are not dividing.

For calculation of protein turnover rates and half-lives we adopted approach from Schwanhausser et al [152]; see Methods. In order to obtain more reliable results, for the turnover rate calculation we considered proteins with at least 3 SILAC ratios in all time points and with coefficient of determination (R_2, correlation coefficient between measured and estimated ratios) higher than 0.7 in all biological replicates of WT and *Fmr1*-KO. After we applied this filter, we were left with 622 proteins with a SILAC ratio in all samples (**Supplementary Table IV.11**). Pearson correlation coefficients of protein half-lives between biological replicates were ≥ 0.99, indicating high reproducibility (**Figure IV.13 A and Figure IV.13 B**), and pearson correlation between mean of WT and *Fmr1*-KO was ≥ 0.99, indicating high similarity between different genotypes (**Figure IV.13 C**). Interestingly, however the measured protein half-lives were shorter in the WT than in KO cells. This was reflected in the median of half- lives: in *Fmr1*-KO neurons median was 102 hours, while in WT was 88 hours, indicating faster turnover in WT neurons.

IV.3.2. Proteins with high and low turnover

In order to determine which proteins have high or low turnover, we binned distributions of the protein half-lives into four quartiles (**Figure IV.14**). Proteins with half-lives in quartile 1 are defined as proteins with high turnover, in quartile 2 as moderately high turnover, quartile 3 as moderately low turnover, and quartile 4 as ones with low protein turnover.

Although proteins in *Fmr1*-KO have somewhat lower turnover rate, statistically, our data confirms that most of the proteins have similar half-life in WT and *Fmr1*-KO neurons. Functional enrichment analysis of Gene Ontology (GO), Pfam and KEGG terms was performed in order to see which processes and pathways differ in each quartile for WT and *Fmr1*-KO neurons, separately.

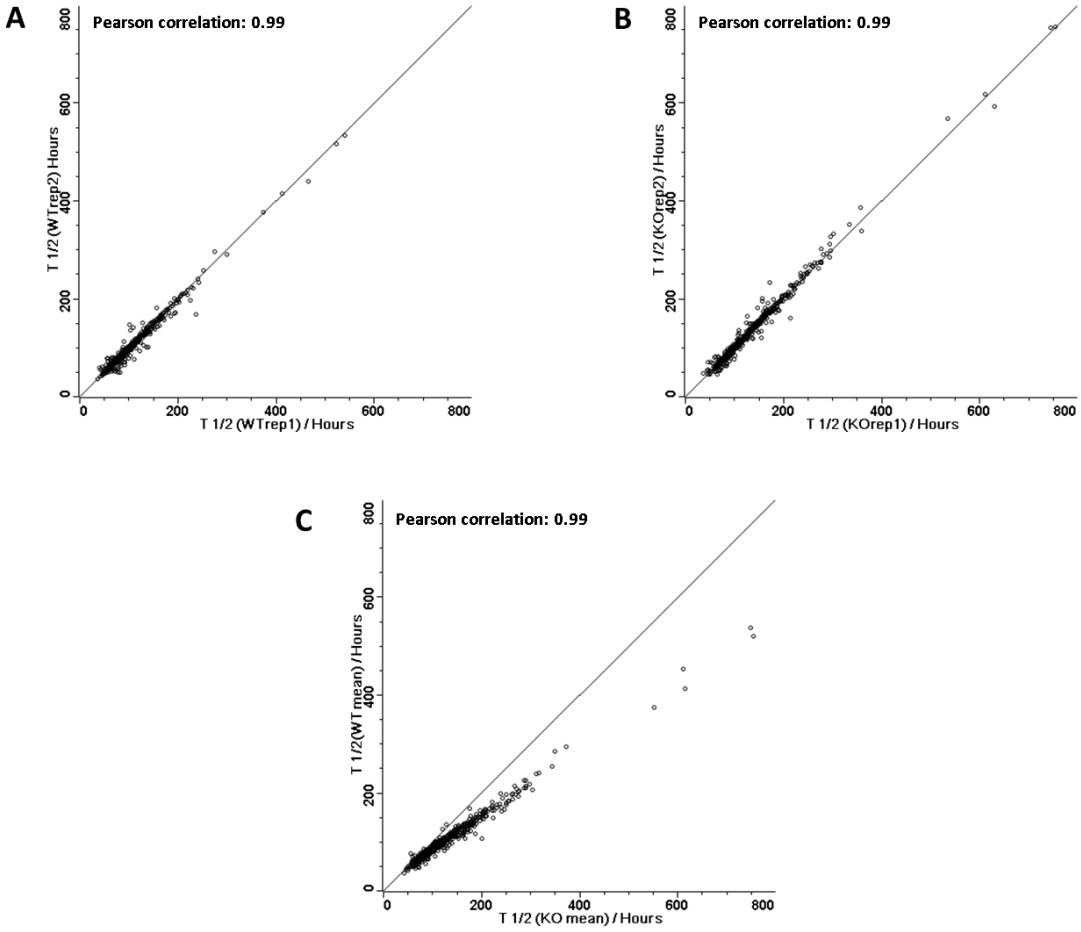

Figure IV.13 | Correlation of half-lives. A) *Between biological replicates in WT cortical neurons;* ***B)*** *Between biological replicates in Fmr1-KO cortical neurons;* ***C)*** *Between mean of biological replicates - WT and KO.*

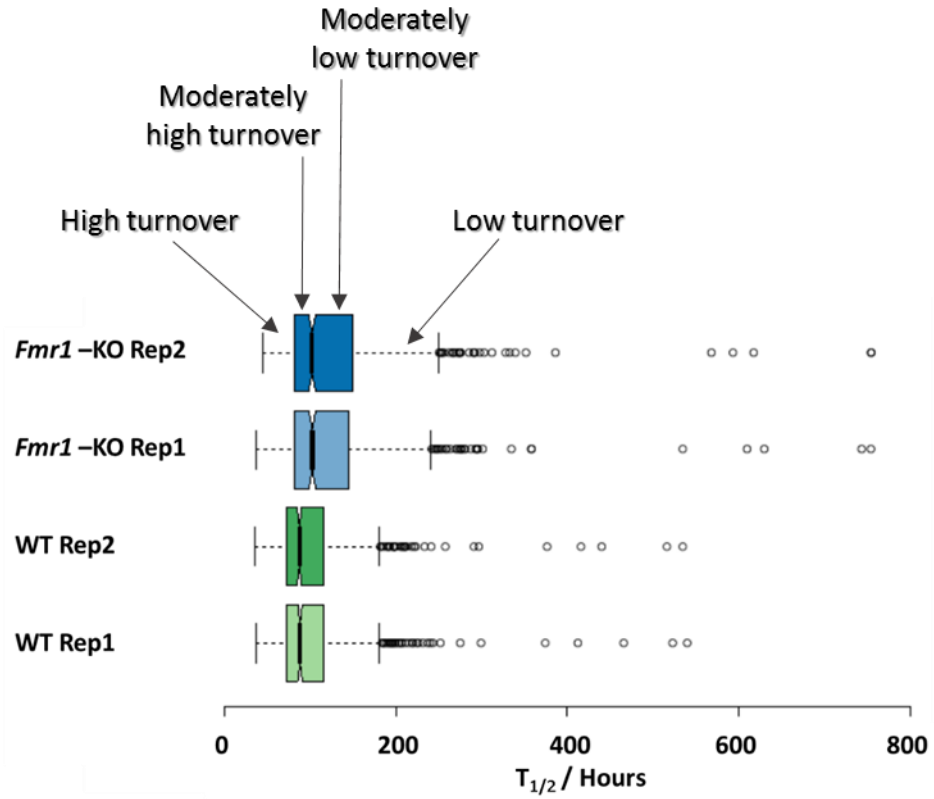

Figure IV.14 | Box plots of protein half-lives. *Green box plots represent WT and blue one Fmr1-KO.*

In WT and *Fmr1*-KO neurons proteins with the lowest turnover rate are proteins involved in oxidative phosphorylation, Alzheimer's, Parkinson's and Huntington's disease (**Figure IV.15 A**), whereas proteins with the highest turnover rate are involved in phagosome, Wnt signaling pathway and gap junction (**Figure IV.15 B**). Results of functional enrichment analysis for other processes are shown in **Supplementary Tables 12-15**. This analysis confirmed that the pool of proteins with high or low protein turnover does not differ between WT and *Fmr1*-KO neurons. However, it is evidently possible to distinguish proteins from different quartiles based on their involvement in different pathways and processes.

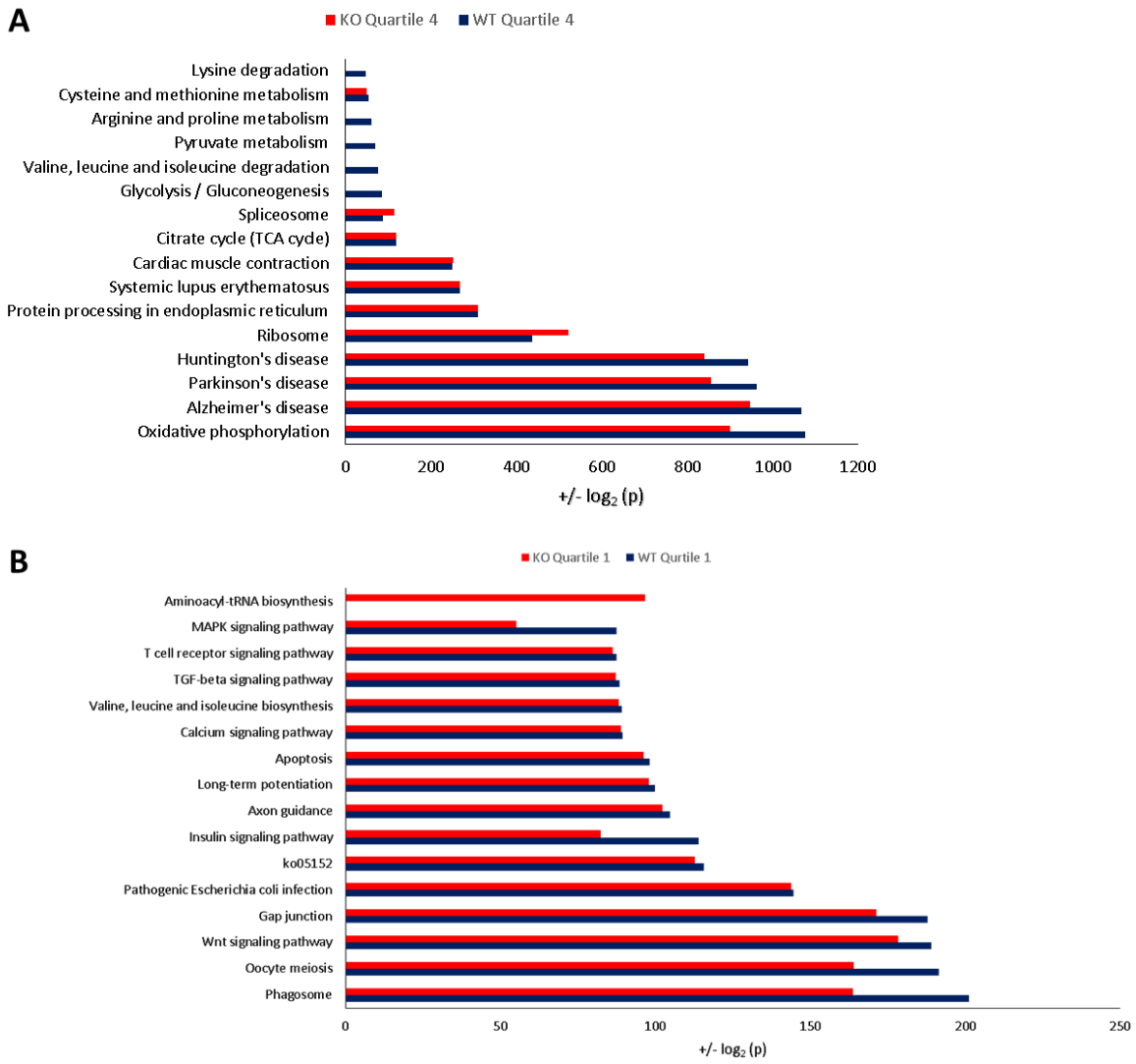

Figure IV.15 | Functional enrichment analysis in WT and Fmr1-KO neurons. A) *Enrichment of KEGG terms in quartile 4;* ***B)*** *Enrichment of KEGG terms in quartile 1 in first top 15 KEGG terms based on corrected p-values.*

IV.4. Global identification of differentially regulated proteins in mouse models of Fragile X Syndrome

This chapter of the thesis is manuscript in preparation from Matic el al.

It is believed that dysregulated translation and elevated protein synthesis is the main cause of the symptoms in fragile X patients. To this end, it is not clear which proteins are affected by this imbalance. Additionally, the connection between FXS and exaggerated mGluR5 signaling [78] was confirmed by pharmacological and genetic approaches (development of *Fmr1*-KO/*mGluR5* het KO cross – genetic rescue model of FXS). Therefore, in this part of the project we aimed to analyze differences in protein expression levels in the WT, the FXS mouse model, and the "FXS rescue" mouse model. To that end we measured nine biological replicates of the WT, *Fmr1* KO and *Fmr1*-KO/*mGluR5*-het cross mice hippocampi by employing label-free quantification. Furthermore, we applied total protein approach (TPA) to determine absolute protein levels [164].

All samples were measured using high resolution mass spectrometry, resulting in 81 LC/MS runs during 14 days of measuring time LTQ Orbitrap Velos or LTQ Orbitrap Elite (Thermo Fisher Scientific) coupled to the EASY-nLC II liquid chromatographer (Proxeon Biosystems). Workflow overview is shown in **Supplementary Figure IV.12**.

IV.4.1. Reproducibility and data validation

To test reproducibility we investigated Pearson correlation coefficient between protein intensities recorded in biological and technical replicates (**Figure IV.16**). As expected, correlation between measurements of same genotype was high (>0.8), and there was no major difference between different experiments and genotypes in comparison with biological replicates measured in the same experiment. Similar correlation between 27

samples pointed out that measured proteomes of the corresponding mice are very similar to each other.

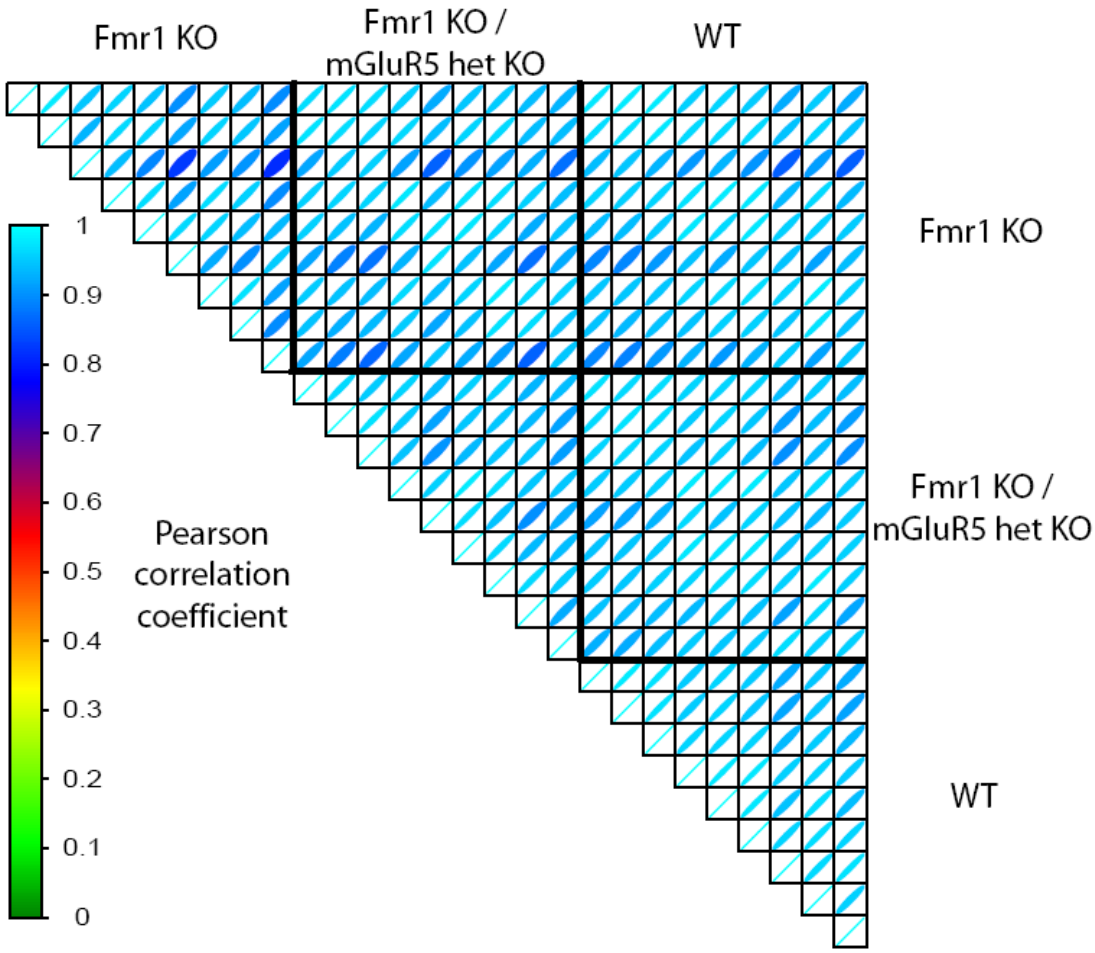

Figure IV.16 | Correlation matrix of all WT, Fmr1-KO and Fmr1-KO/mGluR5 het samples*. Color and thickness of the lines indicate correlation. The thicker the line is, correlation is higher.*

In order to validate our data, we looked for the positive controls: FMRP, which should be absent in *Fmr1*-KO mice; and mGluR5, which should be reduced by ca. 50% in *Fmr1*-KO/*mGluR5*-het mice (**Figure IV.17 A and Figure IV.17 B**). Although a low amount of FMRP was observed *Fmr1*-KO mice, manual inspection of the data revealed that this was an artifact of the "match between run (MBR)" option used during data processing

(**Supplementary Figure IV.13**). Additional validation for FMRP protein was done by Western blot in which FMRP is detectable in WT, but not in knockout mice (**Figure IV.17 C**). Importantly, the levels of mGluR5 were measured to be ca. 50% reduced in the *Fmr1*-KO/*mGluR5*-het mice, validating the ability of the label-free approach to quantify 2-fold changes in protein abundance in our dataset.

The connection between FXS and exaggerated mGluR5 activity was suggested by Bear et al. [78]. Still, it was unclear whether increased activity comes from increased expression of mGluR5, its increased activity, or both. There are few studies addressing this question [236, 237]. In our data, relative protein expression of mGluR5 in *Fmr1*-KO revealed no significant difference in comparison with WT, which is in agreement with results of Dolen et al [81]. (**Figure IV.17 B**).

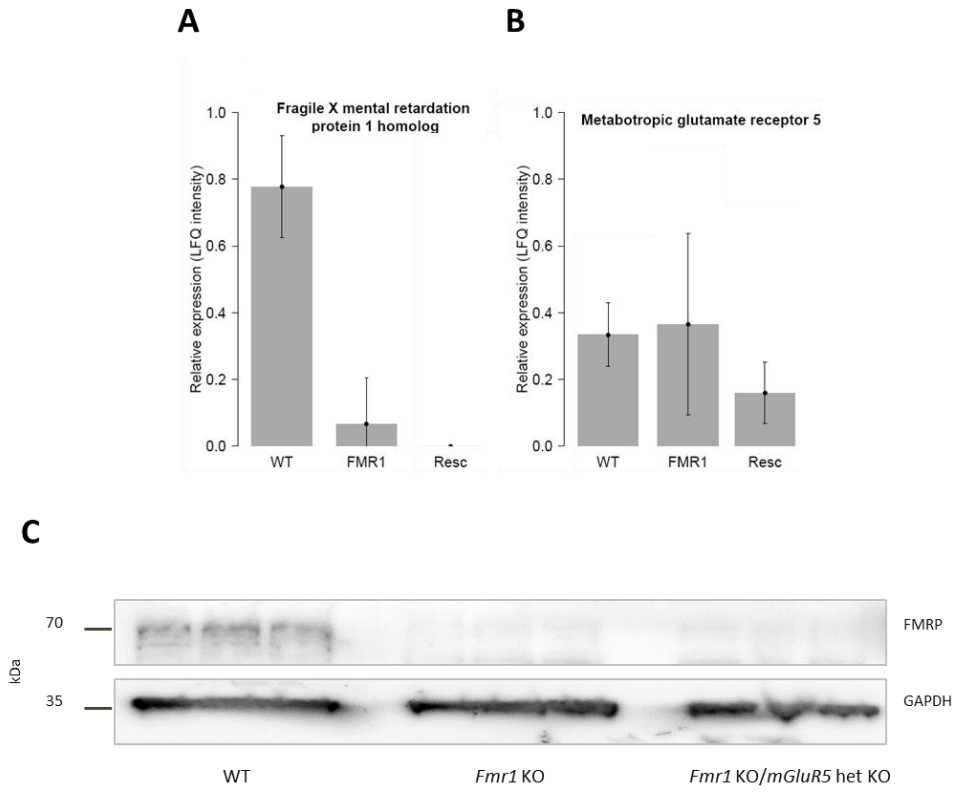

Figure IV.17 | Positive controls and data validation. A*) Relative expression of FMRP in WT, Fmr1-KO and Fmr1-KO/mGluR5;* ***B)*** *relative expression of mGluR5 in WT, Fmr1-KO and Fmr1-KO/mGluR5 het;* ***C)*** *Western blot analysis of FMRP in WT, Fmr1-KO and Fmr1-KO/mGluR5 het.*

IV.4.2. Quantitative proteome of FXS mouse models

Label free quantification analysis of WT, *Fmr1*-KO and *Fmr1*-KO/*mGluR5*-het cross mice resulted in 2,627,231 MS/MS spectra that identified 61,479 non-redundant peptides and 5,238 protein groups (**Supplementary table IV.16**). Estimation for the false discovery rate at the peptide level was 0.39% and at the protein group level 1.76%. After data was imputed, normalized, and LFQ intensities were log-transformed as described in the Methods, we applied ANOVA to test for differential expression of proteins among different genotypes. ANOVA analysis resulted in 68 significantly changing proteins between WT and *Fmr1*-KO, 45 between *Fmr1*-KO and *Fmr1*-KO/*mGluR5*-het cross mice and 106 between WT and *Fmr1*-KO/*mGluR5*-het cross mice. Summary of significantly upregulated and downregulated proteins is showed in **Table IV.7**.

Table IV.7 | Overview of significantly changing proteins in pairwise comparison. *Significantly changing proteins Fmr1-KO vs WT, Fmr1-KO vs Fmr1-KO_mGluR5-het and Fmr1-KO_mGluR5-het vs WT.*

	Significantly changing proteins		
	Fmr1-KO / WT	*Fmr1*-KO / *Fmr1*-KO_*mGluR5*-het	*Fmr1*-KO_mGluR5-het / WT
Downregulated	19	17	57
Upregulated	49	28	49

Principal component analysis (PCA) applied to the whole dataset initially could not show any significant difference between different genotypes **(Figure IV.18 A)**; however, it could separate genotypes when applied to significantly changing proteins only, indicating that these proteins indeed have different expression levels between tested mice **(Figure IV.18 B)**. As expected, PCA shows that two most distinct genotypes are WT and rescue mouse model. Next, we compared our dataset with known mRNA targets of FMRP [44]. Although 582 proteins overlapped with mRNA dataset, only two proteins had higher expression, while two had lower expression level in *Fmr1*-KO in comparison with WT. Although it is expected that a higher number of mRNA targets would have a higher

expression in *Fmr1*-KO (considering that FMRP should repress translation [68]), it seems that other controlling mechanisms are influencing protein level in the brain. We also note that the HITS-CLIP study that detected FMRP targets (41) was performed in a different tissue (whole mouse brain) and that it is lately debated whether it correctly reported endogenous FMRP targets [49].

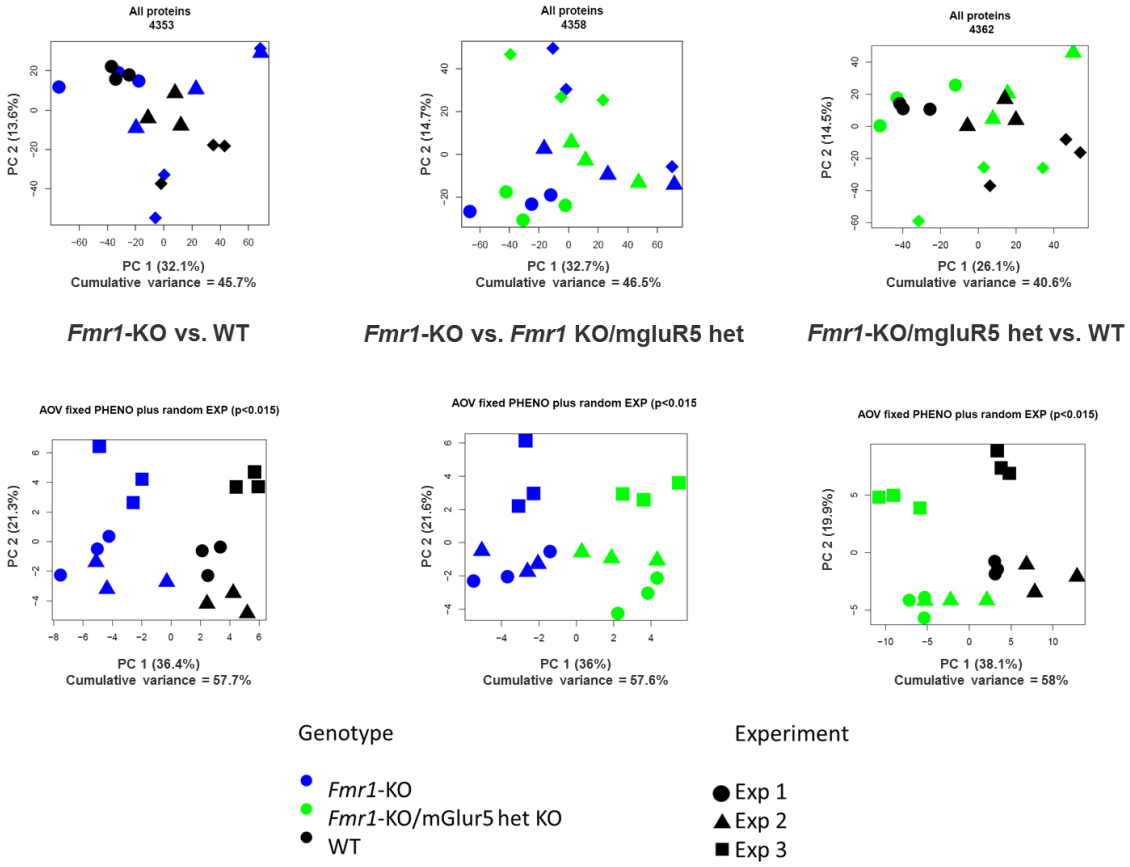

Figure IV.18 | Principal component analysis. ***A****) All proteins from corresponding compared pairs;* ***B)*** *Significantly changing proteins from corresponding compared pairs.*

One of the proteins with significantly different expression between WT and *Fmr*1-KO mice was the Major prion protein (PrP), which was shown to be downregulated in *Fmr*1-KO brain (**Figure IV.19 A**). Since Prp has a role in short and long memory processing [238,

239] and it could potentially be involved in pathogenesis of FXS, we validated the MS data by western blotting. Western blot results were in agreement with MS data, confirming that Prp has higher expression level in WT in comparison with *Fmr1*-KO (**Figure IV.19 B**).

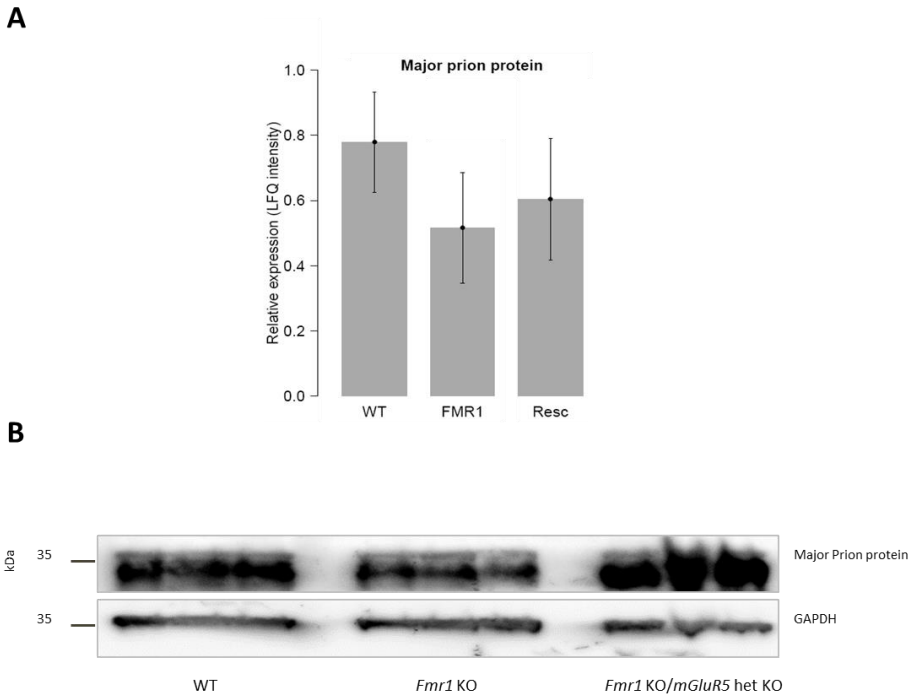

Figure IV.19 | Data validation. A*) Relative expression of PrP in WT, Fmr1-KO and Fmr1-KO/mGluR5 het;* ***B)*** *Western blot analysis of Prp in WT, Fmr1-KO and Fmr1-KO/mGluR5 het.*

IV.4.3. STRING analysis of significantly regulated proteins

A list of significantly changing proteins between WT and *Fmr1*-KO, *Fmr1*-KO and *Fmr1*-KO/*mGluR5*-het cross mice and WT and *Fmr1*-KO/*mGluR5*-het cross mice were separately uploaded to STRING (The Search Tool for the Retrieval of Interacting Genes) database [240, 241] to look for known and predicted protein interactions. Significantly changing proteins were uploaded together for every pairwise comparison.

STRING analysis of *Fmr1*-KO and WT revealed a node of ribosomal proteins which have higher protein expression in *Fmr1*-KO (**Figure IV.20**). It was reported that FMRP is associated with ribosomes [42, 242], mostly with the 60s ribosomal subunit, but association with the 40s ribosomal subunit was detected as well [243]. We detected many ribosomal proteins, but found six from 60s and three from 40s ribosomal subunit with higher expression in *Fmr1*-KO. Additionally, the same trend in terms of direction is observed for mitochondrial ribosomal proteins and mitochondrial transcription factors *Tfam* and *Gfm1*. Mitochondrial dysfunction was previously connected to Fragile X-associated tremor/ataxia syndrome and autism caused by increased nitrative/oxidative stress [244, 245]. Our data suggests that mitochondrial transcription regulation is also likely to be disturbed in FXS.

Moreover, some other proteins like scaffold proteins of the postsynaptic density (PSD) *Dlgap3*, AMPA-type glutamate receptor (AMPAR) subunit *Gria4* and dynamin-1 were detected as significantly downregulated. Considering their known function, they could be involved in FXS pathogenesis (see discussion).

Network analysis of *Fmr1*-KO and *Fmr1*-KO/*mGluR5*-het cross mice was performed in order to see a difference in mechanism between FXS mouse model and its rescue. Mostly, predicted interactions are between proteins involved in metabolism (**Supplementary Figure IV.14**). Small node with Citron Rho-interacting kinase (*Cit*) and Rho guanine nucleotide exchange factor 17 (*Afhgef17*), RNA targets reported by Darnell et al. [44], and Cell division control protein 42 homolog are downregulated in *Fmr1*-KO. These proteins are known to be involved in neurogenesis [246, 247]. Moreover, it was shown that *Cit* is functionally linked to *Fmr1* gene [248] and that this kinase is interacting with mGluR5 receptor[249]. Citron kinase is also known to form a complex with PSD-95 and it is concentrated at the postsynaptic side of glutaminergic synapses [250], therefore it is possible that this kinase plays an important role in the rescue mechanism of FXS. The most numerous group of significantly changing proteins resulted from WT and *Fmr1*-KO/*mGluR5*-het cross mice comparison (**Supplementary Figure IV.16**).

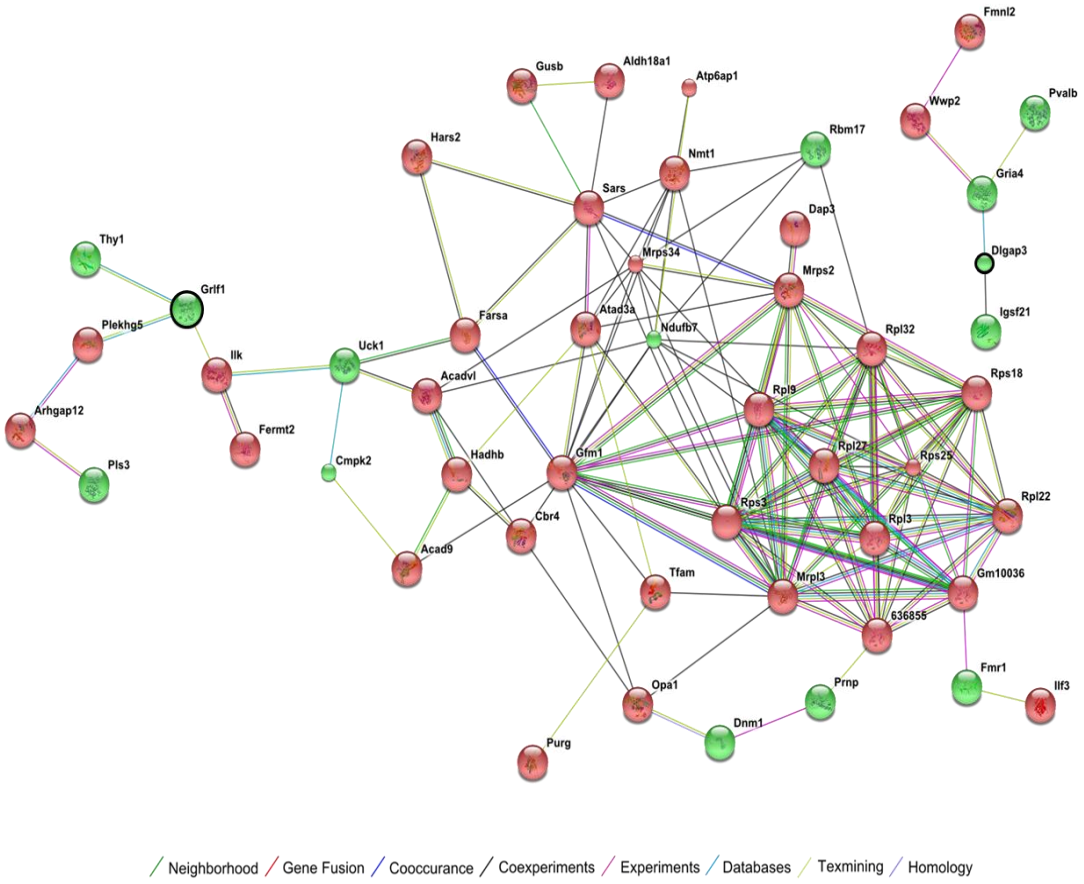

Figure IV.20 | STRING analysis*. Network of significantly changing proteins from pairwise analysis of Fmr1-KO and WT genotype. Red color indicates increased protein expression, and green decreased protein expression in Fmr1-KO, respectively. Black circles indicate that these proteins are overlapping with proteins from Darnell et al. dataset.*

This comparison shows that WT and rescue mouse model are the most diverse genotype groups, despite the fact that the FXS phenotype of the rescue model is more similar to WT than it is to Fmr1 KO. STRING analysis revealed a node of ribosomal proteins that have higher expression levels in the rescue model than in the WT. This indicates that the higher expression level of ribosomal proteins in FXS mouse model was not reverted by the reduction of mGluR5 activity and therefore likely does not play role in the rescue mechanism.

IV.4.4. Estimation of absolute protein levels

It was previously reported that protein synthesis is elevated in the hippocampus of Fragile X mouse model [51, 81, 181]. We applied the total protein approach (TPA) to estimate the absolute level of measured proteins in all three analyzed genotypes. Briefly, individual LFQ intensities were divided by the sum of all LFQ intensities of every protein of a sample which corresponds to the total MS signal of the proteome in that sample [164]. Comparison of absolute protein levels did not show any significant difference in absolute level between WT, *Fmr1*-KO and rescue mouse model. Surprisingly, when TPA was applied separately to significantly changing proteins, we observed that proteins with higher expression level in *Fmr1*-KO (in comparison to WT) tend to be more abundant than those with lower expression levels (**Figure IV.21**). We argue that this fact may be the reason for seemingly higher overall protein expression levels reported in previous studies (see discussion). Conversely, abundance of significantly changing proteins was similar in WT and the rescue model.

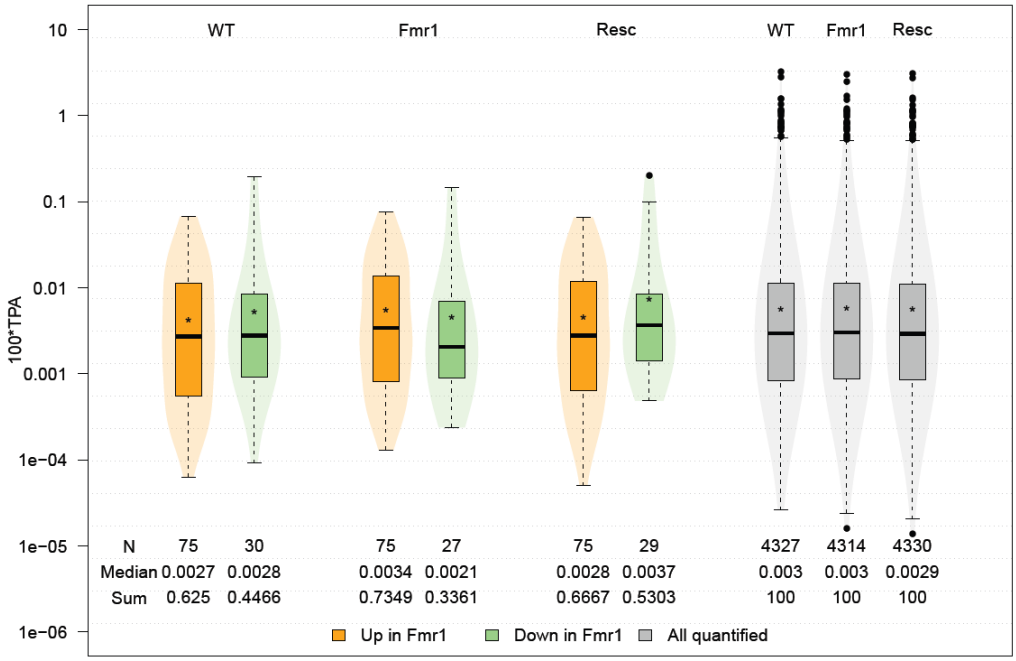

Figure IV.21 | Comparison of absolute protein abundance between WT, Fmr1-KO and Fmr1-KO/mGluR5 het. *TPA was calculated by dividing individual LFQ intensities by the sum of all LFQ intensities of every protein of a sample. Next, TPA values were multiply by 100 in order to get percentage scale (y axis).*

V DISCUSSION

Fragile X Syndrome (FXS), caused by silencing of the *Fmr1* gene and its product FMRP, is still a disorder with unclear pathology. Function of FMRP as an RNA binding protein with many targets related to protein synthesis and signal transduction pathways makes this disorder attractive to study using proteomic tools. Although lot of research was done in this field in the last decade, only a few studies applied global proteomic approaches [52, 53, 251]. Therefore, this thesis presents the first systematic proteomic large-scale analysis of different FXS models.

V.1. Quantitative phosphoproteomics of murine *Fmr1*-KO cell lines provides new insights into FMRP-dependent signal transduction mechanisms

Comparison of the proteome and phosphoproteome of the *Fmr1*-KO MEF cell lines, performed in this thesis, is the first global large-scale study on this cellular model of FXS. We detected 266 proteins and 146 phosphorylation events that are significantly changing between *Fmr1*$^{-}$ and *Fmr1*$^{+}$ MEF cells in both replicate measurements. By mapping proteins and phosphorylation events to the signaling pathways we confirmed downregulation of MAPK signaling pathway in *Fmr1*- cells, which was previously associated with FXS [224] and is dysregulated in other neurological disorders related to intellectual impairment [252, 253]. Other pathways like mTOR, Wnt, p53 and MAPK signaling pathway express several dysregulated proteins that were known to be associated with autism, but not with FXS. cPLA is an example which we validated by western blot. This enzyme is associated with long term potentiation (LTP), memory process, gene transcription and phospholipid turnover. Its increased protein level leads to disruption of the membrane structure which leads to cognitive impairment and increased oxidative stress [254] which is known to be associated with FXS [255]. In general, strong molecular overlap is connecting FXS and autism. Up to 35% individuals

with FXS are diagnosed with autism [6], therefore better understanding of molecular mechanism in FXS can be beneficial for better understanding of autism as well.

V.2. Inhibition of GSK-3β kinase in murine *Fmr1*-KO cell lines

This chapter of the thesis is manuscript in preparation from Matic el al.

When a kinase plays an important role in diverse pathways like GSK-3, it is not surprising that its regulation is implicated in different diseases. One of the disorders with disturbed GSK-3β activity is FXS. In different FXS models, increased GSK-3β activity has been inhibited using lithium (unspecific GSK-3β inhibitor), which showed a reversal of mGluR-dependent LTD [91], hyperactivity [92], learning deficits, dendritic spine shape, anxiety [93] and macroorchidism [94]. Therefore, GSK-3β is a promising target in treatment of FXS.

In order to better understand the function of the kinase, it is crucial to know its substrates. So far, around 100 substrates of GSK-3 are known, but it is believed that some are still undiscovered [229]. In order to look for new substrates in a large scale experiment, proteomics is a great tool of choice, which thus far has not been used in this context. Conventional approaches are normally labor- and time-consuming, with an outcome of one or few substrates, therefore proteomics screening could indeed result in a much higher number of substrates.

Here we applied a SILAC approach to compare the phosphoproteome of *Fmr1*$^{+}$ and *Fmr1*$^{-}$ MEF cells treated with lithium as an unspecific, and TDZD-8 as a specific inhibitor of GSK-3β kinase. Experiments were performed in biological replicates and showed low reproducibility in lithium treatment between replicates on the level of the proteome and phosphoproteome. One of the possible reasons for this could be weak and unspecific

interaction of lithium with GSK-3β, which would lead to unspecific inhibition of the kinase. Indeed, off-target effects of lithium have been previously reported [256]. Conversely, treatment with TDZD-8 showed a good correlation between biological replicates ($r > 0.7$) in *Fmr1*$^{+}$ MEF cells and a weak correlation in the *Fmr1*$^{-}$ MEF cells. We were interested in proteins with downregulated phosphorylation upon TDZD-8 treatment, since TDZD-8 is known to specifically inhibit GSK-3β and reduction of kinase activity should inevitably lead to a reduction of phosphorylation levels on its direct substrates. We focused on a total of 91 significantly decreased phosphorylation events in *Fmr1*$^{+}$ and 146 decreased phosphorylation events in *Fmr1*$^{-}$ MEF cells. Although the number of downregulated phosphorylation events seems to be higher in *Fmr1*$^{-}$ cells, it is important to note that poor reproducibility between replicates and generally lower extent of regulation point to impaired specificity of the kinase (or inhibitor) in *Fmr1*$^{-}$ cells. This result alone may reflect dysregulation of the kinase in FXS.

By comparing our data with the list of the reported GSK-3β substrates [229], we were able to confirm several of them; however most of our significantly decreased phosphorylation events present potential new substrates of the kinase. Approximately half of the potential substrates contain a GSK-3 motif, which is an additional supporting argument for a direct substrate, although it is known that the GSK-3 motif is not very specific, as one of the best known targets (β-catenin) does not contain it [231].

Correlation between TDZD-8 treatment in *Fmr1*$^{-}$ and *Fmr1*$^{+}$ cells showed different influence of the inhibitor in these two cell lines. Interestingly, overlap of significantly decreased phosphorylation events in *Fmr1*$^{-}$ and *Fmr1*$^{+}$ MEF cell lines revealed only two events that are common to both. Both phosphorylation events belong to the same tumor protein D54 that was previously not known as a GSK-3β substrate and is involved in cell growth and apoptosis. Moreover, functional enrichment analysis revealed implication of the potential substrates in cytoskeleton organization and actin binding in *Fmr1*$^{+}$ MEFs, while in *Fmr1*$^{-}$ MEFs potential substrates seem to be more involved in cell cycle, DNA

replication and RNA processing. Involvement of GSK-3β in cytoskeletal reorganization is well known [257], however the role of the kinase in DNA replication and mismatch repair was recently reported [258]. A study showed that inhibition of the kinase protects mouse hippocampal neurons from radiation by accelerating double strand–break efficiency [258]. Another study showed downregulation of DNA damage/repair pathway in FXS patients [259]. Therefore, these results could indeed implicate a different role of GSK-3β in MEF cells. Moreover, downregulation of 6 phosphorylation event on *MAP1B*, a well know substrate, was detected only in *Fmr1*$^{+}$ MEF cell line. When phosphorylated, *MAP1B* is coordinating microtubule dynamics and inhibition of these dynamics results in disturbed axon guidance and branching [260]. Since abnormal axon branching is one of the leading symptoms in FXS, we speculate that this could be a direct consequence of a dysregulation of the GSK-3β kinase in FXS. This could be due to disturbed priming phosphorylation, which is often required for GSK-3β substrate phosphorylation. Another reason could be disturbed MAPK pathway in FXS, or more specific ERK 1/2 kinases. It was shown that phosphorylation of *MAP1B* by GSK-3β requires activity of ERK 1/2 [261]. Since we showed a downregulation of the MAPK pathway in the FXS model, it is possible that the lack of regulation of *MAP1B* by GSK-3β in *Fmr1*$^{-}$ MEFs is a consequence of this aberrant signaling.

Fmr1-KO mouse embryonic fibroblasts (MEFs) is well established FXS model [67, 68], however, when studying implications of GSK-3β targets in neuronal development, another model (as neuronal cell line) with a similar approach should be considered due to a lack of expression of certain receptors and proteins that are not present in fibroblastic cell line.

V.3. Dynamic SILAC of WT and *Fmr1*-KO primary cortical neurons

In the cell, proteins are constantly synthetized and degraded. Therefore, different methods were developed in order to measure protein synthesis and turnover [122] , such

as different tagging strategies coupled with inhibition of translation [262]. Recent advances in proteomics have allowed a large scale determination of the protein turnover in cells using SILAC metabolic labeling. By using this approach, determination of protein half-lives was possible for hundreds of proteins at the same time [152]. While it is possible to completely label “standard” cells, neurons are considered more problematic due to the fact that they are not dividing. In 2008, Spellman et al. showed that neurons can achieve high level of SILAC incorporation (≥ 80%), and that SILAC can be applied to non-dividing cells [155]. We combined this knowledge and applied dynamic SILAC labeling of WT and *Fmr1*-KO primary cortical neurons in order to measure protein turnover and retrieve information about protein half-lives. To our knowledge, this is the first study of protein turnover in neurons.

Our first time point (DIV 2) had an incorporation rate of ~ 50%. Unfortunately, in this experimental design we were not able to get proteins with lower incorporation rates. Specifically, when neurons are seeded in the SILAC media they take 2 days to adhere, therefore earlier points would not be biologically appropriate. As a consequence, in this data we are missing proteins with fast protein turnover.

In addition to a global measurement of protein half-lives, we aimed to compare protein turnover between neurons derived from WT and *Fmr1*-KO mice. WT neurons showed approximately 5% higher incorporation rate than *Fmr1*-KO neurons, pointing to the higher overall turnover in WT neurons. This was also reflected in the median of the half-lives in *Fmr1*-KO neurons median, which was 102 hours compared to only 88 hours in the WT, again indicating higher turnover in WT neurons. This was surprising, considering the fact that one of the main problems in FXS is elevated protein synthesis, which, if compensated by protein degradation, should lead to higher turnover in *Fmr1*-KO neurons. However, as mentioned before, we could not cover earlier time points and it is possible that faster protein synthesis, combined with rapid protein degradation, lead to turnover times that were below the limit of our detection.

In general, when we looked at the individual protein half-live difference between WT and *Fmr1*-KO we were not able to find any statistically significant change. However, we could see the difference between the proteins with high and low protein turnover based on their involvement in different pathways and processes. In addition, it is possible that proteins with fast protein turnover are carrying the difference between WT and *Fmr1*-KO, which we are not able to see with our current experimental design. The experimental design could be changed in a way that two groups of neurons are grown at the same time. The first group of the neurons should be grown in "light" and the second in "heavy" medium. After the neurons are attached (around two days), "light" medium can be exchanged with "heavy" medium because it should contain all different factors that neurons excreted in first two days, and that are needed for neuronal survival. Since neurons should be starting to incorporate "heavy" labels after they are attached, early points could be collected. This experimental approach currently being implemented.

Nevertheless, even without early time points, for the first time, we showed that it is possible to use the SILAC approach in primary neurons to retrieve information about protein half-lives which is useful for the research community.

V.4. Global identification of differentially regulated proteins in mouse models of Fragile X Syndrome

This chapter of the thesis is manuscript in preparation from Matic el al.

The main problem in FXS is dysregulated translation and elevated protein synthesis. So far, it is not very clear which and how many proteins, and their levels are influenced by this dysregulation. In addition, suggested connection of FXS and exaggerated mGluR5 signaling [78] led to the development of *Fmr1*-KO/*mGluR5* het KO cross – genetic rescue model of FXS , which showed correction of most of FXS symptoms [78]. Therefore, we

aimed to analyze differences in protein expression levels in the WT, the FXS mouse model, and the "FXS rescue" mouse model. This data represents the biggest proteome-wide quantitative comparison of protein levels in the hippocampi between WT, *Fmr1*-KO mice and *Fmr1*-KO/*mGluR5*-het cross mice. *Fmr1*-KO mouse model is a reliable FXS model that recapitulates several cellular and behavioral phenotypes of FXS, while *Fmr1*-KO/*mGluR5* het KO cross is a great genetic rescue model whose better understanding could help to gain more insights in the FXS pathogenesis.

Phenotypically these three mice models are easily distinguishable. However, Pearson correlation between biological replicates and different genotypes revealed no major difference at the proteome level, which means that these mice are, surprisingly, very similar to each other. Nevertheless, we aimed to look for proteins that are significantly changing between these genotypes by applying pairwise ANOVA analysis and looking for known protein interactions among them. In *Fmr1*-KO and WT comparison we found significantly regulated proteins that are known to be involved in involved in memory, learning and LTP and moreover, our data suggests that mitochondrial transcription regulation is disturbed in FXS model.

Interestingly, scaffold proteins of the postsynaptic density (PSD) *Dlgap3* and AMPA-type glutamate receptor (AMPAR) subunit *Gria4* were detected as significantly downregulated. The mRNA of *Dlgap3* is a reported target of FMRP [44, 196, 263]. Schütt et al. analyzed protein levels of PSD in 2 weeks and 2 months old mice and observed an increase in protein levels of *Dlgap3* only in hippocampus of 2-month old mice. Another study reported a decreased level of *Dlgap3* in prefrontal cortex of 2-4 months old *Fmr1*-KO mice [264]. Among other symptoms, FXS mouse model includes compulsive repetitive behaviors. It is known that a loss of *Dlgap3* leads to the same behaviors which was shown in *Dlgap3* KO mouse model [265]. Wan et al. studied effects of *Dlgap3* deletion on AMPAR synaptic transmission [266]. They found that a *Dlgap3* deletion is causing a reduction in AMPAR-mediated neurotransmission which can be reversed by reducing

mGluR5 activity. It is known that regulation of AMPAR trafficking has an important role in synaptic plasticity process involved in memory and learning [72, 267]. Nakamoto et al. observed that AMPAR internalization, a major mechanism for synaptic depression, is increased in FMRP deficient dendrites as a result of exaggerated mGluR5 signaling [80]. Our data suggests that a decreased protein level of *Gria4* can be the consequence of a decreased protein level of *Dlgap3.* In addition, it is possible that the protein level of *Dlgap3* depends on the age of the mice and that its decreased level plays important role during early development that can influence mice behavior later.

It is known that AMPAR endocytosis which occurs via clathrin-mediated endocytosis requires activity of dynamin [268]. Dynamin 1 is the main dynamin isoform in the neurons [269]. Recently, it was shown that dynamin-1 is involved in memory formation and its inhibition leads to reduced LTP [270]. In our dataset we observed downregulation of dynamin-1 in *Fmr1*-KO mice.

In the network analysis of FXS and rescue model, we expected to see proteins involved in the rescue mechanism. Considering mGluR5 theory, these proteins should be upregulated in FXS model in comparison with rescue model. Most of the proteins with this trend seem to be involved in metabolism. Unexpectedly, ones that are overlapping with known RNA targets from FMRP [44] are showing the opposite effect.

Overlapping our data with known RNA targets [44] of FMRP serves as an additional validation of our data. However, overlap in this project, as well in proteome and the phosphoproteome of the *Fmr1*-KO MEF cell lines project, turns to be quite poor when it comes to a significantly changing proteins. Since FMRP is established as an RNA-binding protein which inhibits translation [68], it is expected, if certain protein is a FMRP target, to have increased protein level in FXS model. However, in our data we have only few proteins with increased protein levels, while others are having decreased levels. “Proteomic” cause of limited overlap could come from uncompleted proteome coverage or additional regulatory mechanisms that could influence the final protein level. Recently published work showed that previously reported FMRP targets disproportionally

represent the most abundant mRNAs, as well as ones with the longest coding sequence [49]. Thus, it seems to be clear that there is a certain bias in the reported list of mRNA targets of FMRP. Moreover, we showed that most of the proteins that are significantly changing in our data are in the range of lower abundant proteins and therefore more prone to quantification error. Therefore, we note that the overlap of proteomic and transcriptomic data should not be strictly required to validate direct targets of FMRP.

Increased protein synthesis is one of the hallmarks of FXS. By using radioactive metabolic labeling in mouse hippocampal slices it was shown that total protein content is elevated around 10% in the FXS model [81, 181]. Since it is not clear whether this is a consequence of increased synthesis of the whole proteome or only of its fraction, we estimated absolute protein amount in the measured samples. Our results showed no difference in the total proteome of all three genotypes. However, we did observe the change in the FXS model when absolute protein amounts were calculated only for significantly changing proteins: proteins with higher expression level in *Fmr1*-KO tend to be more abundant that those that have lower expression level, which leads to imbalance that – when analyzed by methods that address only complete proteome, such as global 32S incorporation – may be reflected as overall increase of protein expression. Therefore, our results indicates that the previously reported increased global protein synthesis in *Fmr1*-KO can rather be driven by a relatively small number of upregulated proteins rather than the whole proteome. Our additional observation was that regulated proteins in WT and rescue model have a similar abundance. This observation is in agreement with the study from Dolen et al. [81] which reported a reduction of increased protein synthesis level in hippocampal slices by selective reduction in the mGluR*5* gene. However, considering the fact that the portion of the proteins that are changing is rather small (<1%), this hypothesis is not statistically significant. Our results can be explained by the fact that we measured only around one quarter of estimated proteome or that we cannot detect very small change in the proteome due to technical lack of our method.

VI CONCLUSIONS

In this thesis several different proteomic approaches were applied to different cellular and animal models of fragile X syndrome in order to gain better understanding of the molecular mechanisms of the disorder. The following conclusions can be drawn from the obtained results:

1) Analysis of signal transduction pathways involved in the pathogenesis of FXS at the phosphoproteome level in SILAC-labeled murine *Fmr1*$^{-}$ and *Fmr1*$^{+}$ fibroblastic cell lines
    a. Our study represents the first global large-scale analysis of proteome and phosphoproteome of the *Fmr1*-KO MEF cell lines in which we detected 266 proteins and 142 phosphorylation sites that are significantly changing in both biological replicates.
    b. We confirmed a downregulation of the MEK/ERK pathway in absence of FMRP, with decreased phosphorylation on ERK1/2. We detected differential expression of several proteins involved in mTOR, Wnt, p53 and MAPK signaling cascades, that were known to be associated with autism, but not with FXS. Significant increase of p53 and several related proteins revealed for the first time involvement of p53 signaling in molecular pathogenesis of FXS, while decrease in Wnt/calcium pathway pointed to problems in calcium homeostasis. In addition, we detected a significantly reduced level of the major prion protein that could have an important role in cognitive deficits in FXS patients.
2) Identification of potential new GSK-3β substrates in SILAC-labeled murine *Fmr1*$^{-}$ and *Fmr1*$^{+}$ fibroblastic cell lines using GSK-3β inhibition by lithium and TDZD-8
    a. Our study revealed a total of 180 phosphorylation sites in *Fmr1*$^{+}$ MEF cells and 276 phosphorylation sites in *Fmr1*$^{-}$ MEF cells that were significantly changing in at least one biological replicate upon lithium treatment; 215

phosphorylation sites were significantly changing in *Fmr1*$^{+}$ MEF cells and 265 phosphorylation sites in *Fmr1*$^{-}$ MEF cells upon TDZD-8 treatment.

b. Lithium treatment led to unspecific inhibition of the kinase, as reflected in poor reproducibility between biological replicates. Reproducibility was much better in TDZD-8 treatment, where we quantified 91 significantly downregulated phosphorylation sites in *Fmr1*$^{+}$ MEF cells and 146 in *Fmr1*$^{-}$ MEF cells. Most of these events are potential new substrates of GSK-3β.

c. We postulate that specificity of the GSK-3β kinase is decreased in *Fmr1*$^{-}$ MEF cells but not in *Fmr1*$^{+}$ cells. Expected downregulation of multiple phosphorylation events on *MAP1B*, a well characterized GSK-3β substrate, was observed only in *Fmr1*$^{+}$ MEF cell line treated with TDZD-8. Since *MAP1B* is coordinating microtubule dynamics and abnormal axon branching is one of the leading symptoms of FXS, therefore we postulate that the lack of regulation of *MAP1B* by GSK-3β is a likely cause for aberrant morphology of neurons in FXS.

3) Measurement of protein turnover based on dynamic-SILAC method in primary cortical neuronal culture (*Fmr1*-KO and WT)

a. This data represents the first large scale analysis of protein turnover in primary neuronal culture of WT and FXS model. We identified 2,557 proteins, and calculated half-lifes for 622 proteins.

b. WT neurons showed slightly higher incorporation rate than *Fmr1*-KO neurons. However, there was no significant change in individual protein half-live between WT and *Fmr1*-KO.

4) Analysis of pathways involved in the pathogenesis and genetic rescue of FXS at the proteome level in mouse hippocampus

a. This data represents the largest proteome-wide quantitative comparison of protein levels in the hippocampi between WT, *Fmr1* KO mice and *Fmr1* KO/*mGluR5*-het cross mice. Pairwise comparison of the genotypes

confirmed known data, but also revealed dysregulation of additional proteins known to be involved in involved in memory, learning and LTP. Moreover, we also detected potential disruption of mitochondrial transcription regulation in FXS model. We confirmed a reduced level of the major prion protein in the FXS mouse model, observed in the first part of the thesis, which additionally pointed to its involvement in pathogenesis of FXS.

b. We did not observe a significant difference in the total proteome expression levels between the three analyzed genotypes. Data showed a modest change in FXS model when absolute protein amounts were observed separately for significantly changing proteins. This points to the fact that previously observed global increase of protein synthesis in the neurons of FXS mice may in fact be carried by relatively few abundant proteins that are increasingly synthesized in FXS.

VII REFERENCES

1. Martin, J.P. and J. Bell, *A Pedigree of Mental Defect Showing Sex-Linkage.* J Neurol Psychiatry, 1943. **6**(3-4): p. 154-7.
2. Coffee, B., et al., *Incidence of fragile X syndrome by newborn screening for methylated FMR1 DNA.* Am J Hum Genet, 2009. **85**(4): p. 503-14.
3. Belmonte, M.K. and T. Bourgeron, *Fragile X syndrome and autism at the intersection of genetic and neural networks.* Nat Neurosci, 2006. **9**(10): p. 1221-5.
4. Rossignol, R., et al., *Visual sensorial impairments in neurodevelopmental disorders: evidence for a retinal phenotype in fragile x syndrome.* PLoS One, 2014. **9**(8): p. e105996.
5. Sullivan, K., et al., *ADHD symptoms in children with FXS.* Am J Med Genet A, 2006. **140**(21): p. 2275-88.
6. Wang, L.W., E. Berry-Kravis, and R.J. Hagerman, *Fragile X: leading the way for targeted treatments in autism.* Neurotherapeutics, 2010. **7**(3): p. 264-74.
7. Lubs, H.A., *A marker X chromosome.* Am J Hum Genet, 1969. **21**(3): p. 231-44.
8. Krawczun, M.S., E.C. Jenkins, and W.T. Brown, *Analysis of the fragile-X chromosome: localization and detection of the fragile site in high resolution preparations.* Hum Genet, 1985. **69**(3): p. 209-11.
9. Verkerk, A.J., et al., *Identification of a gene (FMR-1) containing a CGG repeat coincident with a breakpoint cluster region exhibiting length variation in fragile X syndrome.* Cell, 1991. **65**(5): p. 905-14.
10. Pfeiffer, B.E. and K.M. Huber, *The state of synapses in fragile X syndrome.* Neuroscientist, 2009. **15**(5): p. 549-67.
11. Kenneson, A., et al., *Reduced FMRP and increased FMR1 transcription is proportionally associated with CGG repeat number in intermediate-length and premutation carriers.* Hum Mol Genet, 2001. **10**(14): p. 1449-54.
12. Tassone, F., et al., *Elevated FMR1 mRNA in premutation carriers is due to increased transcription.* RNA, 2007. **13**(4): p. 555-62.
13. Penagarikano, O., J.G. Mulle, and S.T. Warren, *The pathophysiology of fragile x syndrome.* Annu Rev Genomics Hum Genet, 2007. **8**: p. 109-29.
14. Feng, Y., et al., *Translational suppression by trinucleotide repeat expansion at FMR1.* Science, 1995. **268**(5211): p. 731-4.
15. Hagerman, R., G. Hoem, and P. Hagerman, *Fragile X and autism: Intertwined at the molecular level leading to targeted treatments.* Mol Autism, 2010. **1**(1): p. 12.
16. Gedeon, A.K., et al., *Fragile X syndrome without CCG amplification has an FMR1 deletion.* Nat Genet, 1992. **1**(5): p. 341-4.
17. Hammond, L.S., et al., *Fragile X syndrome and deletions in FMR1: new case and review of the literature.* Am J Med Genet, 1997. **72**(4): p. 430-4.
18. Hirst, M., et al., *Two new cases of FMR1 deletion associated with mental impairment.* Am J Hum Genet, 1995. **56**(1): p. 67-74.

19. Wohrle, D., et al., *A microdeletion of less than 250 kb, including the proximal part of the FMR-I gene and the fragile-X site, in a male with the clinical phenotype of fragile-X syndrome.* Am J Hum Genet, 1992. **51**(2): p. 299-306.
20. De Boulle, K., et al., *A point mutation in the FMR-1 gene associated with fragile X mental retardation.* Nat Genet, 1993. **3**(1): p. 31-5.
21. Fisch, G.S., et al., *Longitudinal study of cognitive abilities and adaptive behavior levels in fragile X males: a prospective multicenter analysis.* Am J Med Genet, 1996. **64**(2): p. 356-61.
22. Fisch, G.S., et al., *Longitudinal changes in cognitive and adaptive behavior in fragile X females: a prospective multicenter analysis.* Am J Med Genet, 1999. **83**(4): p. 308-12.
23. Tassone, F., et al., *Clinical involvement and protein expression in individuals with the FMR1 premutation.* Am J Med Genet, 2000. **91**(2): p. 144-52.
24. Kanellopoulos, A.K., et al., *Learning and Memory Deficits Consequent to Reduction of the Fragile X Mental Retardation Protein Result from Metabotropic Glutamate Receptor-Mediated Inhibition of cAMP Signaling in Drosophila.* The Journal of Neuroscience, 2012. **32**(38): p. 13111-13124.
25. Bhakar, A.L., G. Dölen, and M.F. Bear, *The Pathophysiology of Fragile X (and What It Teaches Us about Synapses).* Annual Review of Neuroscience, 2012. **35**(1): p. 417-443.
26. Pirozzi, F., E. Tabolacci, and G. Neri, *The FRAXopathies: definition, overview, and update.* Am J Med Genet A, 2011. **155A**(8): p. 1803-16.
27. Frolli, A., S. Piscopo, and M. Conson, *Developmental changes in cognitive and behavioural functioning of adolescents with fragile-X syndrome.* J Intellect Disabil Res, 2014.
28. Talisa, V.B., et al., *Autism and anxiety in males with fragile X syndrome: an exploratory analysis of neurobehavioral profiles from a parent survey.* Am J Med Genet A, 2014. **164A**(5): p. 1198-203.
29. Wheeler, A., et al., *Anxiety, attention problems, hyperactivity, and the Aberrant Behavior Checklist in fragile X syndrome.* Am J Med Genet A, 2014. **164A**(1): p. 141-55.
30. Heard, T.T., et al., *EEG abnormalities and seizures in genetically diagnosed Fragile X syndrome.* Int J Dev Neurosci, 2014.
31. Musumeci, S.A., et al., *Epilepsy and EEG findings in males with fragile X syndrome.* Epilepsia, 1999. **40**(8): p. 1092-9.
32. Turner, G., A. Daniel, and M. Frost, *X-linked mental retardation, macro-orchidism, and the Xq27 fragile site.* J Pediatr, 1980. **96**(5): p. 837-41.
33. Opitz, J.M., J.M. Westphal, and A. Daniel, *Discovery of a connective tissue dysplasia in the Martin-Bell syndrome.* Am J Med Genet, 1984. **17**(1): p. 101-9.
34. Hagerman, R.J., et al., *Consideration of connective tissue dysfunction in the fragile X syndrome.* Am J Med Genet, 1984. **17**(1): p. 111-21.
35. Rousseau, F., et al., *A multicenter study on genotype-phenotype correlations in the fragile X syndrome, using direct diagnosis with probe StB12.3: the first 2,253 cases.* Am J Hum Genet, 1994. **55**(2): p. 225-37.
36. Verkerk, A.J., et al., *Alternative splicing in the fragile X gene FMR1.* Hum Mol Genet, 1993. **2**(4): p. 399-404.
37. Bailey, D.B., Jr., et al., *Co-occurring conditions associated with FMR1 gene variations: findings from a national parent survey.* Am J Med Genet A, 2008. **146A**(16): p. 2060-9.

38. Devys, D., et al., *The FMR-1 protein is cytoplasmic, most abundant in neurons and appears normal in carriers of a fragile X premutation.* Nat Genet, 1993. **4**(4): p. 335-40.
39. Santoro, M.R., S.M. Bray, and S.T. Warren, *Molecular Mechanisms of Fragile X Syndrome: A Twenty-Year Perspective.* Annu Rev Pathol, 2011.
40. Feng, Y., et al., *Fragile X mental retardation protein: nucleocytoplasmic shuttling and association with somatodendritic ribosomes.* J Neurosci, 1997. **17**(5): p. 1539-47.
41. Ashley, C.T., Jr., et al., *FMR1 protein: conserved RNP family domains and selective RNA binding.* Science, 1993. **262**(5133): p. 563-6.
42. Khandjian, E.W., et al., *The fragile X mental retardation protein is associated with ribosomes.* Nat Genet, 1996. **12**(1): p. 91-3.
43. Corbin, F., et al., *The fragile X mental retardation protein is associated with poly(A)+ mRNA in actively translating polyribosomes.* Hum Mol Genet, 1997. **6**(9): p. 1465-72.
44. Darnell, J.C., et al., *FMRP stalls ribosomal translocation on mRNAs linked to synaptic function and autism.* Cell, 2011. **146**(2): p. 247-61.
45. Bagni, C. and W.T. Greenough, *From mRNP trafficking to spine dysmorphogenesis: the roots of fragile X syndrome.* Nat Rev Neurosci, 2005. **6**(5): p. 376-87.
46. Darnell, J.C. and E. Klann, *The translation of translational control by FMRP: therapeutic targets for FXS.* Nat Neurosci, 2013. **16**(11): p. 1530-6.
47. Ule, J., et al., *CLIP Identifies Nova-Regulated RNA Networks in the Brain.* Science, 2003. **302**(5648): p. 1212-1215.
48. Ascano, M., et al., *FMRP targets distinct mRNA sequence elements to regulate protein expression.* Nature, 2012.
49. Ouwenga, R.L. and J. Dougherty, *Fmrp targets or not: long, highly brain-expressed genes tend to be implicated in autism and brain disorders.* Mol Autism, 2015. **6**: p. 16.
50. Li, Z., et al., *The fragile X mental retardation protein inhibits translation via interacting with mRNA.* Nucleic Acids Res, 2001. **29**(11): p. 2276-83.
51. Qin, M., et al., *Postadolescent changes in regional cerebral protein synthesis: an in vivo study in the FMR1 null mouse.* J Neurosci, 2005. **25**(20): p. 5087-95.
52. Liao, L., et al., *Quantitative proteomic analysis of primary neurons reveals diverse changes in synaptic protein content in fmr1 knockout mice.* Proc Natl Acad Sci U S A, 2008. **105**(40): p. 15281-6.
53. Klemmer, P., et al., *Proteomics, Ultrastructure, and Physiology of Hippocampal Synapses in a Fragile X Syndrome Mouse Model Reveal Presynaptic Phenotype.* Journal of Biological Chemistry, 2011. **286**(29): p. 25495-25504.
54. Xu, P., et al., *Stable Isotope Labeling with Amino Acids in Drosophila for Quantifying Proteins and Modifications.* Journal of Proteome Research, 2012.
55. Hamada, A., et al., *Loss-of-function analyses of the fragile X-related and dopamine receptor genes by RNA interference in the cricket Gryllus bimaculatus.* Dev Dyn, 2009. **238**(8): p. 2025-33.
56. Winograd, C. and S. Ceman, *Exploring the zebra finch Taeniopygia guttata as a novel animal model for the speech-language deficit of fragile X syndrome.* Results Probl Cell Differ, 2012. **54**: p. 181-97.
57. Zhang, Y.Q., et al., *Drosophila fragile X-related gene regulates the MAP1B homolog Futsch to control synaptic structure and function.* Cell, 2001. **107**(5): p. 591-603.
58. Morales, J., et al., *Drosophila fragile X protein, DFXR, regulates neuronal morphology and function in the brain.* Neuron, 2002. **34**(6): p. 961-72.

59. Dockendorff, T.C., et al., *Drosophila lacking dfmr1 activity show defects in circadian output and fail to maintain courtship interest.* Neuron, 2002. **34**(6): p. 973-84.
60. The Dutch-Belgian Fragile, X.C., et al., *Fmr1 knockout mice: A model to study fragile X mental retardation.* Cell, 1994. **78**(1): p. 23-33.
61. Comery, T.A., et al., *Abnormal dendritic spines in fragile X knockout mice: maturation and pruning deficits.* Proc Natl Acad Sci U S A, 1997. **94**(10): p. 5401-4.
62. Dobkin, C., et al., *Fmr1 knockout mouse has a distinctive strain-specific learning impairment.* Neuroscience, 2000. **100**(2): p. 423-9.
63. Chen, L. and M. Toth, *Fragile X mice develop sensory hyperreactivity to auditory stimuli.* Neuroscience, 2001. **103**(4): p. 1043-50.
64. Musumeci, S.A., et al., *Audiogenic seizures susceptibility in transgenic mice with fragile X syndrome.* Epilepsia, 2000. **41**(1): p. 19-23.
65. Mazroui, R., et al., *Trapping of messenger RNA by Fragile X Mental Retardation protein into cytoplasmic granules induces translation repression.* Hum Mol Genet, 2002. **11**(24): p. 3007-17.
66. Mazroui, R., et al., *Fragile X Mental Retardation protein determinants required for its association with polyribosomal mRNPs.* Hum Mol Genet, 2003. **12**(23): p. 3087-96.
67. Castets, M., et al., *FMRP interferes with the Rac1 pathway and controls actin cytoskeleton dynamics in murine fibroblasts.* Human Molecular Genetics, 2005. **14**(6): p. 835-844.
68. Bechara, E.G., et al., *A novel function for fragile X mental retardation protein in translational activation.* PLoS Biol, 2009. **7**(1): p. e16.
69. Matic, K., et al., *Quantitative Phosphoproteomics of Murine Fmr1-KO Cell Lines Provides New Insights into FMRP-Dependent Signal Transduction Mechanisms.* J Proteome Res, 2014. **13**(10): p. 4388-97.
70. Cajal, S.R.Y., *The Croonian Lecture: La Fine Structure des Centres Nerveux.* Proceedings of the Royal Society of London, 1894. **55**(331-335): p. 444-468.
71. Hughes, J.R., *Post-tetanic potentiation.* Physiol Rev, 1958. **38**(1): p. 91-113.
72. Malenka, R.C. and M.F. Bear, *LTP and LTD: An Embarrassment of Riches.* Neuron, 2004. **44**(1): p. 5-21.
73. Oliet, S.H., R.C. Malenka, and R.A. Nicoll, *Two distinct forms of long-term depression coexist in CA1 hippocampal pyramidal cells.* Neuron, 1997. **18**(6): p. 969-82.
74. Cracco, J.B., et al., *Protein synthesis-dependent LTP in isolated dendrites of CA1 pyramidal cells.* Hippocampus, 2005. **15**(5): p. 551-556.
75. Huber, K.M., M.S. Kayser, and M.F. Bear, *Role for rapid dendritic protein synthesis in hippocampal mGluR-dependent long-term depression.* Science, 2000. **288**(5469): p. 1254-7.
76. Weiler, I.J., et al., *Fragile X mental retardation protein is translated near synapses in response to neurotransmitter activation.* Proc Natl Acad Sci U S A, 1997. **94**(10): p. 5395-400.
77. Laggerbauer, B., et al., *Evidence that fragile X mental retardation protein is a negative regulator of translation.* Hum Mol Genet, 2001. **10**(4): p. 329-38.
78. Bear, M.F., K.M. Huber, and S.T. Warren, *The mGluR theory of fragile X mental retardation.* Trends Neurosci, 2004. **27**(7): p. 370-7.
79. de Vrij, F.M., et al., *Rescue of behavioral phenotype and neuronal protrusion morphology in Fmr1 KO mice.* Neurobiol Dis, 2008. **31**(1): p. 127-32.

80. Nakamoto, M., et al., *Fragile X mental retardation protein deficiency leads to excessive mGluR5-dependent internalization of AMPA receptors.* Proc Natl Acad Sci U S A, 2007. **104**(39): p. 15537-42.
81. Dolen, G., et al., *Correction of fragile X syndrome in mice.* Neuron, 2007. **56**(6): p. 955-62.
82. Krueger, D.D. and M.F. Bear, *Toward fulfilling the promise of molecular medicine in fragile X syndrome.* Annu Rev Med, 2011. **62**: p. 411-29.
83. Frame, S. and P. Cohen, *GSK3 takes centre stage more than 20 years after its discovery.* Biochem J, 2001. **359**(Pt 1): p. 1-16.
84. Soutar, M.P., et al., *Evidence that glycogen synthase kinase-3 isoforms have distinct substrate preference in the brain.* J Neurochem, 2010. **115**(4): p. 974-83.
85. Jope, R.S., C.J. Yuskaitis, and E. Beurel, *Glycogen synthase kinase-3 (GSK3): inflammation, diseases, and therapeutics.* Neurochem Res, 2007. **32**(4-5): p. 577-95.
86. Mines, M.M. and R.S. Jope, *Glycogen synthase kinase-3: A promising therapeutic target for Fragile X Syndrome.* Frontiers in Molecular Neuroscience, 2011. **4**.
87. Portis, S., et al., *The role of glycogen synthase kinase-3 signaling in neurodevelopment and fragile X syndrome.* Int J Physiol Pathophysiol Pharmacol, 2012. **4**(3): p. 140-8.
88. Jope, R.S. and G.V. Johnson, *The glamour and gloom of glycogen synthase kinase-3.* Trends Biochem Sci, 2004. **29**(2): p. 95-102.
89. Min, W.W., et al., *Elevated glycogen synthase kinase-3 activity in Fragile X mice: key metabolic regulator with evidence for treatment potential.* Neuropharmacology, 2009. **56**(2): p. 463-72.
90. McBride, S.M., et al., *Pharmacological rescue of synaptic plasticity, courtship behavior, and mushroom body defects in a Drosophila model of fragile X syndrome.* Neuron, 2005. **45**(5): p. 753-64.
91. Choi, C.H., et al., *Pharmacological reversal of synaptic plasticity deficits in the mouse model of fragile X syndrome by group II mGluR antagonist or lithium treatment.* Brain Res, 2011. **1380**: p. 106-19.
92. Miller, L., et al., *Electrodermal responses to sensory stimuli in individuals with fragile X syndrome.* Am J Med Genet, 1999. **83**: p. 268-279.
93. Liu, Z.-H., D.-M. Chuang, and C.B. Smith, *Lithium ameliorates phenotypic deficits in a mouse model of fragile X syndrome.* International Journal of Neuropsychopharmacology, 2011. **14**(5): p. 618-630.
94. Yuskaitis, C.J., E. Beurel, and R.S. Jope, *Evidence of reactive astrocytes but not peripheral immune system activation in a mouse model of Fragile X syndrome.* Biochimica et Biophysica Acta (BBA)-Molecular Basis of Disease, 2010. **1802**(11): p. 1006-1012.
95. Eldar-Finkelman, H. and A. Martinez, *GSK-3 inhibitors: preclinical and clinical focus on CNS.* Frontiers in molecular neuroscience, 2011. **4**.
96. Bente, M., et al., *Developmentally induced changes of the proteome in the protozoan parasite Leishmania donovani.* Proteomics, 2003. **3**(9): p. 1811-29.
97. Wilkins, M.R., et al., *From proteins to proteomes: large scale protein identification by two-dimensional electrophoresis and amino acid analysis.* Biotechnology (N Y), 1996. **14**(1): p. 61-5.
98. Chandramouli, K. and P.Y. Qian, *Proteomics: challenges, techniques and possibilities to overcome biological sample complexity.* Hum Genomics Proteomics, 2009. **2009**.

99. Prabakaran, S., et al., *Post-translational modification: nature's escape from genetic imprisonment and the basis for dynamic information encoding.* Wiley Interdiscip Rev Syst Biol Med, 2012. **4**(6): p. 565-83.
100. Mann, M. and O.N. Jensen, *Proteomic analysis of post-translational modifications.* Nat Biotechnol, 2003. **21**(3): p. 255-61.
101. Beck-Sickinger, A.G. and K. Mörl, *Posttranslational Modification of Proteins. Expanding Nature's Inventory. By Christopher T. Walsh.* Angewandte Chemie International Edition, 2006. **45**(7): p. 1020-1020.
102. Seo, J. and K.J. Lee, *Post-translational modifications and their biological functions: proteomic analysis and systematic approaches.* J Biochem Mol Biol, 2004. **37**(1): p. 35-44.
103. Beltrao, P., et al., *Evolution and functional cross-talk of protein post-translational modifications.* Mol Syst Biol, 2013. **9**: p. 714.
104. Johnson, L.N., *The regulation of protein phosphorylation.* Biochem Soc Trans, 2009. **37**(Pt 4): p. 627-41.
105. Ciesla, J., T. Fraczyk, and W. Rode, *Phosphorylation of basic amino acid residues in proteins: important but easily missed.* Acta Biochim Pol, 2011. **58**(2): p. 137-48.
106. Feng, J., et al., *Phosphoproteome analysis of isoflurane-protected heart mitochondria: phosphorylation of adenine nucleotide translocator-1 on Tyr194 regulates mitochondrial function.* Cardiovasc Res, 2008. **80**(1): p. 20-9.
107. Matthews, H.R., *Protein kinases and phosphatases that act on histidine, lysine, or arginine residues in eukaryotic proteins: a possible regulator of the mitogen-activated protein kinase cascade.* Pharmacol Ther, 1995. **67**(3): p. 323-50.
108. Fuhrmann, J., et al., *McsB is a protein arginine kinase that phosphorylates and inhibits the heat-shock regulator CtsR.* Science, 2009. **324**(5932): p. 1323-7.
109. Macek, B., M. Mann, and J.V. Olsen, *Global and site-specific quantitative phosphoproteomics: principles and applications.* Annu Rev Pharmacol Toxicol, 2009. **49**: p. 199-221.
110. Ubersax, J.A. and J.E. Ferrell Jr, *Mechanisms of specificity in protein phosphorylation.* Nat Rev Mol Cell Biol, 2007. **8**(7): p. 530-541.
111. De Corte, V., et al., *Identification of Tyr438 as the major in vitro c-Src phosphorylation site in human gelsolin: a mass spectrometric approach.* Protein Sci, 1999. **8**(1): p. 234-41.
112. Villen, J. and S.P. Gygi, *The SCX/IMAC enrichment approach for global phosphorylation analysis by mass spectrometry.* Nat Protoc, 2008. **3**(10): p. 1630-8.
113. Beausoleil, S.A., et al., *Large-scale characterization of HeLa cell nuclear phosphoproteins.* Proc Natl Acad Sci U S A, 2004. **101**(33): p. 12130-5.
114. Pinkse, M.W., et al., *Selective isolation at the femtomole level of phosphopeptides from proteolytic digests using 2D-NanoLC-ESI-MS/MS and titanium oxide precolumns.* Anal Chem, 2004. **76**(14): p. 3935-43.
115. Edelmann, M.J., *Strong Cation Exchange Chromatography in Analysis of Posttranslational Modifications: Innovations and Perspectives.* Journal of Biomedicine and Biotechnology, 2011. **2011**: p. 7.
116. Zhou, H., et al., *Robust phosphoproteome enrichment using monodisperse microsphere-based immobilized titanium (IV) ion affinity chromatography.* Nat Protoc, 2013. **8**(3): p. 461-80.

117. Hughes, C. and J. Krijgsveld, *Developments in quantitative mass spectrometry for the analysis of proteome dynamics.* Trends Biotechnol, 2012. **30**(12): p. 668-76.
118. Pratt, J.M., et al., *Dynamics of Protein Turnover, a Missing Dimension in Proteomics.* Molecular & Cellular Proteomics, 2002. **1**(8): p. 579-591.
119. Vogel, C. and E.M. Marcotte, *Insights into the regulation of protein abundance from proteomic and transcriptomic analyses.* Nat Rev Genet, 2012. **13**(4): p. 227-32.
120. Schwanhausser, B., et al., *Global analysis of cellular protein translation by pulsed SILAC.* PROTEOMICS, 2009. **9**(1): p. 205-9.
121. Boisvert, F.M., et al., *A quantitative spatial proteomics analysis of proteome turnover in human cells.* Mol Cell Proteomics, 2012. **11**(3): p. M111 011429.
122. Hinkson, I.V. and J.E. Elias, *The dynamic state of protein turnover: It's about time.* Trends Cell Biol, 2011. **21**(5): p. 293-303.
123. *Reaping the Benefits of Genomic and Proteomic Research*, in *Reaping the Benefits of Genomic and Proteomic Research: Intellectual Property Rights, Innovation, and Public Health*, S.A. Merrill and A.M. Mazza, Editors. 2006: Washington (DC).
124. Cox, J. and M. Mann, *Quantitative, high-resolution proteomics for data-driven systems biology.* Annu Rev Biochem, 2011. **80**: p. 273-99.
125. Tyers, M. and M. Mann, *From genomics to proteomics.* Nature, 2003. **422**(6928): p. 193-197.
126. Hu, L., et al., *Advances in hyphenated analytical techniques for shotgun proteome and peptidome analysis--a review.* Anal Chim Acta, 2007. **598**(2): p. 193-204.
127. Domon, B. and R. Aebersold, *Mass Spectrometry and Protein Analysis.* Science, 2006. **312**(5771): p. 212-217.
128. Cravatt, B.F., G.M. Simon, and J.R. Yates Iii, *The biological impact of mass-spectrometry-based proteomics.* Nature, 2007. **450**(7172): p. 991-1000.
129. Steen, H. and M. Mann, *The abc's (and xyz's) of peptide sequencing.* Nat Rev Mol Cell Biol, 2004. **5**(9): p. 699-711.
130. Hubner, N.C., S. Ren, and M. Mann, *Peptide separation with immobilized pI strips is an attractive alternative to in-gel protein digestion for proteome analysis.* Proteomics, 2008. **8**(23-24): p. 4862-72.
131. Shevchenko, A., et al., *In-gel digestion for mass spectrometric characterization of proteins and proteomes.* Nat Protoc, 2006. **1**(6): p. 2856-60.
132. Fenn, J.B., et al., *Electrospray ionization for mass spectrometry of large biomolecules.* Science, 1989. **246**(4926): p. 64-71.
133. Altelaar, A.F.M., J. Munoz, and A.J.R. Heck, *Next-generation proteomics: towards an integrative view of proteome dynamics.* Nat Rev Genet, 2013. **14**(1): p. 35-48.
134. Hu, Q., et al., *The Orbitrap: a new mass spectrometer.* Journal of Mass Spectrometry, 2005. **40**(4): p. 430-443.
135. Michalski, A., et al., *Ultra high resolution linear ion trap Orbitrap mass spectrometer (Orbitrap Elite) facilitates top down LC MS/MS and versatile peptide fragmentation modes.* Molecular & Cellular Proteomics, 2011.
136. Lam, H., et al., *Development and validation of a spectral library searching method for peptide identification from MS/MS.* Proteomics, 2007. **7**(5): p. 655-67.
137. Perkins, D.N., et al., *Probability-based protein identification by searching sequence databases using mass spectrometry data.* Electrophoresis, 1999. **20**(18): p. 3551-67.

138. Cox, J., et al., *Andromeda: a peptide search engine integrated into the MaxQuant environment.* J Proteome Res, 2011. **10**(4): p. 1794-805.
139. Eng, J.K., A.L. McCormack, and J.R. Yates Iii, *An approach to correlate tandem mass spectral data of peptides with amino acid sequences in a protein database.* Journal of the American Society for Mass Spectrometry, 1994. **5**(11): p. 976-989.
140. Meissner, F. and M. Mann, *Quantitative shotgun proteomics: considerations for a high-quality workflow in immunology.* Nat Immunol, 2014. **15**(2): p. 112-117.
141. Elias, J.E. and S.P. Gygi, *Target-decoy search strategy for increased confidence in large-scale protein identifications by mass spectrometry.* Nat Methods, 2007. **4**(3): p. 207-14.
142. Ong, S.E., L.J. Foster, and M. Mann, *Mass spectrometric-based approaches in quantitative proteomics.* Methods, 2003. **29**(2): p. 124-30.
143. Ong, S.E. and M. Mann, *Mass spectrometry-based proteomics turns quantitative.* Nat Chem Biol, 2005. **1**(5): p. 252-62.
144. Bantscheff, M., et al., *Quantitative mass spectrometry in proteomics: a critical review.* Analytical and Bioanalytical Chemistry, 2007. **389**(4): p. 1017-1031.
145. Gygi, S.P., et al., *Quantitative analysis of complex protein mixtures using isotope-coded affinity tags.* Nat Biotechnol, 1999. **17**(10): p. 994-9.
146. Ross, P.L., et al., *Multiplexed protein quantitation in Saccharomyces cerevisiae using amine-reactive isobaric tagging reagents.* Mol Cell Proteomics, 2004. **3**(12): p. 1154-69.
147. Thompson, A., et al., *Tandem mass tags: a novel quantification strategy for comparative analysis of complex protein mixtures by MS/MS.* Anal Chem, 2003. **75**(8): p. 1895-904.
148. Yao, X., et al., *Proteolytic 18O labeling for comparative proteomics: model studies with two serotypes of adenovirus.* Anal Chem, 2001. **73**(13): p. 2836-42.
149. Oda, Y., et al., *Accurate quantitation of protein expression and site-specific phosphorylation.* Proc Natl Acad Sci U S A, 1999. **96**(12): p. 6591-6.
150. Ong, S.-E., et al., *Stable Isotope Labeling by Amino Acids in Cell Culture, SILAC, as a Simple and Accurate Approach to Expression Proteomics.* Molecular & Cellular Proteomics, 2002. **1**(5): p. 376-386.
151. Claydon, A.J. and R.J. Beynon, *Protein turnover methods in single-celled organisms: dynamic SILAC.* Methods Mol Biol, 2011. **759**: p. 179-95.
152. Schwanhausser, B., et al., *Global quantification of mammalian gene expression control.* Nature, 2011. **473**(7347): p. 337-342.
153. Andersen, J.S., et al., *Nucleolar proteome dynamics.* Nature, 2005. **433**(7021): p. 77-83.
154. Ong, S.E., et al., *Stable isotope labeling by amino acids in cell culture, SILAC, as a simple and accurate approach to expression proteomics.* Mol Cell Proteomics, 2002. **1**(5): p. 376-86.
155. Spellman, D.S., et al., *Stable isotopic labeling by amino acids in cultured primary neurons: application to brain-derived neurotrophic factor-dependent phosphotyrosine-associated signaling.* Mol Cell Proteomics, 2008. **7**(6): p. 1067-76.
156. Sury, M.D., J.X. Chen, and M. Selbach, *The SILAC fly allows for accurate protein quantification in vivo.* Mol Cell Proteomics, 2010. **9**(10): p. 2173-83.
157. Kruger, M., et al., *SILAC mouse for quantitative proteomics uncovers kindlin-3 as an essential factor for red blood cell function.* Cell, 2008. **134**(2): p. 353-64.
158. Wong, J.W. and G. Cagney, *An overview of label-free quantitation methods in proteomics by mass spectrometry.* Methods Mol Biol, 2010. **604**: p. 273-83.

159. Asara, J.M., et al., *A label-free quantification method by MS/MS TIC compared to SILAC and spectral counting in a proteomics screen.* PROTEOMICS, 2008. **8**(5): p. 994-9.
160. Hanke, S., et al., *Absolute SILAC for accurate quantitation of proteins in complex mixtures down to the attomole level.* J Proteome Res, 2008. **7**(3): p. 1118-30.
161. Ben-Tabou de-Leon, S. and E.H. Davidson, *Experimentally based sea urchin gene regulatory network and the causal explanation of developmental phenomenology.* Wiley Interdisciplinary Reviews: Systems Biology and Medicine, 2009. **1**(2): p. 237-246.
162. Gerber, S.A., et al., *Absolute quantification of proteins and phosphoproteins from cell lysates by tandem MS.* Proc Natl Acad Sci U S A, 2003. **100**(12): p. 6940-5.
163. Zhu, W., J.W. Smith, and C.M. Huang, *Mass spectrometry-based label-free quantitative proteomics.* J Biomed Biotechnol, 2010. **2010**: p. 840518.
164. Wisniewski, J.R., et al., *Extensive quantitative remodeling of the proteome between normal colon tissue and adenocarcinoma.* Mol Syst Biol, 2012. **8**: p. 611.
165. Castets, M., et al., *FMRP interferes with the Rac1 pathway and controls actin cytoskeleton dynamics in murine fibroblasts.* Hum Mol Genet, 2005. **14**(6): p. 835-44.
166. Macek, B., et al., *The serine/threonine/tyrosine phosphoproteome of the model bacterium Bacillus subtilis.* Molecular & Cellular Proteomics, 2007. **6**(4): p. 697-707.
167. Ishihama, Y., J. Rappsilber, and M. Mann, *Modular stop and go extraction tips with stacked disks for parallel and multidimensional peptide fractionation in proteomics.* Journal of proteome research, 2006. **5**(4): p. 988-994.
168. Olsen, J.V. and B. Macek, *High accuracy mass spectrometry in large-scale analysis of protein phosphorylation.* Methods Mol Biol, 2009. **492**: p. 131-42.
169. Cox, J. and M. Mann, *MaxQuant enables high peptide identification rates, individualized p.p.b.-range mass accuracies and proteome-wide protein quantification.* Nat Biotechnol, 2008. **26**(12): p. 1367-72.
170. Cox, J., et al., *A practical guide to the MaxQuant computational platform for SILAC-based quantitative proteomics.* Nat Protoc, 2009. **4**(5): p. 698-705.
171. Benjamini, Y. and Y. Hochberg, *Controlling the False Discovery Rate - a Practical and Powerful Approach to Multiple Testing.* Journal of the Royal Statistical Society Series B-Methodological, 1995. **57**(1): p. 289-300.
172. Jensen, L.J., et al., *STRING 8--a global view on proteins and their functional interactions in 630 organisms.* Nucleic Acids Res, 2009. **37**(Database issue): p. D412-6.
173. Franceschini, A., et al., *STRING v9.1: protein-protein interaction networks, with increased coverage and integration.* Nucleic Acids Res, 2013. **41**(Database issue): p. D808-15.
174. Davidovic, L., et al., *A metabolomic and systems biology perspective on the brain of the fragile X syndrome mouse model.* Genome Res, 2011. **21**(12): p. 2190-202.
175. Davidovic, L., et al., *The nuclear MicroSpherule protein 58 is a novel RNA-binding protein that interacts with fragile X mental retardation protein in polyribosomal mRNPs from neurons.* Human Molecular Genetics, 2006. **15**(9): p. 1525-1538.
176. Khandjian, E.W., et al., *Novel Isoforms of the Fragile X Related Protein FXR1P are Expressed During Myogenesis.* Human Molecular Genetics, 1998. **7**(13): p. 2121-2128.
177. Demart, S., et al., *New insight into abnormal prion protein using monoclonal antibodies.* Biochem Biophys Res Commun, 1999. **265**(3): p. 652-7.

178. Huang da, W., B.T. Sherman, and R.A. Lempicki, *Systematic and integrative analysis of large gene lists using DAVID bioinformatics resources.* Nat Protoc, 2009. **4**(1): p. 44-57.
179. Huang da, W., B.T. Sherman, and R.A. Lempicki, *Bioinformatics enrichment tools: paths toward the comprehensive functional analysis of large gene lists.* Nucleic Acids Res, 2009. **37**(1): p. 1-13.
180. Ishihama, Y., J. Rappsilber, and M. Mann, *Modular stop and go extraction tips with stacked disks for parallel and multidimensional Peptide fractionation in proteomics.* J Proteome Res, 2006. **5**(4): p. 988-94.
181. Osterweil, E.K., et al., *Hypersensitivity to mGluR5 and ERK1/2 Leads to Excessive Protein Synthesis in the Hippocampus of a Mouse Model of Fragile X Syndrome.* Journal of Neuroscience, 2010. **30**(46): p. 15616-15627.
182. Deeb, S.J., et al., *Super-SILAC allows classification of diffuse large B-cell lymphoma subtypes by their protein expression profiles.* Mol Cell Proteomics, 2012. **11**(5): p. 77-89.
183. Bolstad, B.M., et al., *A comparison of normalization methods for high density oligonucleotide array data based on variance and bias.* Bioinformatics, 2003. **19**(2): p. 185-93.
184. Benjamini, Y. and Y. Hochberg, *Controlling the False Discovery Rate: A Practical and Powerful Approach to Multiple Testing.* Journal of the Royal Statistical Society. Series B (Methodological), 1995. **57**(1): p. 289-300.
185. Siomi, M.C., et al., *FXR1, an autosomal homolog of the fragile X mental retardation gene.* EMBO J, 1995. **14**(11): p. 2401-8.
186. Zhang, Y., et al., *The fragile X mental retardation syndrome protein interacts with novel homologs FXR1 and FXR2.* EMBO J, 1995. **14**(21): p. 5358-66.
187. Sung, Y.J., et al., *RNAs That Interact with the Fragile X Syndrome RNA Binding Protein FMRP.* Biochemical and Biophysical Research Communications, 2000. **275**(3): p. 973-980.
188. Brown, V., et al., *Microarray Identification of FMRP-Associated Brain mRNAs and Altered mRNA Translational Profiles in Fragile X Syndrome.* Cell, 2001. **107**(4): p. 477-487.
189. Schaeffer, C., et al., *The fragile X mental retardation protein binds specifically to its mRNA via a purine quartet motif.* EMBO J, 2001. **20**(17): p. 4803-13.
190. Schenck, A., et al., *A highly conserved protein family interacting with the fragile X mental retardation protein (FMRP) and displaying selective interactions with FMRP-related proteins FXR1P and FXR2P.* Proc Natl Acad Sci U S A, 2001. **98**(15): p. 8844-9.
191. Chen, L., et al., *The fragile x mental retardation protein binds and regulates a novel class of mRNAs containing u rich target sequences.* Neuroscience, 2003. **120**(4): p. 1005-1017.
192. Dolzhanskaya, N., et al., *The fragile X mental retardation protein interacts with U-rich RNAs in a yeast three-hybrid system.* Biochemical and Biophysical Research Communications, 2003. **305**(2): p. 434-441.
193. Miyashiro, K.Y., et al., *RNA Cargoes Associating with FMRP Reveal Deficits in Cellular Functioning in Fmr1 Null Mice.* Neuron, 2003. **37**(3): p. 417-431.
194. Westmark, C.J. and J.S. Malter, *FMRP mediates mGluR5-dependent translation of amyloid precursor protein.* PLoS Biol, 2007. **5**(3): p. e52.

195. Zhang, M., Q. Wang, and Y. Huang, *Fragile X mental retardation protein FMRP and the RNA export factor NXF2 associate with and destabilize Nxf1 mRNA in neuronal cells.* Proceedings of the National Academy of Sciences, 2007. **104**(24): p. 10057-10062.
196. Schütt, J., et al., *Fragile X Mental Retardation Protein Regulates the Levels of Scaffold Proteins and Glutamate Receptors in Postsynaptic Densities.* Journal of Biological Chemistry, 2009. **284**(38): p. 25479-25487.
197. Bechara, E.G., et al., *A novel function for fragile X mental retardation protein in translational activation.* PLoS Biol, 2009. **7**(1): p. e16-e16.
198. Khandjian, E.W., et al., *Novel isoforms of the fragile X related protein FXR1P are expressed during myogenesis.* Hum Mol Genet, 1998. **7**(13): p. 2121-8.
199. Kanaani, J., et al., *Recombinant prion protein induces rapid polarization and development of synapses in embryonic rat hippocampal neurons in vitro.* J Neurochem, 2005. **95**(5): p. 1373-1386.
200. Criado, J.R., et al., *Mice devoid of prion protein have cognitive deficits that are rescued by reconstitution of PrP in neurons.* Neurobiology of Disease, 2005. **19**(1-2): p. 255-265.
201. Le, T.D., et al., *Lipid signaling in cytosolic phospholipase A2alpha-cyclooxygenase-2 cascade mediates cerebellar long-term depression and motor learning.* Proc Natl Acad Sci U S A, 2010. **107**(7): p. 3198-203.
202. Huber, K.M., *The fragile X-cerebellum connection.* Trends Neurosci, 2006. **29**(4): p. 183-5.
203. Bell, J.G., et al., *Essential fatty acids and phospholipase A2 in autistic spectrum disorders.* Prostaglandins Leukot Essent Fatty Acids, 2004. **71**(4): p. 201-204.
204. el Bekay, R., et al., *Enhanced markers of oxidative stress, altered antioxidants and NADPH-oxidase activation in brains from Fragile X mental retardation 1-deficient mice, a pathological model for Fragile X syndrome.* Eur J Neurosci, 2007. **26**(11): p. 3169-80.
205. Kanehisa, M. and S. Goto, *KEGG: kyoto encyclopedia of genes and genomes.* Nucleic Acids Res, 2000. **28**(1): p. 27-30.
206. Lugo, J.N., et al., *Deletion of PTEN produces deficits in conditioned fear and increases fragile X mental retardation protein.* Learn Mem, 2013. **20**(12): p. 670-3.
207. Butler, M.G., et al., *Subset of individuals with autism spectrum disorders and extreme macrocephaly associated with germline PTEN tumour suppressor gene mutations.* J Med Genet, 2005. **42**(4): p. 318-21.
208. Chiu, S., et al., *Early acceleration of head circumference in children with fragile x syndrome and autism.* J Dev Behav Pediatr, 2007. **28**(1): p. 31-5.
209. Bhattacharya, A., et al., *Genetic removal of p70 S6 kinase 1 corrects molecular, synaptic, and behavioral phenotypes in fragile X syndrome mice.* Neuron, 2012. **76**(2): p. 325-37.
210. Hay, N. and N. Sonenberg, *Upstream and downstream of mTOR.* Genes Dev, 2004. **18**(16): p. 1926-1945.
211. Sharma, A., et al., *Dysregulation of mTOR signaling in fragile X syndrome.* J Neurosci, 2010. **30**(2): p. 694-702.
212. Osterweil, E.K., et al., *Hypersensitivity to mGluR5 and ERK1/2 leads to excessive protein synthesis in the hippocampus of a mouse model of fragile X syndrome.* J Neurosci, 2010. **30**(46): p. 15616-15627.

213. Luo, Y., et al., *Fragile x mental retardation protein regulates proliferation and differentiation of adult neural stem/progenitor cells.* PLoS Genet, 2010. **6**(4): p. e1000898.
214. Liu, W., et al., *Drosophila FMRP participates in the DNA damage response by regulating G2/M cell cycle checkpoint and apoptosis.* Human Molecular Genetics, 2012. **21**(21): p. 4655-4668.
215. Zhang, W., et al., *A feed-forward mechanism involving Drosophila fragile X mental retardation protein triggers a replication stress-induced DNA damage response.* Hum Mol Genet, 2014.
216. Alpatov, R., et al., *A Chromatin-Dependent Role of the Fragile X Mental Retardation Protein FMRP in the DNA Damage Response.* Cell, 2014. **157**(4): p. 869-81.
217. Decorsiere, A., et al., *Essential role for the interaction between hnRNP H/F and a G quadruplex in maintaining p53 pre-mRNA 3'-end processing and function during DNA damage.* Genes Dev, 2011. **25**(3): p. 220-5.
218. Melko, M. and B. Bardoni, *The role of G-quadruplex in RNA metabolism: involvement of FMRP and FMR2P.* Biochimie, 2010. **92**(8): p. 919-26.
219. Sheikh, A.M., et al., *BDNF-Akt-Bcl2 antiapoptotic signaling pathway is compromised in the brain of autistic subjects.* J Neurosci Res, 2010. **88**(12): p. 2641-2647.
220. Jessberger, S., et al., *Dentate gyrus-specific knockdown of adult neurogenesis impairs spatial and object recognition memory in adult rats.* Learn Mem, 2009. **16**(2): p. 147-154.
221. Lie, D.-C., et al., *Wnt signalling regulates adult hippocampal neurogenesis.* Nature, 2005. **437**(7063): p. 1370-1375.
222. Luo, Y., et al., *Fragile x mental retardation protein regulates proliferation and differentiation of adult neural stem/progenitor cells.* PLoS Genet, 2010. **6**(4): p. e1000898-e1000898.
223. Allen, N.J., et al., *Astrocyte glypicans 4 and 6 promote formation of excitatory synapses via GluA1 AMPA receptors.* Nature, 2012. **486**(7403): p. 410-414.
224. Cheng, P., I. Alberts, and X. Li, *The role of ERK1/2 in the regulation of proliferation and differentiation of astrocytes in developing brain.* Int J Dev Neurosci, 2013. **31**(8): p. 783-9.
225. CastrÃ©n, M., et al., *Altered differentiation of neural stem cells in fragile X syndrome.* Proc Natl Acad Sci U S A, 2005. **102**(49): p. 17834-17839.
226. Bolduc, F.V., et al., *Fragile x mental retardation 1 and filamin a interact genetically in Drosophila long-term memory.* Front Neural Circuits, 2010. **3**: p. 22.
227. Dolan, B.M., et al., *Rescue of fragile X syndrome phenotypes in Fmr1 KO mice by the small-molecule PAK inhibitor FRAX486.* Proc Natl Acad Sci U S A, 2013. **110**(14): p. 5671-6.
228. Hayashi, M.L., et al., *Inhibition of p21-activated kinase rescues symptoms of fragile X syndrome in mice.* Proc Natl Acad Sci U S A, 2007. **104**(27): p. 11489-94.
229. Sutherland, C., *What Are the bona fide GSK3 Substrates?* Int J Alzheimers Dis, 2011. **2011**: p. 505607.
230. Hur, E.-M. and F.-Q. Zhou, *GSK3 signalling in neural development.* Nat Rev Neurosci, 2010. **11**(8): p. 539-551.
231. Kimelman, D. and W. Xu, *beta-catenin destruction complex: insights and questions from a structural perspective.* Oncogene, 2006. **25**(57): p. 7482-91.

232. Oh, M., et al., *GSK-3 Phosphorylates δ-Catenin and Negatively Regulates Its Stability via Ubiquitination/Proteosome-mediated Proteolysis.* Journal of Biological Chemistry, 2009. **284**(42): p. 28579-28589.
233. Arikkath, J., et al., *δ-catenin regulates spine and synapse morphogenesis and function in hippocampal neurons during development.* The Journal of Neuroscience, 2009. **29**(17): p. 5435-5442.
234. Abu-Elneel, K., et al., *A δ-Catenin Signaling Pathway Leading to Dendritic Protrusions.* Journal of Biological Chemistry, 2008. **283**(47): p. 32781-32791.
235. Yang, M., et al., *Tumor protein D52-like 2 contributes to proliferation of breast cancer cells.* Cancer Biother Radiopharm, 2015. **30**(1): p. 1-7.
236. Giuffrida, R., et al., *A Reduced Number of Metabotropic Glutamate Subtype 5 Receptors Are Associated with Constitutive Homer Proteins in a Mouse Model of Fragile X Syndrome.* The Journal of Neuroscience, 2005. **25**(39): p. 8908-8916.
237. Lohith, T., et al., *Is metabotropic glutamate receptor 5 upregulated in prefrontal cortex in fragile X syndrome?* Molecular Autism, 2013. **4**(1): p. 15.
238. Criado, J.R., et al., *Mice devoid of prion protein have cognitive deficits that are rescued by reconstitution of PrP in neurons.* Neurobiol Dis, 2005. **19**(1-2): p. 255-65.
239. Coitinho, A.S., et al., *Short-term memory formation and long-term memory consolidation are enhanced by cellular prion association to stress-inducible protein 1.* Neurobiol Dis, 2007. **26**(1): p. 282-90.
240. Jensen, L.J., et al., *STRING 8—a global view on proteins and their functional interactions in 630 organisms.* Nucleic Acids Research, 2009. **37**(suppl 1): p. D412-D416.
241. Franceschini, A., et al., *STRING v9.1: protein-protein interaction networks, with increased coverage and integration.* Nucleic Acids Research, 2013. **41**(D1): p. D808-D815.
242. Chen, E., et al., *Fragile X Mental Retardation Protein Regulates Translation by Binding Directly to the Ribosome.* Molecular Cell, 2014. **54**(3): p. 407-417.
243. Siomi, M.C., et al., *Specific sequences in the fragile X syndrome protein FMR1 and the FXR proteins mediate their binding to 60S ribosomal subunits and the interactions among them.* Molecular and Cellular Biology, 1996. **16**(7): p. 3825-32.
244. Ross-Inta, C., et al., *Evidence of mitochondrial dysfunction in fragile X-associated tremor/ataxia syndrome.* Biochem J, 2010. **429**(3): p. 545-52.
245. Valenti, D., et al., *Mitochondrial dysfunction as a central actor in intellectual disability-related diseases: An overview of Down syndrome, autism, Fragile X and Rett syndrome.* Neurosci Biobehav Rev, 2014.
246. Di Cunto, F., et al., *Defective neurogenesis in citron kinase knockout mice by altered cytokinesis and massive apoptosis.* Neuron, 2000. **28**: p. 115 - 27.
247. Vadodaria, K.C., et al., *Stage-specific functions of the small Rho GTPases Cdc42 and Rac1 for adult hippocampal neurogenesis.* J Neurosci, 2013. **33**(3): p. 1179-89.
248. Bauer, C., et al., *Genetic and systems level analysis of Drosophila sticky/citron kinase and dFmr1 mutants reveals common regulation of genetic networks.* BMC Systems Biology, 2008. **2**(1): p. 101.
249. Farr, C.D., et al., *Proteomic analysis of native metabotropic glutamate receptor 5 protein complexes reveals novel molecular constituents.* J Neurochem, 2004. **91**(2): p. 438-50.

250. Zhang, W., et al., *Citron Binds to PSD-95 at Glutamatergic Synapses on Inhibitory Neurons in the Hippocampus.* The Journal of Neuroscience, 1999. **19**(1): p. 96-108.
251. Monzo, K., et al., *Proteomic analysis reveals CCT is a target of Fragile X mental retardation protein regulation in Drosophila.* Developmental Biology, 2010. **340**(2): p. 408-418.
252. McMillan, E.L., et al., *Gene expression changes in the MAPK pathway in both Fragile X and Down syndrome human neural progenitor cells.* Am J Stem Cells, 2012. **1**(2): p. 154-162.
253. Kim, E.K. and E.-J. Choi, *Pathological roles of MAPK signaling pathways in human diseases.* Biochimica et Biophysica Acta (BBA) - Molecular Basis of Disease, 2010. **1802**(4): p. 396-405.
254. Ong, W.-Y., et al., *Synthetic and Natural Inhibitors of Phospholipases A2: Their Importance for Understanding and Treatment of Neurological Disorders.* ACS Chemical Neuroscience, 2015.
255. El Bekay, R., et al., *Enhanced markers of oxidative stress, altered antioxidants and NADPH-oxidase activation in brains from Fragile X mental retardation 1-deficient mice, a pathological model for Fragile X syndrome.* European Journal of Neuroscience, 2007. **26**(11): p. 3169-3180.
256. Phiel, C.J. and P.S. Klein, *MOLECULAR TARGETS OF LITHIUM ACTION.* Annual Review of Pharmacology and Toxicology, 2001. **41**(1): p. 789-813.
257. Lucas, F.R., et al., *Inhibition of GSK-3beta leading to the loss of phosphorylated MAP-1B is an early event in axonal remodelling induced by WNT-7a or lithium.* J Cell Sci, 1998. **111 (Pt 10)**: p. 1351-61.
258. Yang, E.S., et al., *Glycogen synthase kinase 3β inhibition enhances repair of DNA double-strand breaks in irradiated hippocampal neurons.* Neuro-Oncology, 2011.
259. Xu, H., et al., *DNA repair/replication transcripts are down regulated in patients with Fragile X Syndrome.* BMC Res Notes, 2013. **6**: p. 90.
260. Zhou, F.-Q. and W.D. Snider, *GSK-3β and Microtubule Assembly in Axons.* Science, 2005. **308**(5719): p. 211-214.
261. Goold, R.G. and P.R. Gordon-Weeks, *The MAP kinase pathway is upstream of the activation of GSK3β that enables it to phosphorylate MAP1B and contributes to the stimulation of axon growth.* Molecular and Cellular Neuroscience, 2005. **28**(3): p. 524-534.
262. Hughes, C. and J. Krijgsveld, *Developments in quantitative mass spectrometry for the analysis of proteome dynamics.* Trends in Biotechnology, 2012. **30**(12): p. 668-676.
263. Brown, V., et al., *Microarray identification of FMRP-associated brain mRNAs and altered mRNA translational profiles in fragile X syndrome.* Cell, 2001. **107**(4): p. 477-87.
264. Krueger, D.D., et al., *Cognitive dysfunction and prefrontal synaptic abnormalities in a mouse model of fragile X syndrome.* Proc Natl Acad Sci U S A, 2011. **108**(6): p. 2587-92.
265. Welch, J.M., et al., *Cortico-striatal synaptic defects and OCD-like behaviours in Sapap3-mutant mice.* Nature, 2007. **448**(7156): p. 894-900.
266. Wan, Y., G. Feng, and N. Calakos, *Sapap3 Deletion Causes mGluR5-Dependent Silencing of AMPAR Synapses.* The Journal of Neuroscience, 2011. **31**(46): p. 16685-16691.
267. Bredt, D.S. and R.A. Nicoll, *AMPA Receptor Trafficking at Excitatory Synapses.* Neuron, 2003. **40**(2): p. 361-379.

268. Carroll, R.C., et al., *Dynamin-dependent endocytosis of ionotropic glutamate receptors.* Proc Natl Acad Sci U S A, 1999. **96**(24): p. 14112-7.
269. Ferguson, S.M., et al., *A Selective Activity-Dependent Requirement for Dynamin 1 in Synaptic Vesicle Endocytosis.* Science, 2007. **316**(5824): p. 570-574.
270. Fà, M., et al., *Dynamin 1 Is Required for Memory Formation.* PLoS One, 2014. **9**(3): p. e91954.

Curriculum Vitae

PERSONAL INFORMATION

Name: Katarina Matic

Date of Birth: 25th March 1985

Nationality: Croatian

EDUCATIONAL QUALIFICATIONS

11/2011 – 7/2015	**PhD Student in Cellular and Molecular Neuroscience** Proteome Center Tuebingen, University of Tuebingen, Germany Graduate School of Cellular and Molecular Neuroscience, University of Tuebingen, Germany
9/2004 - 9/2010	**MD Degree** School of Medicine, University of Split, Split, Croatia Thesis: "The existence of geographical clusters of rheumatoid arthritis in a tertiary care based register according to their origin in Split-Dalmatia County"

RESEARCH EXPERIENCE

5 - 10/2010	**Research traning** School of Medicine, Cancer Biology group University of Split, Split, Croatia

List of publications

1. **Matic K**, Bardoni B, Davidovic L, Macek B.
   Inhibition of GSK-3β kinase in murine *Fmr1*-KO cell lines
   (manuscript in preparation)

2. **Matic K**, Krug K, Osterweil E, Bear M, Macek B.
   Global identification of differentially regulated proteins in mouse models of Fragile X Syndrome
   (manuscript in preparation)

3. Burian M, Velic A, **Matic K**, Gunther S, Kraft B, Gonser L, et al.
   Quantitative Proteomics of the Human Skin Secretome reveal a Reduction of Immune Defense Mediators in Ectodermal Dysplasia Patients.
   J Invest Dermatol. 2014.

4. **Matic K**, Eninger T, Bardoni B, Davidovic L, Macek B.
   Quantitative Phosphoproteomics of Murine Fmr1-KO Cell Lines Provides New Insights into FMRP-Dependent Signal Transduction Mechanisms.
   J Proteome Res. 2014;13(10):4388-97.

5. Utrobicic I, Novak I, Marinovic-Terzic I, **Matic K**, Lessel D, Salamunic I, et al.
   Carpal tunnel syndrome is associated with high fibrinogen and fibrinogen deposits. Neurosurgery. 2014;75(3):276-85; discussion 85.

6. Degoricija M, Situm M, Korac J, Miljkovic A, **Matic K**, Paradzik M, et al.
   High NF-kappaB and STAT3 activity in human urothelial carcinoma: a pilot study.
   World J Urol. 2014.

7. Krug K, Carpy A, Behrends G, **Matic K**, Soares NC, Macek B.
   Deep coverage of the Escherichia coli proteome enables the assessment of false discovery rates in simple proteogenomic experiments.
   Mol Cell Proteomics. 2013;12(11):3420-30.

8. Kaliterna DM, Krstulovic DM, **Matic K**, Perkovic D, Radic M, Marinovic I.
   The existence of geographical clusters of rheumatiod arhritis according to their origin in a tertiary care based register.
   Reumatizam. 2013;60(1):14-8.

.

Acknowledgements

Veliko hvala na nesebicnoj potpori i razumijevanju mojim roditeljima koji su uvijek bili blizu mene, iako smo kilometrima daleko. Posebno hvala mojoj majci koja me “pustila da otidem u svijet”, iako je to bila jedna od tezih stvari koje je napravila.

I would like to express warmest thanks to my supervisor Prof. Dr. Boris Macek. He gave me opportunity to come and work in the proteomics lab when I did not know what the real lab or proteomics really is. Happy, sad, hard and easy moments made my PhD making process an incredible experience.

I also want to thank my lab members. Firstly, to a fantastic group – Dr. Alejandro Carpy, Dr. Boumediene Soufi and Dr. Karsten Krug. Sharing my life with you inside and outside of the lab was really a lot of fun. Next to great scientific discussions, lot of “hääääääääää” and “special” moments made great memories that I will always remember. Special thanks goes to our great “lab mom” Urlike Grammig, without her help lot of us would be lost. Also, I need to thank the best student ever – Timo Eninger, he showed me how supervision can be a fun job. Additionally, special thanks goes to “my brother” Dr. Nelson Soares, Philipp Spät, Vaishnavi Ravikumar, Elias Probst, Christoph Täumer, Maja Semanjski, Dr. Mirita Franz-Wachtel, Dr. Ana Velic, Johannes Madlung, Silke Wahl, Irina Droste-Borel, Bianca Kuhn , Boris Günther and all ex-members, visiting scientists and students for a great working environment.

I would like to thank my Thesis Advisory Committee members - Prof. Dr. Alfred Nordheim and Prof. Dr. Olaf Riess for useful discussions and advices. In addition, I would like to thank Prof. Dr. Mathias Jucker for being part of my committee for my thesis defense.

I would like to thank all the scientist that collaborated with me especially Dr. Laetitia Davidovic, Dr. Barbara Bardoni, Dr. Mark Bear and Dr. Emily Osterweil.

Special thank you goes to Prof. Dr. Matko Marusic and Prof. Dr. Janos Terzic for a great support before and during my PhD process.

Also big thanks you goes to all my friends at home, especially to the first and the second Ivana and Tea. Although I am not at home for almost five years, every time when I talk to you or see you, it feels like I never left.

Manuscripts related to this thesis

Matic K, Eninger T, Bardoni B, Davidovic L, Macek B.
Quantitative Phosphoproteomics of Murine Fmr1-KO Cell Lines Provides New Insights into FMRP-Dependent Signal Transduction Mechanisms.
J Proteome Res. 2014;13(10):4388-97.

Journal of proteome research

Article

pubs.acs.org/jpr

Quantitative Phosphoproteomics of Murine *Fmr1*-KO Cell Lines Provides New Insights into FMRP-Dependent Signal Transduction Mechanisms

Katarina Matic,[⊥,†,‡] Timo Eninger,[⊥,†] Barbara Bardoni,[§,∥] Laetitia Davidovic,[*,§,∥] and Boris Macek[*,†]

[†]Proteome Center Tübingen and [‡]Graduate School of Cellular and Molecular Neuroscience, University of Tübingen, Österbergstrasse 3, 72074 Tübingen, Germany

[§]Institut de Pharmacologie Moléculaire et Cellulaire, CNRS UMR 7275, 660 route des Lucioles, 06560 Valbonne, France

[∥]Université de Nice-Sophia Antipolis, 28 Avenue Valrose, 06103 Nice, France

Supporting Information

ABSTRACT: Fragile X mental retardation protein (FMRP) is an RNA-binding protein that has a major effect on neuronal protein synthesis. Transcriptional silencing of the *FMR1* gene leads to loss of FMRP and development of Fragile X syndrome (FXS), the most common known hereditary cause of intellectual impairment and autism. Here we utilize SILAC-based quantitative phosphoproteomics to analyze murine *FMR1*$^{-}$ and *FMR1*$^{+}$ fibroblastic cell lines derived from *FMR1*-KO embryos to identify proteins and phosphorylation sites dysregulated as a consequence of FMRP loss. We quantify FMRP-related changes in the levels of 5,023 proteins and 6,133 phosphorylation events and map them onto major signal transduction pathways. Our study confirms global downregulation of the MAPK/ERK pathway and decrease in phosphorylation level of ERK1/2 in the absence of FMRP, which is connected to attenuation of long-term potentiation. We detect differential expression of several key proteins from the p53 pathway, pointing to the involvement of p53 signaling in dysregulated cell cycle control in FXS. Finally, we detect differential expression and phosphorylation of proteins involved in pre-mRNA processing and nuclear transport, as well as Wnt and calcium signaling, such as PLC, PKC, NFAT, and cPLA2. We postulate that calcium homeostasis is likely affected in molecular pathogenesis of FXS.

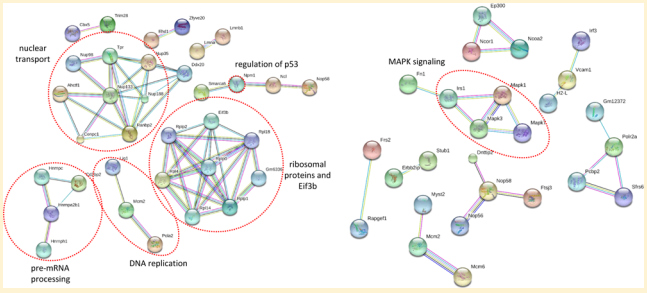

KEYWORDS: *fragile X syndrome, autism, phosphoproteomics, FMRP, FMR1, MEF*

INTRODUCTION

Fragile X syndrome (FXS) is the leading known cause of inherited intellectual disability[1] and autism spectrum disorders (ASD).[2,3] FXS is generally caused by an abnormal CGG trinucleotide repeat expansion and hypermethylation in the 5′ untranslated region of the fragile X mental retardation 1 gene (*FMR1*), resulting in *FMR1* silencing and absence of fragile X mental retardation protein (FMRP).[4,5] FMRP is an RNA-binding protein,[6] which is mainly expressed in neurons and testes.[7] It contains two (central) RNA-binding KH domains and one (C-terminal) RGG box[8] through which it can bind hundreds of mRNA molecules in brain,[9] many of which are encoded by genes related to autism. FMRP associates with polyribosomes[10−12] and influences protein synthesis via translational regulation.[13,14] Overall, the FMRP/RNA interaction is a complex process involving different RNA-binding domains and several RNA motifs. In addition, it can be influenced by other RNA-binding proteins interacting with FMRP.[15−17] It seems clear that FMRP binds to mRNA targets that encode both pre- and postsynaptic proteins and participates in the control of activity-dependent synaptic translation. Some of the target mRNAs encode important signaling proteins such as the metabotropic (mGluR5)[9,18] or ionotropic (NMDA receptor subunits)[9,19] glutamate receptors, members of the mTOR[9] signaling pathways, and other proteins that are involved in regulation of translation, which makes it likely that FMRP influences major signaling pathways in the cell. Furthermore, FMRP was described as a key player in the transport and localization of target mRNA molecules in the neuronal dendritic arborization toward the synapse where they undergo localized translation.[20] A loss of FMRP causes altered synaptic development and function[21] as well as disruptions in synaptic plasticity.[22] These abnormalities are the molecular bases of intellectual disability but also of other neurological/psychiatric pathologies associated with the FXS phenotype, such as autism, epilepsy, hyperactivity, and attention deficit disorder. It is therefore necessary to identify proteins and phosphorylation events dysregulated in FXS, as they may

Received: June 24, 2014
Published: August 29, 2014

dx.doi.org/10.1021/pr5006372 | *J. Proteome Res.* 2014, 13, 4388−4397

contribute to our understanding of the molecular pathogenesis and present drug targets for treatment of the disorder.

FMRP is highly conserved across species, and several *Fmr1*-knockout (KO) cell lines and animals have been established as FXS models.[23−25] One of them is an *Fmr1*-KO mouse SV40-immortalized fibroblast cell line model, termed the STEK cell line, that is derived from *Fmr1*-KO embryos and has previously been used to examine the role of FMRP as a translational repressor in stress granules.[24] Another generation of STEK cells was obtained by stable transfection of the longest isoform of FMRP (human ISO1) in naturally immortalized *Fmr1*-KO mouse embryonic fibroblasts (MEFs).[26] This cellular model, used in this study, has also been used to identify several novel RNA targets of FMRP[16,26,27] and to study the role of FMRP in the dynamics of P bodies.[28]

Modern proteomic workflows allow quantification of changes on the protein and phosphorylation site levels in a global and high throughput fashion. Stable isotope labeling by amino acid in cell culture (SILAC) or isobaric tags for relative and absolute quantitation (iTRAQ) strategies have been previously applied to the study of Drosophila and mouse models of FXS.[29−31] In the SILAC-based quantitative proteomic analysis of synaptosomal preparations from *Fmr1*-KO and WT cortical neurons, Liao et al. detected 132 proteins with altered expression in the absence of FMRP, including proteins related to autism and epilepsy.[29] In another study, iTRAQ was used to quantify proteomes of *FMR1*-KO vs WT mice hippocampi; this study resulted in quantification of 23 proteins with differential expression involved in cell differentiation, neurite outgrowth, and synaptic vesicle release.[30] Finally, heterozygous *dfmr1*$^{\mp}$ *Drosophila* labeled *in vivo* with SILAC allowed profiling of 1,617 proteins and identification of some proteins known to be differentially regulated in FXS, such as actin-binding protein profilin and microtubulin-associated protein futsch.[31]

Phosphorylation can alter protein function and activity and plays a significant regulatory role in a wide range of biochemical and cellular processes,[32] including signaling pathways and transduction cascades. Despite the fact that several signaling pathways are known to be affected in FXS,[33,34] global protein phosphorylation dynamics in FXS-related model systems was so far not investigated. Here we perform a quantitative analysis on the proteome and phosphoproteome of murine *FMR1*$^{-}$ and *FMR1*$^{+}$ MEF cells by using high resolution mass spectrometry in combination with SILAC.[35] Metabolic SILAC-labeling enabled us to identify and quantify thousands of proteins and phosphorylation events and map them to major regulatory pathways, giving unprecedented insights in the pathophysiology of FXS.

MATERIALS AND METHODS

Cell Culture and SILAC Labeling

A spontaneously immortalized fibroblastic murine *Fmr1*-KO cell line was established from mouse embryonic fibroblasts (MEFs) derived from *FMR1*-null C57Bl/6J embryos (mouse strain gR2700 available from Jackson Laboratory). *FMR1*-KO MEFs cells were then transfected with a pTL10 vector containing *FMR1* isoform 1 human cDNA or with an empty pTL10 vector.[36] Simultaneously, cells were cotransfected with a pIREShyg3 plasmid (Clontech-BD Bioscience) containing Hygromycin B resistance. This procedure resulted in two stable cell lines: one stably re-expressing FMRP, termed as STEK-59 (*FMR1*$^{+}$ MEFs), and one *Fmr1*-KO cell line further referred to as STEK-87 (*FMR1*$^{-}$ MEFs). MEF cells were cultured in DMEM medium (Dulbecco's modified eagle medium, High Glucose (4.5 g/L), PAA, or PAN Biotech) lacking arginine, lysine, and L-glutamine. L-Glutamine (2 mM, Gibco), penicillin/streptomycin (100 U/mL, PAN), Hygromycin B (from *Streptomyces hygroscopicus*, 150 μg/mL, Sigma-Aldrich), and dialyzed FBS (10%, Invitrogen) were added to the medium. The "light" SILAC media was further supplemented with 73 mg/L L-lysine Lys0 and 42 mg/L L-arginine Arg0 (both from Silantes), whereas 73 mg/L "heavy" L-lysine Lys8 (13C6,15N2-L-lysine, Silantes) and 42 mg/L "heavy" L-arginine Arg10 (13C6,15N4-L-Arginine, Silantes) were added to the "heavy" SILAC medium. Both cell lines (*FMR1*$^{+}$ MEFs and *FMR1*$^{-}$ MEFs) were grown in an incubator (37 °C, 5% CO2) in either "light" or "heavy" SILAC DMEM medium. A complete overview of applied methods is shown in Figure 1.

Protein Extraction

To extract SILAC-labeled proteins from cell culture, cells were washed twice with 5 mL of DPBS (PAA Laboratories) and put on ice to prevent protein degradation during the following denaturation step with a buffer containing 6 M urea, 2 M thiourea, and 10 mM Tris-Base. Protease (complete Mini EDTA-free Proteinase Inhibitor Cocktail) and phosphatase inhibitors (glycerol-2-phosphate, sodium fluorite, and sodium orthovanadate) were added. DNA and RNA were removed during 10 min incubation with benzonase (EMPROVE bio; Merck) at room temperature (RT) followed by centrifugation at 2800*g* (4000 rpm, 10 °C, 25 min). The DNA- and RNA-containing precipitate was removed afterward.

In-Solution Protein Digestion and Isoelectric Focusing

Extracted proteins from each cell line were mixed 1:1 ("light" to "heavy" and vice versa; according to Bradford assay, Bio-Rad Laboratories). Protein mixtures were digested according to the protocol published by Macek et al.[37] Portions of the tryptic peptides, 100 μg per sample, were further fractionated according to their isoelectric point on 3100 OffGel fractionators (Agilent) by Off-Gel separation using manufacturer's instructions. Focusing was done with 13 cm Immobiline DryStrips pH 3−10 (GE Healthcare), resulting in 12 fractions per sample. Current was limited to 50 μA and fractionation completed as soon as 20 kVh were reached. Fractions were acidified using acidic acid (30% ACN, 10% TFA, and 5% acetic acid in water) before desalting on StageTips, described by Ishihama.[38]

Phosphopeptide Enrichment

Phosphopeptide enrichment was done as described previously[39] with the following modifications: 5 mg of digested peptides per sample (a portion of tryptic digestion described in previous section) were separated using strong cation exchange (SCX) chromatography with a linear gradient of 0−35% of SCX solvent B over 32 min, which resulted in 16 fractions. The resulting 16 fractions were pooled to 11 fractions according to the SCX chromatogram. The flow-through, containing unbound peptides, was collected separately. Eleven fractions per replicate plus flow-through were further processed via TiO_2 chromatography. Hereafter, phosphopeptides were eluted in three steps with elution buffer (40% ammonium hydroxide solution in 60% acetonitrile, pH 10.5). The TiO_2 chromatography was done once or twice per fraction depending on the phosphopeptide quantities expected from the SCX chromatogram. Enrichment of the flow-through was done five times.

dx.doi.org/10.1021/pr5006372 | J. Proteome Res. 2014, 13, 4388−4397

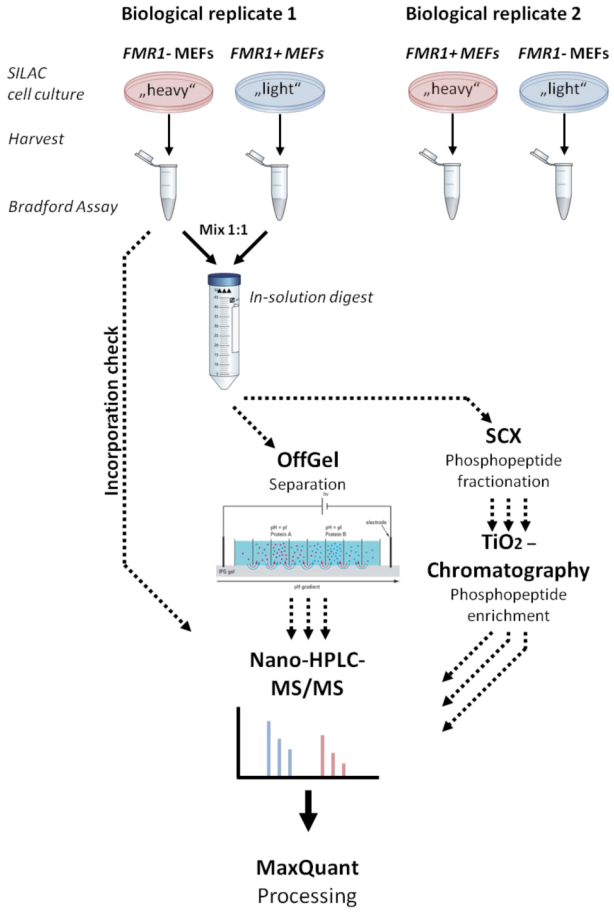

Figure 1. Proteomic and phosphoproteomic workflow for two replicates of SILAC-labeled cells. *FMR1*$^-$ MEFs and *FMR1*$^+$ MEFs cells were grown in SILAC-labeled medium for 14 days. In biological replicate 1, *FMR1*$^-$ MEFs were "heavy" and *FMR1*$^+$ MEFs "light" labeled, while, in biological replicate 2, labeling was inversed. After labeling, cells were harvested, followed by cell lysis and protein extraction. Full incorporation of SILAC amino acids was confirmed. After 1:1 mixing of "heavy" and "light" cell lysates and subsequent in-solution digestion, one part was used for the proteomic workflow, which includes separation by OffGel and measurement by nano-HPLC MS/MS on a LTQ-Orbitrap Elite and further processing by MaxQuant software. The greater part of digested proteins was fractionated by SCX, and phosphopeptides were enriched by TiO_2 chromatography before subsequent measurements by nano-HPLC MS/MS on a LTQ-Orbitrap XL.

Nano-LC-MS/MS Analysis

All peptides were measured on Easy-LC nano-HPLC (Proxeon Biosystems) coupled to an LTQ Orbitrap Elite mass spectrometer (Thermo Fisher Scientific) for the proteome or an LTQ Orbitrap XL (Thermo Fisher Scientific) for the phosphoproteome. Liquid chromatography was done with a 15 cm fused silica emitter with an inner diameter of 75 μm and a tip diameter of 8 μm, in-house made nano-HPLC column, packed with reversed-phase ReproSil-Pur C18-AQ 3 μm resin (Dr. Maisch GmbH). Peptides were flushed with HPLC solvent A (0.5% acetic acid) at a flow rate of 500 nL/min with the maximum pressure of 280 bar. Elution was done using segmented 90 min gradient (LTQ Orbitrap Elite) or 130 min (LTQ Orbitrap XL) of 5−90% HPLC solvent B (80% ACN, 0.5% acetic acid) at a flow rate of 200 nL/min. The eluted peptides were ionized in an electrospray ionization (ESI) source (Proxeon Biosystems) set to positive ion mode. Full scan MS spectra were acquired in the orbitrap analyzer in a mass range from m/z 300−2000 at a resolution of 120,000 (LTQ Orbitrap Elite) or 60,000 (LTQ Orbitrap XL), followed by fragmentation in an LTQ mass analyzer of the top 20 (LTQ Orbitrap Elite) or top 5 (LTQ Orbitrap XL) most intense precursor ions with collision induced dissociation (CID) at a target value of 5000 charges. Dynamic exclusion was used to exclude fragmented masses for 90 s. In addition, for phosphoproteome measurement (LTQ Orbitrap XL), ions were fragmented by multistage activation (MSA) on the neutral loss ions at −98, −49, and −32.6.

Data Processing and Analysis

The mass spectrometer data were processed using MaxQuant suite V 1.3.0.5.[40,41] Spectra were searched using andromeda search engine[42] against the proteome database of *Mus musculus* (UniProt complete proteome database, downloaded on 25 December 2012), consisting of 50,697 protein entries and 247 commonly observed lab contaminants. The mass tolerance for the first search was set to 20 ppm, and to 6 ppm for the main search. The multiplicity was set to two. Lys0, Arg0 and Lys8, Arg10 for "light" and "heavy" samples, respectively. Full tryptic specificity was required, and a maximum of two missed cleavages were allowed. Carbamidomethylation of cysteine was set as fixed modification, while oxidation, acetylation (on N-term), and phosphorylation on Ser/Thr/Tyr were chosen as variable modifications. The initial mass tolerance for the precursor ion was set to 6 ppm and 0.5 Da at the fragment ion level. For quantification of proteins, a minimum of two peptides with at least seven amino acids had to be detected. The maximum allowed posterior error probability (PEP) was set to 1, and the false discovery rate (FDR) to max 1% for peptides and proteins. Requantification was enabled while the second peptides were disabled.

The localization probabilities of potential phosphorylation events on Ser/Thr/Tyr were calculated based on the post-translational modification (PTM). Quantification of phosphorylation sites was normalized with the respective protein abundance, provided the protein was quantified.

Bioinformatic Analysis

Perseus V 1.3.0.4, a module from the MaxQuant suite,[40] was used for calculation of the Pearson correlation for both proteome and phosphoproteome. This was done by extraction of the H/L ratios from the ProteinGroups.txt file, generated in MaxQuant. Contaminants, reverse hits or identified by site, were removed, values Log2 transformed, and the Pearson correlation calculated for the H/L ratios of both replicates.

The calculation of significantly changing proteins and phosphorylation sites was also done in Perseus V 1.3.0.4 (two-tailed "Significance B" test; $p \leq 0.05$). H/L ratios were transformed to Log2, whereas intensities of peptides or phosphorylation sites were Log10 transformed. For significance of phosphorylation sites, H/L ratios were normalized by corresponding protein H/L ratios.

In the same module we performed functional enrichment analysis of Gene Ontology, Pfam, and KEGG terms for increased and decreased classified proteins and phosphorylation sites. We applied truncation based on Benjamini−Hochberg[43] corrected p-values with a threshold value of 0.05 to test whether specific annotation terms are significantly enriched or depleted among the chosen set of proteins of interest. The adjusted p-values were ±log10 transformed and visualized in Excel. The

dx.doi.org/10.1021/pr5006372 | J. Proteome Res. 2014, 13, 4388−4397

list of proteins and phosphorylation sites from classes 1−3 was divided based on their increasing or decreasing levels separately uploaded to the STRING (The Search Tool for the Retrieval of Interacting Genes) database[44,45] to look for known and predicted protein interactions. We requested the highest confidence score of 0.9 for the predicted protein interaction and discarded disconnected nodes.

The available list of FMRP protein−RNA interactions (pri) or protein−protein interactions (ppi) manually curated from the literature[46] was updated with recent references (notably ref 9) and used to appreciate the overlap between dysregulated proteins in the present data sets of protein levels and phosphorylation events.

Western Blotting

Cell extracts were analyzed by Western blotting as described previously.[46,47] The following primary antibodies were used: 1C3 against FMRP (1:500[48]); 3Fx against FXR1P and cross-reacting with FXR2P (1:500[49]), anti-β-actin monoclonal antibody (1:20,000; Sigma), anti-β-tubulin monoclonal antibody (1:500, clone E7, Iowa Developmental Hybridoma Bank, USA), anti-cPLA2 (1:1,000, Santa Cruz), and anti-Prp (1:500, clone SAF70[50]). Digital acquisition of the chemiluminescent signal was performed using the Las-3000 Imager system (Fujifilm). Quantitation of Western blot was performed using the ImageJ software and normalized to the β-actin or β-tubulin signal. GraphPad 4 software was used for statistical analysis.

RESULTS AND DISCUSSION

To compare the proteome and the phosphoproteome of the *FMR1*$^-$ and the control *FMR1*$^+$ MEF cell lines, we performed two SILAC experiments in reverse labeling manner. Briefly, SILAC-labeled cells were lysed, and their proteins were extracted and digested with trypsin. A smaller portion of the digests was separated by isoelectric focusing (for proteome measurement), whereas the larger portion was subjected to two stages of phosphopeptide enrichment, using SCX and TiO_2 chromatographies (for phosphoproteome measurement). All LC-MS/MS measurements were performed on the LTQ-Orbitrap mass spectrometers and MS data were processed by MaxQuant software package (Figure 1). Incorporation of SILAC labels was verified in dedicated mass spectrometry runs, which confirmed full labeling of the MEF proteome (Supporting Information Table 1). "Heavy" (Arg10, Lys8) and "light" (Arg0, Lys0) labeled cell lysates were mixed in equal amounts as verified by MS measurements (Supporting Information Table 2). Pearson correlation coefficients between SILAC ratios measured in two biological replicates were $r = -0.932$ for the proteome and $r = -0.708$ for the phosphoproteome data, indicating high reproducibility at both levels (Figure 2A, B). Inverse correlation is a consequence of inverse SILAC labeling.

Overview of Proteome and Phosphoproteome Results

Combined analysis of 24 MS runs from isoelectric focusing (proteome analysis) and 44 MS runs from phosphopeptide enrichment resulted in 56,352 identified peptide sequences from 6,703 protein groups. Identified protein groups were filtered for contaminants, reverse (decoy) hits, and proteins identified by modification site. The estimated false discovery rate (FDR) was 0.36% at the peptide level and 2.09% at the protein group level. From 6,235 detected endogenous MEF proteins, 4,195 were quantified in both replicates, of which 266 were changing significantly in both biological replicates (134 were increasing and 132 decreasing). Scatter plots of measured protein ratios are shown separately for both replicates in Figure 2C, D.

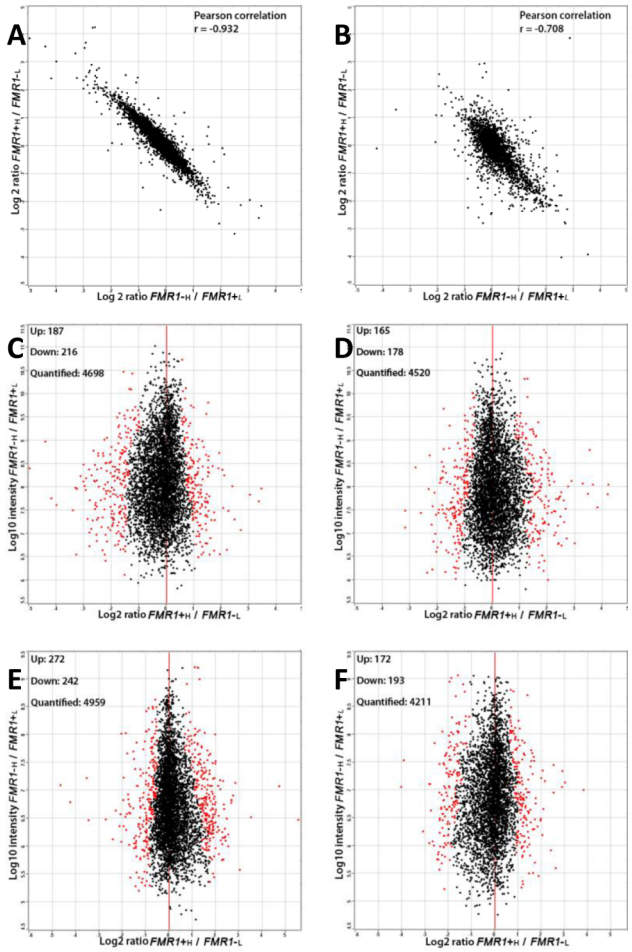

Figure 2. Correlations of proteome and phosphoproteome. Correlation between biological replicates at the (A) proteome and (B) phosphoproteome levels. Each dot represents a SILAC protein or phosphorylation site ratio measured in both biological replicates. Negative correlation is a consequence of inversed SILAC labeling. Distributions of quantified proteins from (C) biological replicate 1; (D) biological replicate 2; (E) phosphorylation sites replicate 1; and (F) biological replicate 2. Intensity is log10, H/L ratios log2 transformed. Red dots represent significant ($p < 0.05$) outliers, which are reported separately for increased and decreased in *FMR1*$^-$ MEF.

The phosphoproteome analysis revealed 9,181 phosphorylation events on 2,494 proteins. Since we expected expression differences at both proteome and phosphoproteome levels, we normalized phosphopeptide ratios with protein ratios. The total number of quantified phosphorylation events that could be normalized by the respective protein ratio was 6,040, of which 142 showed significant changes in both replicates (86 phosphorylation sites were increasing, and 56 phosphorylation sites were decreasing in *FMR1*$^-$ cells compared to the *FMR1*$^+$ cells). Distributions of phosphorylation events measured in both replicates are shown in Figure 2E, F.

We next compared our quantified proteome data set with reported mRNA targets or protein interactors of FMRP[9,51−62] (see Materials and Methods section). This comparison revealed 383 proteins, of which 23 were significantly changing in at least one biological replicate in our data set. Surprisingly, the levels

dx.doi.org/10.1021/pr5006372 | J. Proteome Res. 2014, 13, 4388−4397

of only eight proteins were significantly increasing in *FMR1*$^-$ MEFs, as should be expected for mRNA targets for which FMRP would repress translation,[16] while 15 were significantly decreasing. This limited overlap can have several reasons, starting from the proteome coverage obtained in our study (we estimate that we quantified about one-third of all expressed proteins in the cell), studied system (original mRNA data are derived from the mouse brain), and additional regulatory mechanisms that likely influence the final level of an FMRP target protein in the cell, such as protein degradation. All detected proteins and phosphorylation events of proteins that are known mRNA targets or protein interactors of FMRP are listed in Supporting Information Table 3.

Validation by Western Blotting

The mass spectrometry-based quantification was further validated by Western blot (Figure 3). Analysis using the anti-FMRP mAb1C3 confirmed the expression of FMRP in *FMR1*$^+$ MEFs and its absence in *FMR1*$^-$ MEFs (Figure 3A). Western blot analysis with the 3Fx antibody recognizing the homologues of FMRP, all isoforms of Fxr1p and Fxr2p, showed that the lack of FMRP did not affect their levels of expression (Figure 3B). This confirms the mass spectrometry measurements and previous observations that the absence of FMRP is not compensated by upregulation of its homologues.[63]

We also validated two candidate proteins significantly dysregulated in the MS experiments. First, semiquantitative Western blotting analysis confirmed that *FMR1*$^-$ MEFs express lower levels of the major prion protein (Prp) than *FMR1*$^+$ MEFs (Figure 3C left panel), exhibiting a significant decrease of 62% (p = 0.0361; Figure 3C right panel). Since PrP has a role in the formation of synapses[64] and in memory processing in the rat hippocampus,[65] we hypothesize that reduced levels of Prp could contribute to the cognitive deficits observed in the *FMR1*-KO mouse. Second, we observed a significant increase in cytosolic calcium-dependent phospholipase A2 (Pla2g4a known as cPLA2, Figure 3D left panel) levels which is increased by 82% in *FMR1*$^-$ MEFs as compared to *FMR1*$^+$ MEFs (p = 0.0079; Figure 3D right panel). cPLA2 releases arachidonic acid from membrane phospholipids. Importantly, cPLA2 participates in cerebellar long-term depression and motor learning.[66] It is tempting to speculate that abnormal overexpression of cPLA2 in the brain could participate in the cerebellar dysfunctions observed in *Fmr1*-KO mice.[67] Significantly higher concentrations of cPLA2 have been reported in red blood cells of patients with autism,[68] further linking systemic dysregulations of cPLA2 to autism.

Regulatory Pathway Analysis

For downstream bioinformatic analysis and pathway mapping, detected proteins and phosphorylation events were clustered into three classes based on quantification confidence as described in Table 1. Proteins and phosphorylation events that were not significantly changing in any of the replicates were not further considered.

To investigate general processes and pathways that differ between the *FMR1*$^+$ and *FMR1*$^-$ MEFs, we first used classified proteins and phosphorylation sites to perform functional enrichment analysis of Gene Ontology (GO), Pfam, and KEGG terms. The set of proteins and phosphorylation events with *increased* levels revealed significant overrepresentation of terms related to cell cycle, nucleotide metabolism, and p53 pathway (proteome level), as well as vasopressin-regulated water reabsorption and ribosome (phosphoproteome level)

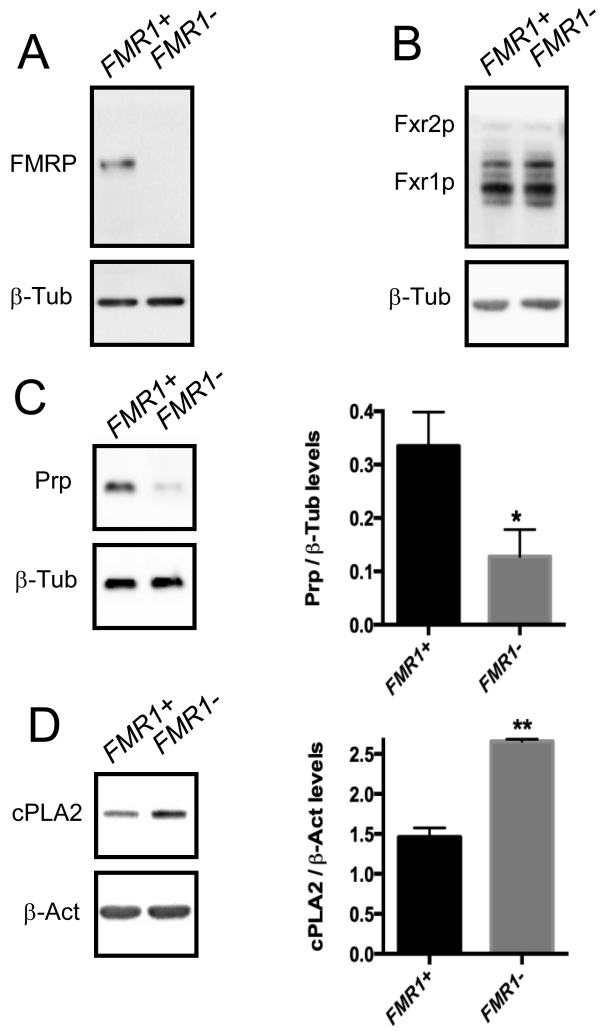

Figure 3. Western blot analysis of *FMR1*-KO MEFs reexpressing (*FMR1*$^+$) or not (*FMR1*$^-$) FMRP. (A) Western blot analysis with anti-FMRP 1C3 antibody. β-tubulin (β-tub) signal is used to verify equal loading of lanes. (B) Western blot analysis of *FMR1*$^+$ or *FMR1*$^-$ MEFs with anti-Fxr1P/Fxr2p antibody #3FX recognizing the homologues of Fmrp, Fxr1p (short and medium isoforms), and Fxr2p. β-tubulin (β-tub) signal is used to verify equal loading of lanes. (C) Representative Western blot of Prp protein levels in *FMR1*$^+$ or *FMR1*$^-$ MEFs. Densitometric quantification of Western blots reveals that depletion of *Fmr1* leads to a significant decrease of Prp protein levels relative to *FMR1*$^+$ cells. (D) Representative Western blot of cPLA2 protein levels in *FMR1*$^+$ or *FMR1*$^-$ MEFs. Densitometric quantification of Western blots shows that depletion of *Fmr1* leads to a significant increase in cPLA2 protein levels. Data are presented as means ± SEM of n = 5 experiments. The asterisks * and ** indicate respectively $p < 0.05$ and $p < 0.01$ of the Mann and Whitney test.

(Supporting Information Table 4). Proteins and phosphorylation events with *decreased* levels pointed to significant overrepresentation of functions related to peroxisome proliferator-activated receptor (PPAR) pathway, lysosome and extracellular matrix interaction (proteome level), as well as gap junction, Alzheimer' s disease, long-term potentiation, long-term depression, axon guidance, and Wnt and MAP kinase pathways (phosphoproteome level) (Supporting Information Table 5).

We next searched the STRING[44,45] database for known and predicted protein−protein interactions among classified proteins and phosphorylation events detected in our data set.

dx.doi.org/10.1021/pr5006372 | J. Proteome Res. 2014, 13, 4388−4397

Table 1. Classification of Quantified Proteins and Phosphorylation Sites[a]

	Proteins		Phosphorylation sites	
	Increased in *FMR1*-KO	Decreased in *FMR1*-KO	Increased in *FMR1*-KO	Decreased in *FMR1*-KO
Class 1	134	132	86	56
Class 2	77	75	131	129
Class 3	34	59	124	157
Classes 1 + 2 + 3	245	266	341	342

[a]Class 1 includes proteins or phosphorylation sites which were significantly changing in both replicates. Class 2 consists of protein phosphorylation sites which were significantly changing in at least one replicate and have the same trend in both replicates. Class 3 was significant in at least one replicate and had a missing value in the other replicate.

The STRING analysis revealed strong clusters of cell cycle-related and ribosomal proteins among proteins with increased levels in *FMR1*$^-$ cells (Supporting Information Figure 1A). Interestingly, a cluster of proteins of the ubiquitin/proteasome system was also present in that part of the data set, pointing to a possible increase of protein degradation as a consequence of FMRP loss. Among proteins with decreased levels in *FMR1*$^-$ cells, the STRING analysis detected several members of the gluthatione-*S*-transferase (GST) protein family, as well as PTEN/phospholipase pathway and Notch signaling (Supporting Information Figure 1B). The decrease in GST members can be linked to the increase in oxidative stress markers observed in the brain of *Fmr1*-KO mice.[46,69] In the phosphoproteome data set, we observed increased phosphorylation on clusters of proteins related to pre-mRNA processing, DNA replication, ribosomal proteins, and several proteins involved in nuclear transport, such as nucleoporins (Figure 4A), revealing that the FMRP influence on these processes is largely mediated at the protein phosphorylation level. Among proteins with decreased phosphorylation levels in *FMR1*$^-$ cells, we detected several proteins from the MAPK pathway (Figure 4B).

To gain a more detailed insight into differences in specific signal transduction networks, we mapped classified proteins and phosphorylation events onto highly conserved pathways from Kyoto Encyclopedia of Genes and Genomes (KEGG),[70] focusing on the mTOR, p53, Wnt, and MAPK pathways.

mTOR Signaling Pathway

In *FMR1*$^-$ cells, we observed that the levels of mTOR and the main proteins of the Akt-mTOR pathway were not significantly changing in steady states (Supporting Information Figure 2). However, our data showed a significant decrease in the phosphorylation level on ERK (see below) and we also observed decreased phosphorylation levels of IRS1 and Rictor. Interestingly, we detected a significant decrease in levels of PTEN, an inhibitor of the PI3K-AKT cascade pathway which is associated with memory and learning process[71] and whose downregulation is connected to autism[72] and FXS.[73] We also observed a significant increase of phosphorylation on the S6 protein, which is a likely consequence of activated p70 S6 kinase[74] and points to an increase of mTOR activity and protein synthesis in *FMR1*$^-$ MEFs.

The mammalian target of rapamycin (mTOR), a serine/threonine kinase, is a signaling node that plays an important role in cellular processes such as protein synthesis and proliferation.[75] Notably, the mTOR/Akt pathway controls mGluR5-mediated activity-dependent protein synthesis involved in synaptic plasticity. There are contradictory statements on the contribution of the Akt-mTOR pathway on the exaggerated global protein synthesis in FXS. While Sharma et al. suppose a possible role for mTOR signaling in increased mGluR-LTD and assume a causal relationship between elevated

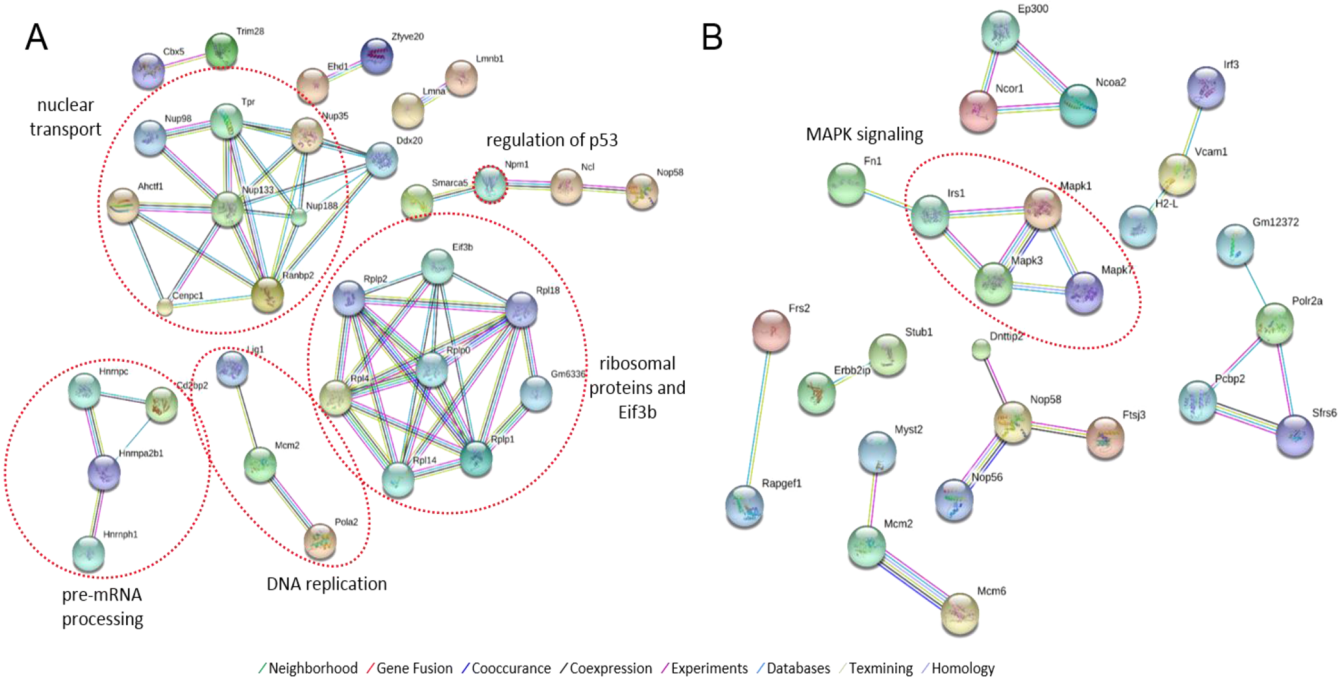

Figure 4. Known and predicted protein interactions of detected phosphoproteins in *Fmr1*$^-$ STEK cells: (A) proteins with increased phosphorylation; (B) proteins with decreased phosphorylation. Interactions were retrieved from the STRING database using all phosphorylation sites from classes 1−3.

dx.doi.org/10.1021/pr5006372 | *J. Proteome Res.* 2014, 13, 4388−4397

mTOR signaling and overactivation of group 1 mGluRs,[76] Osterweil et al. showed that mTOR does not contribute to the increased protein synthesis.[77] These authors also showed that the ERK1/2 pathway is responsible for elevated protein synthesis; still, the pathway by itself is not overactive but rather hypersensitive to stimulation.[76,77]

p53 Signaling Pathway

Our data set revealed a significant increase of the p53 protein in *FMR1*$^{-}$ cells as well as significant changes in eight other proteins linked to p53 signaling. Chk1, Cdk4/6, Cyclin B, Cdc2, and p53R2 were increased, whereas KAI, PTEN, and TSAP6 were decreased (Supporting Information Figure 3).

Using adult neuronal progenitor/stem cells (aNPCs) as a model, Luo et al. showed that FMRP regulates Cyclin D and Cdk4 mRNAs involved in cell cycle progression.[78] In addition, Liu et al. showed that Cyclin B is upregulated in the *Drosophila* FXS model,[79] which supports proposed involvement of FMRP in cell cycle control. Although there is to date very little evidence linking p53 signaling to FXS, recent reports show the involvement of FMRP in the DNA damage response,[80,81] a cellular response which triggers activation of the p53 pathway. Also, p53 mRNA is a putative target of FMRP, since its 3′UTR harbors a G-quadruplex RNA structure[82] that is an RNA motif bound with high affinity by FMRP.[55,83] Furthermore, there are several reports on the role of p53 in autism. Sheikh et al. examined a possible apoptosis signaling deregulation in the brain of autistic subjects and found increased levels of p53.[84] Taken together, our results point to involvement of p53 and its downstream targets in dysregulated cell cycle control in FXS.

WNT Signaling Pathway

The canonical Wnt pathway is crucial for activation of neuronal differentiation during neurogenesis, and its inhibition induces hippocampus-dependent learning deficits.[85,86] For this reason it was hypothesized that defective Wnt signaling might be linked to human mental disorders such as FXS. Indeed, reduced Wnt signaling in aNPCs was found by Luo et al. in the hippocampus of *FMR1*-KO mice.[87] Our data revealed a decrease of FRP level, which normally blocks the Wnt canonical pathway (Supporting Information Figure 4). Since it is reported that Wnt signaling is reduced in FXS, it is possible that this is one of the compensatory mechanisms. In addition, we detected decreased levels of Knypek, which was shown previously to influence synaptic formation and is involved in AMPAR mobility.[88] In the Wnt/calcium pathway we detected a significant decrease both in the PLC levels and those of its phosphorylated forms, significant dephosphorylation of PKC, as well as significant dephosphorylation of the transcription factor NFAT. We therefore postulate that calcium homeostasis and Wnt/calcium-dependent gene expression may be affected in molecular pathogenesis of FXS.

MAPK Signaling Pathway

Our data point to a general downregulation of the canonical MAPK pathway, including related receptors and signaling nodes such as EGF-receptor, Ras, and ERK1/2 (Supporting Information Figure 5). We observed a decrease in ERK2 levels and a significant decrease in the phosphorylation status of ERK2 Thr183 and Tyr185, based on statistical significance mentioned in the Materials and Methods section. Decreased levels of ERK1/2 and its phosphorylation are associated with cell proliferation, migration, and differentiation, also in the central nervous system, and these processes are therefore expected to be affected in FXS.[89] Deficits in proper neurogenesis and neuronal differentiation in the absence of FMRP were previously described.[90] Importantly, a significant reduction in basal phosphorylation of ERK1/2 was also observed previously in the CA1 region of the *FMR1*-KO hippocampus.[77] We also observed a significant increase of Filamin A (FLNA) levels with a concomitant significant decrease in its phosphorylation levels. Interestingly, it was previously reported that Filamin A phosphorylation modulates actin neuronal remodelling[79] and that its downregulation in *dfmr1*-null *Drosophila* participates in abnormal neuronal branching.[91] Importantly, in *Fmr1*$^{-}$ cells we also detected a significant increase in the level of the cytoskeleton regulator PAK kinase, which was previously reported to be a drug target for FXS and autism therapy.[92,93]

CONCLUSIONS

Our data represent the first global large-scale analysis of the proteome and phosphoproteome of the *Fmr1*-KO MEF cell lines, a commonly used *Fmr1*-KO model. Since the control *Fmr1*-KO MEF cells were re-expressing human FMRP ISO1, we expect that the presented data reflect mostly the function of this particular FMRP isoform; however, overlaps with other FMRP isoforms as well with FMRP paralogs (FXR1P or FXR2P) are possible. We detected 266 proteins and 142 phosphorylation sites that are significantly changing in both biological replicates and analyzed them in the context of the major signal transduction implicated in FXS. We confirm downregulation of the MEK/ERK pathway in the absence of FMRP, with decreased phosphorylation on ERK1/2. We report differential expression of several proteins involved in mTOR, Wnt, p53, and MAPK signaling cascades, that were known to be associated with autism, but not with FXS. We detect significant increase of p53 and proteins linked to the p53 signaling. This study opens new avenues and motivates further investigation in neuronal cultures and *in vivo* FXS models to connect current insights to early signaling events from receptors that are not expressed or functional in MEF cells. This will ultimately lead to a better understanding of the molecular mechanisms dysregulated in FXS.

ASSOCIATED CONTENT

Supporting Information

Incorporation rates of "heavy" isotopes of arginine and lysine in cells after 9 days of growth in SILAC media; SILAC heavy/light mixing error; detected proteins and phosphorylation sites; functional enrichment analysis of Gene Ontology, Pfam, and KEGG terms in *increased* proteins and phosphorylation sites from classes 1−3; functional enrichment analysis of Gene Ontology, Pfam, and KEGG terms in *decreased* proteins and phosphorylation sites from classes 1−3; STRING analysis; classified proteins and phosphorylation events mapped onto the mTOR signaling pathway; classified proteins and phosphorylation events mapped onto the p53 signaling pathway; classified proteins and phosphorylation events mapped onto the Wnt signaling pathway; classified proteins and phosphorylation events mapped onto the MAPK signaling pathway. This material is available free of charge via the Internet at http://pubs.acs.org.

AUTHOR INFORMATION

Corresponding Authors

*Phone: +33/(0)493/95 77 62. Fax: + 33/(0)493/95 77 08. E-mail: davidovic@ipmc.cnrs.fr.

*Phone: +49/(0)7071/29-70556. Fax: +49/(0)7071/29-5779. E-mail: boris.macek@uni-tuebingen.de.

Author Contributions

⊥K.M. and T.E. contributed equally to this work.

Notes

The authors declare no competing financial interest.

ACKNOWLEDGMENTS

The authors gratefully thank Prof. E.W. Khandjian (Centre de Recherche Université Laval-Robert Giffard, Québec, Canada) for kindly providing the SV40-transformed STEK cell line in which were performed experiments preliminary to this study. L.D. thanks Joëlle Chabry and Gérard Lambeau (IPMC, Valbonne, France) for providing antibodies and advice for their use. Our work was supported by CNRS, FRAXA Foundation, Université de Nice, and ANR JCJC MetaboXFra (to L.D.), INSERM, Agence Nationale de la Recherche: ANR-11-LABX-0028-01, Blanc SVSE4-2012, and Blanc SVSE8-2012 (to B.B.), and FP7 PRIME-XS Consortium (to B.M.).

REFERENCES

(1) Coffee, B.; Keith, K.; Albizua, I.; Malone, T.; Mowrey, J.; Sherman, S. L.; Warren, S. T. Incidence of Fragile X Syndrome by Newborn Screening for Methylated FMR1 DNA. *Am. J. Human Genet.* **2009**, *85* (4), 503−514.

(2) Wang, L. W.; Berry-Kravis, E.; Hagerman, R. J. Fragile X: leading the way for targeted treatments in autism. *Neurotherapeutics* **2010**, *7* (3), 264−274.

(3) Reddy, K. S. Cytogenetic abnormalities and fragile-X syndrome in Autism Spectrum Disorder. *BMC Med. Genet.* **2005**, *6*, 3.

(4) Pieretti, M.; Zhang, F. P.; Fu, Y. H.; Warren, S. T.; Oostra, B. A.; Caskey, C. T.; Nelson, D. L. Absence of expression of the FMR-1 gene in fragile X syndrome. *Cell* **1991**, *66* (4), 817−822.

(5) Verkerk, A. J.; Pieretti, M.; Sutcliffe, J. S.; Fu, Y. H.; Kuhl, D. P.; Pizzuti, A.; Reiner, O.; Richards, S.; Victoria, M. F.; Zhang, F. P.; et al. Identification of a gene (FMR-1) containing a CGG repeat coincident with a breakpoint cluster region exhibiting length variation in fragile X syndrome. *Cell* **1991**, *65* (5), 905−14.

(6) Ashley, J. C. T.; Wilkinson, K. D.; Reines, D.; Warren, S. T. FMR1 protein: conserved RNP family domains and selective RNA binding. *Science* **1993**, *262* (5133), 563−566.

(7) Hinds, H. L.; Ashley, C. T.; Sutcliffe, J. S.; Nelson, D. L.; Warren, S. T.; Housman, D. E.; Schalling, M. Tissue specific expression of FMR-1 provides evidence for a functional role in fragile X syndrome. *Nat. Genet.* **1993**, *3* (1), 36−43.

(8) Siomi, H.; Siomi, M. C.; Nussbaum, R. L.; Dreyfuss, G. The protein product of the fragile X gene, FMR1, has characteristics of an RNA-binding protein. *Cell* **1993**, *74* (2), 291−298.

(9) Darnell, J. C.; Van Driesche, S. J.; Zhang, C.; Hung, K. Y.; Mele, A.; Fraser, C. E.; Stone, E. F.; Chen, C.; Fak, J. J.; Chi, S. W.; Licatalosi, D. D.; Richter, J. D.; Darnell, R. B. FMRP stalls ribosomal translocation on mRNAs linked to synaptic function and autism. *Cell* **2011**, *146* (2), 247−61.

(10) Khandjian, E. W.; Corbin, F.; Woerly, S.; Rousseau, F. The fragile X mental retardation protein is associated with ribosomes. *Nat. Genet.* **1996**, *12* (1), 91−3.

(11) Siomi, M. C.; Zhang, Y.; Siomi, H.; Dreyfuss, G. Specific sequences in the fragile X syndrome protein FMR1 and the FXR proteins mediate their binding to 60S ribosomal subunits and the interactions among them. *Mol. Cell. Biol.* **1996**, *16* (7), 3825−32.

(12) Feng, Y.; Absher, D.; Eberhart, D. E.; Brown, V.; Malter, H. E.; Warren, S. T. FMRP associates with polyribosomes as an mRNP, and the I304N mutation of severe fragile X syndrome abolishes this association. *Mol. Cell* **1997**, *1* (1), 109−18.

(13) Laggerbauer, B.; Ostareck, D.; Keidel, E. M.; Ostareck-Lederer, A.; Fischer, U. Evidence that fragile X mental retardation protein is a negative regulator of translation. *Hum. Mol. Genet.* **2001**, *10* (4), 329−38.

(14) Li, Z.; Zhang, Y.; Ku, L.; Wilkinson, K. D.; Warren, S. T.; Feng, Y. The fragile X mental retardation protein inhibits translation via interacting with mRNA. *Nucleic Acids Res.* **2001**, *29* (11), 2276−2283.

(15) Davidovic, L.; Huot, M. E.; Khandjian, E. W. Lost once, the Fragile X Mental Retardation protein is now back onto brain polyribosomes. *RNA Biol.* **2005**, *2* (1), 1−3.

(16) Bechara, E. G.; Didiot, M. C.; Melko, M.; Davidovic, L.; Bensaid, M.; Martin, P.; Castets, M.; Pognonec, P.; Khandjian, E. W.; Moine, H.; Bardoni, B. A novel function for fragile X mental retardation protein in translational activation. *PLoS Biol.* **2009**, *7* (1), e16−e16.

(17) Maurin, T.; Zongaro, S.; Bardoni, B. Fragile X Syndrome: From molecular pathology to therapy. *Neurosci. Biobehav. Rev.* **2014**, DOI: 10.1016/j.neubiorev.2014.01.006.

(18) Higashimori, H.; Morel, L.; Huth, J.; Lindemann, L.; Dulla, C.; Taylor, A.; Freeman, M.; Yang, Y. Astroglial FMRP-dependent translational down-regulation of mGluR5 underlies glutamate transporter GLT1 dysregulation in the fragile X mouse. *Hum. Mol. Genet.* **2013**, *22* (10), 2041−54.

(19) Schutt, J.; Falley, K.; Richter, D.; Kreienkamp, H. J.; Kindler, S. Fragile X mental retardation protein regulates the levels of scaffold proteins and glutamate receptors in postsynaptic densities. *J. Biol. Chem.* **2009**, *284* (38), 25479−87.

(20) Dictenberg, J. B.; Swanger, S. A.; Antar, L. N.; Singer, R. H.; Bassell, G. J. A direct role for FMRP in activity-dependent dendritic mRNA transport links filopodial-spine morphogenesis to fragile X syndrome. *Dev. Cell* **2008**, *14* (6), 926−39.

(21) Bassell, G. J.; Warren, S. T. Fragile X syndrome: loss of local mRNA regulation alters synaptic development and function. *Neuron* **2008**, *60* (2), 201−214.

(22) Pfeiffer, B. E.; Huber, K. M. The state of synapses in fragile X syndrome. *Neuroscientist* **2009**, *15* (5), 549−567.

(23) Fmr1 knockout mice: a model to study fragile X mental retardation. The Dutch-Belgian Fragile X Consortium. *Cell* **1994**, *78*, (1), 23−33.

(24) Mazroui, R.; Huot, M. E.; Tremblay, S.; Filion, C.; Labelle, Y.; Khandjian, E. W. Trapping of messenger RNA by Fragile X Mental Retardation protein into cytoplasmic granules induces translation repression. *Hum. Mol. Genet.* **2002**, *11* (24), 3007−17.

(25) Mientjes, E. J.; Nieuwenhuizen, I.; Kirkpatrick, L.; Zu, T.; Hoogeveen-Westerveld, M.; Severijnen, L.; Rife, M.; Willemsen, R.; Nelson, D. L.; Oostra, B. A. The generation of a conditional Fmr1 knock out mouse model to study Fmrp function in vivo. *Neurobiol. Dis.* **2006**, *21* (3), 549−55.

(26) Castets, M.; Schaeffer, C.; Bechara, E.; Schenck, A.; Khandjian, E. W.; Luche, S.; Moine, H.; Rabilloud, T.; Mandel, J.-L.; Bardoni, B. FMRP interferes with the Rac1 pathway and controls actin cytoskeleton dynamics in murine fibroblasts. *Hum. Mol. Genet.* **2005**, *14* (6), 835−844.

(27) Nolze, A.; Schneider, J.; Keil, R.; Lederer, M.; Hüttelmaier, S.; Kessels, M. M.; Qualmann, B.; Hatzfeld, M. FMRP regulates actin filament organization via the armadillo protein p0071. *RNA* **2013**, *19* (11), 1483−1496.

(28) Didiot, M. C.; Subramanian, M.; Flatter, E.; Mandel, J. L.; Moine, H. Cells lacking the fragile X mental retardation protein (FMRP) have normal RISC activity but exhibit altered stress granule assembly. *Mol. Biol. Cell* **2009**, *20* (1), 428−37.

(29) Liao, L.; Park, S. K.; Xu, T.; Vanderklish, P.; Yates, r. J. R. Quantitative proteomic analysis of primary neurons reveals diverse changes in synaptic protein content in fmr1 knockout mice. *Proc. Natl. Acad. Sci. U. S. A.* **2008**, *105* (40), 15281−15286.

(30) Klemmer, P.; Meredith, R. M.; Holmgren, C. D.; Klychnikov, O. I.; Stahl-Zeng, J.; Loos, M.; van der Schors, R. C.; Wortel, J.; de Wit, H.; Spijker, S.; Rotaru, D. C.; Mansvelder, H. D.; Smit, A. B.; Li, K. W. Proteomics, ultrastructure, and physiology of hippocampal synapses in a fragile X syndrome mouse model reveal presynaptic phenotype. *J. Biol. Chem.* **2011**, *286* (29), 25495−25504.
(31) Xu, P.; Tan, H.; Duong, D. M.; Yang, Y.; Kupsco, J.; Moberg, K. H.; Li, H.; Jin, P.; Peng, J. Stable isotope labeling with amino acids in Drosophila for quantifying proteins and modifications. *J. Proteome Res.* **2012**, *11* (9), 4403−4412.
(32) Olsen, J. V.; Blagoev, B.; Gnad, F.; Macek, B.; Kumar, C.; Mortensen, P.; Mann, M. Global, in vivo, and site-specific phosphorylation dynamics in signaling networks. *Cell* **2006**, *127* (3), 635−648.
(33) Bhakar, A. L.; Dolen, G.; Bear, M. F. The pathophysiology of fragile X (and what it teaches us about synapses). *Annu. Rev. Neurosci.* **2012**, *35*, 417−43.
(34) De Rubeis, S.; Bagni, C. Regulation of molecular pathways in the Fragile X Syndrome: insights into Autism Spectrum Disorders. *J. Neurodev. Disord.* **2011**, *3* (3), 257−69.
(35) Ong, S.-E.; Blagoev, B.; Kratchmarova, I.; Kristensen, D. B.; Steen, H.; Pandey, A.; Mann, M. Stable isotope labeling by amino acids in cell culture, SILAC, as a simple and accurate approach to expression proteomics. *Mol. Cell Proteomics* **2002**, *1* (5), 376−386.
(36) Castets, M.; Schaeffer, C.; Bechara, E.; Schenck, A.; Khandjian, E. W.; Luche, S.; Moine, H.; Rabilloud, T.; Mandel, J. L.; Bardoni, B. FMRP interferes with the Rac1 pathway and controls actin cytoskeleton dynamics in murine fibroblasts. *Hum. Mol. Genet.* **2005**, *14* (6), 835−44.
(37) Macek, B.; Mijakovic, I.; Olsen, J. V.; Gnad, F.; Kumar, C.; Jensen, P. R.; Mann, M. The serine/threonine/tyrosine phosphoproteome of the model bacterium Bacillus subtilis. *Mol. Cell. Proteomics* **2007**, *6* (4), 697−707.
(38) Ishihama, Y.; Rappsilber, J.; Mann, M. Modular stop and go extraction tips with stacked disks for parallel and multidimensional peptide fractionation in proteomics. *J. Proteome Res.* **2006**, *5* (4), 988−994.
(39) Olsen, J. V.; Macek, B. High accuracy mass spectrometry in large-scale analysis of protein phosphorylation. *Methods Mol. Biol.* **2009**, *492*, 131−42.
(40) Cox, J.; Mann, M. MaxQuant enables high peptide identification rates, individualized p.p.b.-range mass accuracies and proteome-wide protein quantification. *Nat. Biotechnol.* **2008**, *26* (12), 1367−72.
(41) Cox, J.; Matic, I.; Hilger, M.; Nagaraj, N.; Selbach, M.; Olsen, J. V.; Mann, M. A practical guide to the MaxQuant computational platform for SILAC-based quantitative proteomics. *Nat. Protoc.* **2009**, *4* (5), 698−705.
(42) Cox, J.; Neuhauser, N.; Michalski, A.; Scheltema, R. A.; Olsen, J. V.; Mann, M. Andromeda: a peptide search engine integrated into the MaxQuant environment. *J. Proteome Res.* **2011**, *10* (4), 1794−805.
(43) Benjamini, Y.; Hochberg, Y. Controlling the False Discovery Rate—A Practical and Powerful Approach to Multiple Testing. *J. R. Stat. Soc., Ser. B: Methodological* **1995**, *57* (1), 289−300.
(44) Jensen, L. J.; Kuhn, M.; Stark, M.; Chaffron, S.; Creevey, C.; Muller, J.; Doerks, T.; Julien, P.; Roth, A.; Simonovic, M.; Bork, P.; von Mering, C. STRING 8—a global view on proteins and their functional interactions in 630 organisms. *Nucleic Acids Res.* **2009**, *37* (Database issue), D412−6.
(45) Franceschini, A.; Szklarczyk, D.; Frankild, S.; Kuhn, M.; Simonovic, M.; Roth, A.; Lin, J.; Minguez, P.; Bork, P.; von Mering, C.; Jensen, L. J. STRING v9.1: protein-protein interaction networks, with increased coverage and integration. *Nucleic Acids Res.* **2013**, *41* (Database issue), D808−15.
(46) Davidovic, L.; Navratil, V.; Bonaccorso, C. M.; Catania, M. V.; Bardoni, B.; Dumas, M. E. A metabolomic and systems biology perspective on the brain of the fragile X syndrome mouse model. *Genome Res.* **2011**, *21* (12), 2190−202.
(47) Davidovic, L.; Bechara, E.; Gravel, M.; Jaglin, X. H.; Tremblay, S.; Sik, A.; Bardoni, B.; Khandjian, E. W. The nuclear MicroSpherule protein 58 is a novel RNA-binding protein that interacts with fragile X mental retardation protein in polyribosomal mRNPs from neurons. *Hum. Mol. Genet.* **2006**, *15* (9), 1525−1538.
(48) Devys, D.; Lutz, Y.; Rouyer, N.; Bellocq, J. P.; Mandel, J. L. The FMR-1 protein is cytoplasmic, most abundant in neurons and appears normal in carriers of a fragile X premutation. *Nat. Genet.* **1993**, *4* (4), 335−40.
(49) Khandjian, E. W.; Bardoni, B.; Corbin, F.; Sittler, A.; Giroux, S.; Heitz, D.; Tremblay, S.; Pinset, C.; Montarras, D.; Rousseau, F.; Mandel, J.-L. Novel Isoforms of the Fragile X Related Protein FXR1P are Expressed During Myogenesis. *Hum. Mol. Genet.* **1998**, *7* (13), 2121−2128.
(50) Demart, S.; Fournier, J. G.; Creminon, C.; Frobert, Y.; Lamoury, F.; Marce, D.; Lasmezas, C.; Dormont, D.; Grassi, J.; Deslys, J. P. New insight into abnormal prion protein using monoclonal antibodies. *Biochem. Biophys. Res. Commun.* **1999**, *265* (3), 652−7.
(51) Siomi, M. C.; Siomi, H.; Sauer, W. H.; Srinivasan, S.; Nussbaum, R. L.; Dreyfuss, G. FXR1, an autosomal homolog of the fragile X mental retardation gene. *EMBO J.* **1995**, *14* (11), 2401−8.
(52) Zhang, Y.; O'Connor, J. P.; Siomi, M. C.; Srinivasan, S.; Dutra, A.; Nussbaum, R. L.; Dreyfuss, G. The fragile X mental retardation syndrome protein interacts with novel homologs FXR1 and FXR2. *EMBO J.* **1995**, *14* (21), 5358−66.
(53) Sung, Y. J.; Conti, J.; Currie, J. R.; Brown, W. T.; Denman, R. B. RNAs That Interact with the Fragile X Syndrome RNA Binding Protein FMRP. *Biochem. Biophys. Res. Commun.* **2000**, *275* (3), 973−980.
(54) Brown, V.; Jin, P.; Ceman, S.; Darnell, J. C.; O'Donnell, W. T.; Tenenbaum, S. A.; Jin, X.; Feng, Y.; Wilkinson, K. D.; Keene, J. D.; Darnell, R. B.; Warren, S. T. Microarray Identification of FMRP-Associated Brain mRNAs and Altered mRNA Translational Profiles in Fragile X Syndrome. *Cell* **2001**, *107* (4), 477−487.
(55) Schaeffer, C.; Bardoni, B.; Mandel, J. L.; Ehresmann, B.; Ehresmann, C.; Moine, H. The fragile X mental retardation protein binds specifically to its mRNA via a purine quartet motif. *EMBO J.* **2001**, *20* (17), 4803−13.
(56) Schenck, A.; Bardoni, B.; Moro, A.; Bagni, C.; Mandel, J. L. A highly conserved protein family interacting with the fragile X mental retardation protein (FMRP) and displaying selective interactions with FMRP-related proteins FXR1P and FXR2P. *Proc. Natl. Acad. Sci. U. S. A.* **2001**, *98* (15), 8844−9.
(57) Chen, L.; Yun, S. W.; Seto, J.; Liu, W.; Toth, M. The fragile x mental retardation protein binds and regulates a novel class of mRNAs containing u rich target sequences. *Neuroscience* **2003**, *120* (4), 1005−1017.
(58) Dolzhanskaya, N.; Sung, Y. J.; Conti, J.; Currie, J. R.; Denman, R. B. The fragile X mental retardation protein interacts with U-rich RNAs in a yeast three-hybrid system. *Biochem. Biophys. Res. Commun.* **2003**, *305* (2), 434−441.
(59) Miyashiro, K. Y.; Beckel-Mitchener, A.; Purk, T. P.; Becker, K. G.; Barret, T.; Liu, L.; Carbonetto, S.; Weiler, I. J.; Greenough, W. T.; Eberwine, J. RNA Cargoes Associating with FMRP Reveal Deficits in Cellular Functioning in Fmr1 Null Mice. *Neuron* **2003**, *37* (3), 417−431.
(60) Westmark, C. J.; Malter, J. S. FMRP mediates mGluR5-dependent translation of amyloid precursor protein. *PLoS Biol.* **2007**, *5* (3), e52.
(61) Zhang, M.; Wang, Q.; Huang, Y. Fragile X mental retardation protein FMRP and the RNA export factor NXF2 associate with and destabilize Nxf1 mRNA in neuronal cells. *Proc. Natl. Acad. Sci. U. S. A.* **2007**, *104* (24), 10057−10062.
(62) Schütt, J.; Falley, K.; Richter, D.; Kreienkamp, H.-J.; Kindler, S. Fragile X Mental Retardation Protein Regulates the Levels of Scaffold Proteins and Glutamate Receptors in Postsynaptic Densities. *J. Biol. Chem.* **2009**, *284* (38), 25479−25487.
(63) Khandjian, E. W.; Bardoni, B.; Corbin, F.; Sittler, A.; Giroux, S.; Heitz, D.; Tremblay, S.; Pinset, C.; Montarras, D.; Rousseau, F.; Mandel, J. Novel isoforms of the fragile X related protein FXR1P are expressed during myogenesis. *Hum. Mol. Genet.* **1998**, *7* (13), 2121−8.

(64) Kanaani, J.; Prusiner, S. B.; Diacovo, J.; Baekkeskov, S.; Legname, G. Recombinant prion protein induces rapid polarization and development of synapses in embryonic rat hippocampal neurons in vitro. *J. Neurochem.* **2005**, *95* (5), 1373−1386.
(65) Criado, J. R.; Sanchez-Alavez, M.; Conti, B.; Giacchino, J. L.; Wills, D. N.; Henriksen, S. J.; Race, R.; Manson, J. C.; Chesebro, B.; Oldstone, M. B. A. Mice devoid of prion protein have cognitive deficits that are rescued by reconstitution of PrP in neurons. *Neurobiol. Disease* **2005**, *19* (1−2), 255−265.
(66) Le, T. D.; Shirai, Y.; Okamoto, T.; Tatsukawa, T.; Nagao, S.; Shimizu, T.; Ito, M. Lipid signaling in cytosolic phospholipase A2alpha-cyclooxygenase-2 cascade mediates cerebellar long-term depression and motor learning. *Proc. Natl. Acad. Sci. U. S. A.* **2010**, *107* (7), 3198−203.
(67) Huber, K. M. The fragile X-cerebellum connection. *Trends Neurosci.* **2006**, *29* (4), 183−5.
(68) Bell, J. G.; MacKinlay, E. E.; Dick, J. R.; MacDonald, D. J.; Boyle, R. M.; Glen, A. C. A. Essential fatty acids and phospholipase A2 in autistic spectrum disorders. *Prostaglandins Leukot Essent. Fatty Acids* **2004**, *71* (4), 201−204.
(69) el Bekay, R.; Romero-Zerbo, Y.; Decara, J.; Sanchez-Salido, L.; Del Arco-Herrera, I.; Rodriguez-de Fonseca, F.; de Diego-Otero, Y. Enhanced markers of oxidative stress, altered antioxidants and NADPH-oxidase activation in brains from Fragile X mental retardation 1-deficient mice, a pathological model for Fragile X syndrome. *Eur. J. Neurosci.* **2007**, *26* (11), 3169−80.
(70) Kanehisa, M.; Goto, S. KEGG: kyoto encyclopedia of genes and genomes. *Nucleic Acids Res.* **2000**, *28* (1), 27−30.
(71) Lugo, J. N.; Smith, G. D.; Morrison, J. B.; White, J. Deletion of PTEN produces deficits in conditioned fear and increases fragile X mental retardation protein. *Learn. Mem.* **2013**, *20* (12), 670−3.
(72) Butler, M. G.; Dasouki, M. J.; Zhou, X. P.; Talebizadeh, Z.; Brown, M.; Takahashi, T. N.; Miles, J. H.; Wang, C. H.; Stratton, R.; Pilarski, R.; Eng, C. Subset of individuals with autism spectrum disorders and extreme macrocephaly associated with germline PTEN tumour suppressor gene mutations. *J. Med. Genet.* **2005**, *42* (4), 318−21.
(73) Chiu, S.; Wegelin, J. A.; Blank, J.; Jenkins, M.; Day, J.; Hessl, D.; Tassone, F.; Hagerman, R. Early acceleration of head circumference in children with fragile x syndrome and autism. *J. Dev. Behav. Pediatr.* **2007**, *28* (1), 31−5.
(74) Bhattacharya, A.; Kaphzan, H.; Alvarez-Dieppa, A. C.; Murphy, J. P.; Pierre, P.; Klann, E. Genetic removal of p70 S6 kinase 1 corrects molecular, synaptic, and behavioral phenotypes in fragile X syndrome mice. *Neuron* **2012**, *76* (2), 325−37.
(75) Hay, N.; Sonenberg, N. Upstream and downstream of mTOR. *Genes Dev.* **2004**, *18* (16), 1926−1945.
(76) Sharma, A.; Hoeffer, C. A.; Takayasu, Y.; Miyawaki, T.; McBride, S. M.; Klann, E.; Zukin, R. S. Dysregulation of mTOR signaling in fragile X syndrome. *J. Neurosci.* **2010**, *30* (2), 694−702.
(77) Osterweil, E. K.; Krueger, D. D.; Reinhold, K.; Bear, M. F. Hypersensitivity to mGluR5 and ERK1/2 leads to excessive protein synthesis in the hippocampus of a mouse model of fragile X syndrome. *J. Neurosci.* **2010**, *30* (46), 15616−15627.
(78) Luo, Y.; Shan, G.; Guo, W.; Smrt, R. D.; Johnson, E. B.; Li, X.; Pfeiffer, R. L.; Szulwach, K. E.; Duan, R.; Barkho, B. Z.; Li, W.; Liu, C.; Jin, P.; Zhao, X. Fragile x mental retardation protein regulates proliferation and differentiation of adult neural stem/progenitor cells. *PLoS Genet.* **2010**, *6* (4), e1000898.
(79) Liu, W.; Jiang, F.; Bi, X.; Zhang, Y. Q. Drosophila FMRP participates in the DNA damage response by regulating G2/M cell cycle checkpoint and apoptosis. *Hum. Mol. Genet.* **2012**, *21* (21), 4655−4668.
(80) Zhang, W.; Cheng, Y.; Li, Y.; Chen, Z.; Jin, P.; Chen, D. A feed-forward mechanism involving Drosophila fragile X mental retardation protein triggers a replication stress-induced DNA damage response. *Hum. Mol. Genet.* **2014**, DOI: 10.1093/hmg/ddu241.
(81) Alpatov, R.; Lesch, B. J.; Nakamoto-Kinoshita, M.; Blanco, A.; Chen, S.; Stutzer, A.; Armache, K. J.; Simon, M. D.; Xu, C.; Ali, M.; Murn, J.; Prisic, S.; Kutateladze, T. G.; Vakoc, C. R.; Min, J.; Kingston, R. E.; Fischle, W.; Warren, S. T.; Page, D. C.; Shi, Y. A Chromatin-Dependent Role of the Fragile X Mental Retardation Protein FMRP in the DNA Damage Response. *Cell* **2014**, *157* (4), 869−81.
(82) Decorsiere, A.; Cayrel, A.; Vagner, S.; Millevoi, S. Essential role for the interaction between hnRNP H/F and a G quadruplex in maintaining p53 pre-mRNA 3′-end processing and function during DNA damage. *Genes Dev.* **2011**, *25* (3), 220−5.
(83) Melko, M.; Bardoni, B. The role of G-quadruplex in RNA metabolism: involvement of FMRP and FMR2P. *Biochimie* **2010**, *92* (8), 919−26.
(84) Sheikh, A. M.; Malik, M.; Wen, G.; Chauhan, A.; Chauhan, V.; Gong, C.-X.; Liu, F.; Brown, W. T.; Li, X. BDNF-Akt-Bcl2 antiapoptotic signaling pathway is compromised in the brain of autistic subjects. *J. Neurosc.i Res.* **2010**, *88* (12), 2641−2647.
(85) Jessberger, S.; Clark, R. E.; Broadbent, N. J.; Clemenson, J. G. D.; Consiglio, A.; Lie, D. C.; Squire, L. R.; Gage, F. H. Dentate gyrus-specific knockdown of adult neurogenesis impairs spatial and object recognition memory in adult rats. *Learn. Mem.* **2009**, *16* (2), 147−154.
(86) Lie, D.-C.; Colamarino, S. A.; Song, H.-J.; DÃ©sirÃ©, L.; Mira, H.; Consiglio, A.; Lein, E. S.; Jessberger, S.; Lansford, H.; Dearie, A. R.; Gage, F. H. Wnt signalling regulates adult hippocampal neurogenesis. *Nature* **2005**, *437* (7063), 1370−1375.
(87) Luo, Y.; Shan, G.; Guo, W.; Smrt, R. D.; Johnson, E. B.; Li, X.; Pfeiffer, R. L.; Szulwach, K. E.; Duan, R.; Barkho, B. Z.; Li, W.; Liu, C.; Jin, P.; Zhao, X. Fragile x mental retardation protein regulates proliferation and differentiation of adult neural stem/progenitor cells. *PLoS Genet.* **2010**, *6* (4), e1000898−e1000898.
(88) Allen, N. J.; Bennett, M. L.; Foo, L. C.; Wang, G. X.; Chakraborty, C.; Smith, S. J.; Barres, B. A. Astrocyte glypicans 4 and 6 promote formation of excitatory synapses via GluA1 AMPA receptors. *Nature* **2012**, *486* (7403), 410−414.
(89) Cheng, P.; Alberts, I.; Li, X. The Role of ERK1/2 in the Regulation of Proliferation and Differentiation of Astrocytes in Developing Brain. *Int. J. Dev. Neurosci.* **2013**, *31*, 783.
(90) Castrén, M.; Tervonen, T.; Kärkkäinen, V.; Heinonen, S.; CastrÃ©n, E.; Larsson, K.; Bakker, C. E.; Oostra, B. A.; Akerman, K. Altered differentiation of neural stem cells in fragile X syndrome. *Proc. Natl. Acad. Sci. U. S. A.* **2005**, *102* (49), 17834−17839.
(91) Bolduc, F. V.; Bell, K.; Rosenfelt, C.; Cox, H.; Tully, T. Fragile x mental retardation 1 and filamin a interact genetically in Drosophila long-term memory. *Front. Neural Circuits* **2010**, *3*, 22.
(92) Dolan, B. M.; Duron, S. G.; Campbell, D. A.; Vollrath, B.; Shankaranarayana Rao, B. S.; Ko, H. Y.; Lin, G. G.; Govindarajan, A.; Choi, S. Y.; Tonegawa, S. Rescue of fragile X syndrome phenotypes in Fmr1 KO mice by the small-molecule PAK inhibitor FRAX486. *Proc. Natl. Acad. Sci. U. S. A.* **2013**, *110* (14), 5671−6.
(93) Hayashi, M. L.; Rao, B. S.; Seo, J. S.; Choi, H. S.; Dolan, B. M.; Choi, S. Y.; Chattarji, S.; Tonegawa, S. Inhibition of p21-activated kinase rescues symptoms of fragile X syndrome in mice. *Proc. Natl. Acad. Sci. U. S. A.* **2007**, *104* (27), 11489−94.